Fischer Tropsch Catalyst Structures & Process Design for JP-5 Fuel Integrated with MFEC

by

Tunde B.A Dokun

A thesis submitted to the Graduate Faculty of
Auburn University
in partial fulfillment of the
requirements for the Degree of
Master of Science

Auburn, Alabama
August 9, 2010

Keywords: Process and Product Design, Gas-to-Liquids
Fischer Tropsch Synthesis, Packed Bed, Aspen Simulation, MFEC

Approved by

Bruce J. Tatarchuck, Chair, Professor of Chemical Engineering
Mario R. Eden, Associate Professor of Chemical Engineering
Robert W. Ashurst, Assistant Professor of Chemical Engineering

Abstract

Modern societies are seeking new sources and corresponding technology as traditional fossil fuels are becoming more difficult to access because of their remote locations. A potentially attractive solution is to convert natural gas to a synthesis gas and then synthesize longer-chain hydrocarbons through a Fischer-Tropsch (FTS) reaction. However, conventional FTS reactors are faced with the challenge of heat removal due to the reaction being highly exothermic.

A design framework has been established, which incorporates functionality of the FTS catalyst and its impact on the FTS balance of plant (BOP). Process simulation tools are used in an iterative design to develop a unique plant optimized for the production of JP-5 and other value-added hydrocarbons under process constraints and size limitations.

The focus of this work is to evaluate the effects of utilizing a micro-fibrous entrapped catalyst (MFEC) on FTS plant scalability, physical plant design, and critical front-end capital cost in order to design a mobilized Fischer-Tropsch process for the purpose of producing JP-5. The product distribution of the FTS reaction is given by the Anderson-Schulz-Flory distribution. MFEC is comprised of a small grain catalyst entrapped within a sinter-locked network of a metal. With the use of this metal fiber network, we are able to increase the effective thermal conductivity within the reactor by about 90%, and reduce the temperature rise within the reactor as compared to a conventional Packed bed reactor. MFEC are readily manufactured and provide high intra-particle and mass transport properties. The temperature uniformity within the reactor will ensure and enhance JP-5 selectivity.

Using an implicit finite integrating scheme, we are able to determine the reactor temperature profile by modeling a plug flow reactor which includes the energy balances on the gas phase. The catalyst temperature will be assumed to be uniform inside the catalyst particles, so all heat of reaction is generated inside the catalyst particles. Moreover, with Aspen^{TM} integrated simulation, we are able to simulate an overall GTL plant capable of producing 500 bpd of JP-5. The simulation takes into account a vapor-liquid relationship of the different FTS hydrocarbon products with the intrinsic kinetics of the FTS and a water gas shift reaction for a promoted Iron catalyst, Fe/Cu/K as a basis of development.

The application of applied mathematics and numerical methods in solving the sets of differential equations is the key to fully understanding the temperature profile. By effectively designing an FTS reactor that has an effective heat transfer mechanism due to a high effective intra-bed thermal conductivity, a better control on intra-bed hot spots and product selectivity is achieved. A High selectivity towards JP-5 will be observed and thus, we are able to reduce the balance of plant (BOP) requirements for the FTS reactor and downstream operations.

Acknowledgements

The project undertaken for this research thesis has involved collaboration not only between academia and industry, but among a vast number of educational disciplines, family and friends. Due to the broad interdisciplinary nature of this project, there are many people in many walks of life that have contributed to the success of the project, and I would like to recognize and thank all of them. First, I would first like to thank my parents; Tele and Tope Dokun for their unconditional love and encouraging support throughout my life. I would like to thank my major professor, Dr. Bruce Tatarchuk, research committee; Dr. Mario Eden, and Dr. Bob Ashurst for their guidance and constructive feedback during the completion of this project. I would like to thank Ms. Karen Cochran and Ms. Kim Dennis for their support and services with academic and non-academic related issues. I would also like to thank the expertise of co-authors during my publications and presentations in relation to the project, particularly Dr. Donald Cahela, Dr. Hongyun Yang and Dr. Norm Sammons. Finally, I would like to thank all of my office mates and collaborators; Min Sheng, Josh Jackson, Pavielle Lockhart and Steve Saunders for their ability to provide alternative viewpoints needed to tackle the problem from all angles. To each of you – My sincerest gratitude and love.

Table of Contents

Abstract ii

Acknowledgements iv

List of Tables vii

List of Figures ix

List of Abbreviations xi

Chapter 1 – Introduction 1

Chapter 2 – Theoretical Background 3

2.1 History 3

2.2 FTS Catalyst 3

2.2.1 Product Selectivity 6

2.3 FTS Reactor 8

2.3.1 Reactor Design 9

2.3.2 Fixed Bed 11

2.3.3 Fluidized Bed 12

2.3.4 Slurry Bed 12

2.4 FTS Polymerization Reaction 14

2.5 FTS Mechanism/Kinetics 14

2.5.1 Fischer - Tropsch Synthesis 14

2.5.2 Water- Gas Shift Reaction 18

Chapter 3 – FTS Catalyst Design for Jet Fuel 20
3.1 Catalyst Design and Optimization 21
3.2 Catalyst Matrix 24
3.2.1 Catalyst for Jet Fuel Production 26
3.2.2 Phase Changes during Synthesis 35
3.2.3 Influence of Promoters on Physical Properties and Synthesis 36
3.2.4 Catalyst Size and Shape 38
3.3 Thermal Conductivity 40
Chapter 4 FTS Process Design for Jet Fuel 44
4.1 Introduction 45
4.2 Integrated Simulated Design 51
4.2.1 Upstream 52
4.2.2 FTS Reactor 57
4.2.3 Downstream 65
4.3 Weight/Volume BOP Analysis 66
Chapter 5 – Accomplishments and Future Directions 79
5.1 Accomplishments 79
5.2 Future Direction 80
Bibliography 81
Appendices 88

List of Tables

Table 2.1 Existing plants and plants under construction for Fischer-Tropsch synthesis 4

Table 2.2 Summary of Catalyst, Alpha values and Operating Conditions 7

Table 2.3 Advantages and disadvantages of established reactors for FTS 13

Table 3.1 Summary of Premium Products, Catalyst and technology used 24

Table 3.2 Chain Growth Probability factors for different Catalyst 27

Table 3.3 Estimated constants A and B 29

Table 3.4 Summary of FT Kinetics and Parameter 31

Table 3.5 Characterization data of Catalyst 33

Table 3.6 Optimization of Fe Catalyst Design 34

Table 3.7 Influence of alkali content on synthesis performance of precipitated iron catalyst 38

Table 3.8 Some common catalyst shape 39

Table 3.9 Thermal Conductivity and wall heat transfer coefficients 42

Table 4.1 Selected Fuel Properties for Jet Fuel and Diesel 49

Table 4.2 Comparison of Syngas generation technologies (Natural Gas Feed) I 52

Table 4.3 Comparison of Syngas generation technologies. II 53

Table 4.4 Sensitivity Analysis of steam to methane ratio and N.G temperature on GTL Performance. 56

Table 4.5 MFEC Reactors versus Fixed and Slurry Reactors. 58

Table 4.6 Conventional Packed Bed Reactors vs. MFEC. 62

Table 4.7 Overall Product Yield of JP-5 64

Table 4.8 Case A: Overall Product Yield of JP-5 - HTFT..... 69

Table 4.9 Case A: Overall Product Yield of JP-5 - LTFT. 70

Table 4.10 Products for Case Scenarios 74

Table 4.11 Weight and Volume of Major Process Equipments for Case A 74

Table 4.12 Weight and Volume of Major Process Equipments for Case B & C..... 75

Table 4.13 General Comparison Cases for 500 bpd of JP-5..... 76

Table 4.14 Composition of Recycled Streams..... 77

List of Figures

Figure 2.1 Hydrocarbon Selectivity 6

Figure 2.2 Types of Fischer-Tropsch Synthesis Reactors 9

Figure 2.3 Selectivity of FTS for LTFT and HTFT on Fe Catalyst 10

Figure 2.4 kinetic scheme of the successive hydrogenation of surface carbon 17

Figure 3.1 An Integrated Approach in FTS Catalyst Design 22

Figure 3.2 ASF Weight distributions as a function of chain growth probability 23

Figure 3.3 Influence of SiO_2 on pore volume of Fe_2O_3 25

Figure 3.4 Influence of SiO_2 on Surface Area of Fe_2O_3 25

Figure 3.5 Alpha versus Temperature for Promoted Iron 28

Figure 3.6 Alpha versus Syngas ratio for Promoted Iron 29

Figure 3.7 CO hydrogenation activities I 32

Figure 3.8 CO hydrogenation activities II 32

Figure 3.9 CO hydrogenation activities III 33

Figure 3.10 Iron Catalyst Phase Change during FT 35

Figure 3.11 Influence on the unit cell size of magnetite. 37

Figure 3.12 The surface area of fully reduced catalyst 37

Figure 3.13 Effect of particle size of the catalyst on CO Conversion 38

Figure 3.14 Catalyst Effectiveness Factor 39

Figure 3.15 Diagram of Location of Thermocouples 41

Figure 3.16 Temperature Bed comparisons between Packed Bed and MFEC 42

Figure 3.17 Steady-State data and segregated 2-D simulation result for heat-up of a tube packed with MFEC 42

Figure 4.1 U.S Energy Consumption 45

Figure 4.2 Comparison of FT Products with conventional Refinery barrel 47

Figure 4.3 Block Flow Diagram of an FT Process 51

Figure 4.4 Process Flow Sheet of FTS - Upstream 54

Figure 4.5 CO Conversion in FTS reactor 60

Figure 4.6 Temperature profile in FTS reactor 61

Figure 4.7 CO Conversion in FTS reactor 61

Figure 4.8 Product Selectivity Comparisons between Packed bed and MFEC 62

Figure 4.9 Product Yield from Hydro-cracking 64

Figure 4.10 Process Flow Sheet of FTS – Downstream 65

Figure 4.11 Fischer Tropsch Possibilities for Mobile Skid Unit 67

Figure 4.12 Process Flow Diagram Case A (Single Pass) 68

Figure 4.13 HTFT for Case A (Single Pass) 69

Figure 4.14 Case A (Single Pass) Simulation validation 70

Figure 4.15 LTFT for Case A (Single Pass) 71

Figure 4.16 Process Flow Diagram for Case B (Single Pass with Hydro-cracking unit) 72

Figure 4.17 Process Flow Diagram for Case C (Single Pass with Hydro-cracking unit/Lt. Naphta) 72

Figure 4.18 Reactor Productivity 77

Abbreviations

β	Biot number, $h_w R_t / k_r$
C_p	fluid specific heat
G	superficial mass flowrate
Nu	Apparent wall Nusselt number
d_p	Particle Diameter
Nu_{fw}	Apparent fluid/wall Nusselt number $h_{wf} d_p / k_f$
Pe_{RF}	Radial fluid Peclet number, $GC_p d_p / k_{rf}$
Re	Reynolds number, Gd_p / μ
Pr	Pradtl number, $\mu C_p / k_g$
k_{rg}	radial bulk thermal conductivity of gas
k_{rs}	radial bulk thermal conductivity of solid
k_{rf}	fluid bulk thermal conductivity
h_{wf}	wall/fluid heart transfer coefficient
h_{fs}	fluid/solid heat transfer coefficient
h_{ws}	wall/solid heat transfer coefficient
Bi	Biot number $h_w r / k_g$
U	Overall heat transfer coefficient
h_w	wall heat transfer coefficient
k_r	Effective thermal conductivity
u_s	superficial mass velocity
r_A	rate of reaction of CO
ε	voidage
ρ_{tap}	tapped density, gm/cc
ρ_{bulk}	bulk density, gm/cc
ρ_{part}	particle density, gm/cc
L	Catalyst loading, gm cat/total gm
V_p	pore volume of support material, cc/gm

"Research is to see what everybody else sees, and to think what nobody else has thought."
Albert Szent-Gyorgyi

Chapter 1

Introduction

1.1 Overview

The United States Department of Defense (DoD) is interested in low-sulfur, environmentally clean Fischer-Tropsch fuels—specifically Jet fuel, JP-5,—due to the inherent security risks associated with and the instability in the crude oil supply. Currently, the world's fuel and chemical production is based predominantly on petroleum crude oil with reserves of methane and coal exceeding that of crude oil. It should then come as no surprise that with increasing crude oil prices, the inaccessibility of crude oil deposits and transportation cost of fuel to its markets, there is a shift toward the utilization of coal, natural gas and other alternatives sources for energy. A logical alternative to refining crude oil is the production of syngas (CO and H_2) from methane, coal or even biomass and furthermore, its conversion to a range of liquid fuels and chemicals through Fischer Tropsch Synthesis (FTS). Advantages of fuels derived from FT processes include the absence of sulfur, nitrogen or heavy metal contaminants, and a low aromatic content. With the focus of this work on JP-5 for the Navy; JP-5 produced from FT has good combustion properties and high smoke points. Potentially useful co-products are also generated such as waste heat which can be converted to electrical power and or reused back in the FT process.

Chapter 2 of this thesis gives a general overview of the fundamental concepts surrounding FT. The focus covers current FT catalyst, reactor types/design and operating conditions, the polymerization reaction and kinetics governing this reaction. Chapter 3 focuses on the choice of an appropriate catalyst for JP-5 production with the use of micro-fibers materials to enhance thermal conductivity. An optimal design for the catalyst is highlighted with respect to product selectivity which requires a comprehensive understanding of influences with promoters and supports. In addition, phase changes and catalyst deactivation are reviewed. The thermal conductivity measurement of a packed bed was compared to that of a micro-fiber catalyst bed showing significant improvement for heat removal. Chapter 4 details the use of this technology for specific case study examples with emphasis on problem formulation and significant results on JP-5 production. The impact of an improved FTS selectivity and the overall balance of plant (BOP) is assessed which includes a unique process design approach using simulation tools for upstream and downstream operations. Chapter 5 highlights the conclusions reached from the use of this technology, framework and iterative design, as well as a detailed plan of action to strengthen and expand this research area. It will be demonstrated that this research provides a method to address the increasing energy demands and crisis we face including those by the DoD.

"The era of procrastination, of half-measures, of soothing and baffling expedients, of delays, is coming to a close. In its place we are entering a period of consequences…"
Sir Winston Churchill, November 1936

Chapter 2

Theoretical Background

2.1 History

In 1902, Sabatier and Senderens discovered that methane could be formed from a mixture of H_2 and CO over nickel and cobalt catalyst. German chemical manufacturer, BASF, produced liquid products such as paraffins, olefins and oxygenates on activated Co-Os catalyst at high pressure.[1] In time, nickel was abandoned as a catalyst because its activity declined due to the formation of nickel carbonyl. Haber and Bosch developed a method for ammonia synthesis in 1908 while Bergius worked directly on the hydrogenation of coal in 1913.[2] Franz Fischer and Hans Tropsch were responsible for the development of the Fischer Tropsch method in 1920 with the intention of producing high-value hydrocarbon molecules from coal-derived gas. Fischer and Tropsch successfully proposed the synthol process from CO and H_2 on alkalized iron chips.[3] In 1935, the first FT industrial application was designed; the Ruhrchemie atmospheric fixed-bed reactor.[4] By 1935, about 4 commercial-size, Ruhrchemie-licensed FT plants were under construction with an estimated annual capacity of producing 725,000 – 868,000 barrels of gasoline, diesel fuel, and lubricating oil.[4] By 1944,

[1] Dry, M. "The Fischer Tropsch Process: 1950-2000." *Catalysis Today* 71 (2002): p227-41
[2] Guettel, R. "Reactors for Fischer Tropsch Synthesis." *Chem. Eng. Tech.* 31 (2008): p746-54
[3] Khodakov, A. "Advances in the Development of Novel Cobalt Fischer Tropsch for Synthesis of Long Chain Hydrocarbon and Clear fuels." *Chemical Reviews* 107 N5 (2007): p1692-1744
[4] Steynberg, A. "Introduction to Fischer Tropsch Technology." *Studies in Surface Science and Catalysis* 152 (2004): p1-63

another catalyst predominantly used in FTS was cobalt with a composition in relative mass units of 100Co:5ThO2:8MgO:200Kieselguhr (silicious diatomatous earth).[5] In 1950, the first FT plant was built in the United States in Brownsville, TX with the capacity to produce 5,000 bpd, but with an increase in feed prices, the plant was shut down.[2] In 2006, Sasol-Chevron embarked on a project to design a Gas-to-Liquid (GTL) plant in Escravos, Nigeria with an estimated production capacity of about 100,000 bpd. Exxon-Mobil signed an agreement with Al-Kaleen Gas Project (AKG) to build 150,000 bpd GTL-FT plants in Qatar. FT technology has reached an industrial full-scale application which has been commercialized worldwide. Table 1 below shows a timeline of FTS plant construction and the average capacity under which they operate.

Table 1. Existing plants and plants under construction for Fischer-Tropsch synthesis.[2]

Company	Site	Capacity [bpd]	Raw Material	Commission Date
Existing plants				
Sasol	Sasolburg	2500	Coal	1955
Sasol	Secunda	85000	Coal	1980
Sasol	Secunda	85000	Coal	1982
MossGas	Mossel Bay	30000	Natural Gas	1992
Shell	Bintulu	12500	Natural Gas	1993
Sasol/Qatar Petroleum	Qatar	34000	Natural Gas	2006
Under Construction				
Sasol-Chevron	Escravos		Natural Gas	2007
Exxon-Mobil	Qatar		Natural Gas	2009

2.2 FTS Catalyst

The four metals currently known to be most active in the hydrogenation of CO to hydrocarbon are Fe, Ni, Co and Ru. While Ni is the most active of the four metals, it is

[5] Dry, M. "The Fischer Tropsch Synthesis." *Catalysis: Science and Technology* 1 (1981): p159-225

known to have a very high selectivity for methane while olefin selectivity is very low.[6] Additionally, the use of nickel as a catalyst creates inherent problems relating to the volatility of nickel carbonyls formed in the FT environment. Ru, Co, and Fe are therefore the catalysts of choice, however, the determination of the most desirable catalyst is still difficult to determine as several factors come into play including cost, availability, desired product spectrum, catalytic life time, and activity.

Alkali-promoted iron catalysts have been industrially utilized in FTS for many years. Iron catalysts have high water-gas shift activity and selectivity toward olefins.[7] There are two types of iron catalyst, fused and precipitated iron. Fused iron catalysts are enhanced with an alkali to increase catalyst activity and selectivity. Precipitated iron catalysts, on the other hand, are doped with metals like Cu to enhance the reduction of iron oxide. The catalyst is then precipitated from an acidic solution with the addition of a basic solution, e.g. sodium carbonate or ammonia.

Cobalt catalysts on the other hand, are usually supported with an alkali. A major difference between a cobalt catalyst and that of iron is that cobalt catalysts are not inhibited by water and thus result in a higher productivity at high syngas conversion. They are also known to give the highest yields and longest lifetime producing linear alkanes.[8] Cobalt disadvantages include a low water-gas shift activity and relatively expensive when compared to an iron catalyst.

[6] Dry, M. "FT synthesis over iron catalyst." *Catalysis Letters* 7 (1990): p241-252
[7] Jager, B. "Advances in low temperature Fischer-Tropsch synthesis." *Catalysis Today* 23 (1995): p17-28
[8] Chaumette, P. "Higher alcohol and paraffin synthesis on cobalt based catalyst: comparisons of mechanistic aspects." *Topics in Catalysis* 2 (1995): p117-126

2.2.1 Product Selectivity

The products from the FT synthesis form a complex, multi-component mixture varying in carbon number and product type. The product distribution of hydrocarbons can be described by the Anderson-Schulz-Flory (ASF)[9] equation;

$$m_n = (1-\alpha)\alpha^{n-1} \tag{1}$$

Thus, one is able to express this product distribution into weight fraction

$$W_n = n(1-\alpha)^2\alpha^{n-1} \tag{2}$$

$$\log\frac{W_n}{n} = n\log\alpha + \log\frac{(1-\alpha)^2}{\alpha} \tag{3}$$

The products of FTS over Co, Fe and Ru are shown on Figure 1.

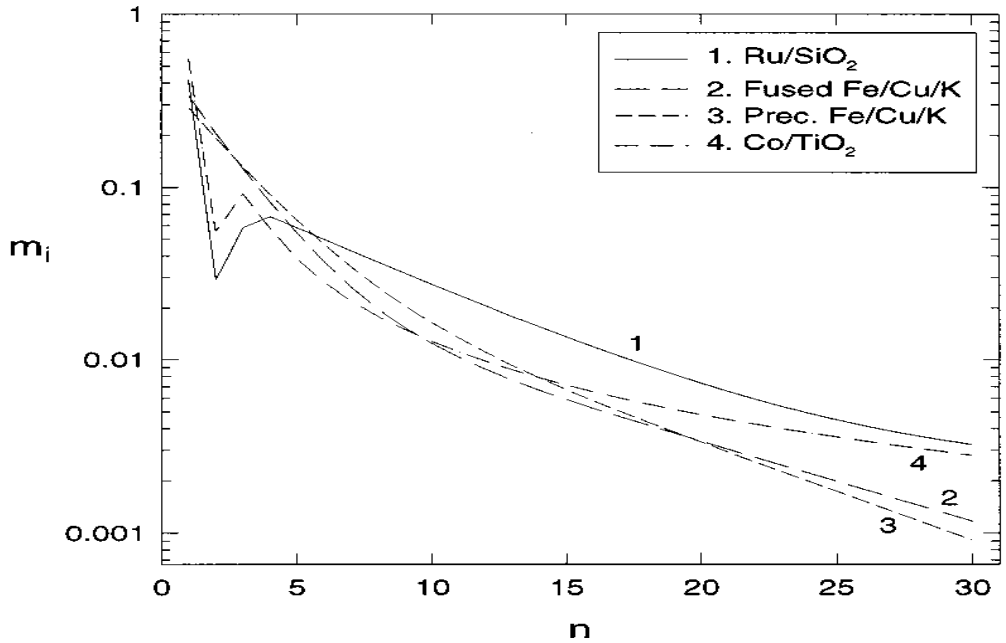

Figure 1 Hydrocarbon Selectivity on Co/TiO_2 200°C; $H_2/CO \sim 2.1$, and $P \sim 20$ bars.[10]
Ru/SiO_2. 212 °C, $H_2/CO \sim 2$, and $P \sim 5$ bars[18]
Fused and precipitated Fe/Cu/K [11]

[9] Anderson, R. "Catalyst for the Fischer-Tropsch Synthesis." *Van Nostrand Reinhold* 4 (1956) New York
[10] Iglesia, E. "Selectivity Control and Catalyst Design in the Fischer-Tropsch Synthesis: Sites, Pellet, and Reactors." *Advances in Catalysis* 39 (1993): p221-298
[11] Donnelly, T.J. "Analysis and Prediction of Product Distributions of the Fischer-Tropsch Synthesis." *Energy & Fuels* 2 (1988): p734-739

where $\alpha = \frac{k_p}{k_p + k_t}$; and k_p represent the propagation rate and k_t represent the termination rate.[12] A summary of catalyst and corresponding alpha values are reported in Table 2.

Table 2. Summary of Catalyst, Alpha values and Operating Conditions.[13]

Element	Alpha	Operation Temperature (ºC)
Ru	0.85-0.95	180-250
Co	0.70-0.80	180-250
Fe	0.50- 0.70	220-250 (LT) 280-350 (HT)

LT/HT – Low/High temperature

There are significant deviations from the ASF due to the uncertainties of not knowing the mechanism on the molecular level. These deviations have been well documented. For example; relatively high yields of methane, which have been explained by reactor hot spots,[13] increase termination of C_1 precursors,[14] low yields of ethane and ethene which is attributed to secondary reaction.[15] Changes in the growth parameter and the exponential decrease of the olefin to paraffin ratio with increasing carbon number have also been reported for most catalysts; iron[16,17], cobalt[6,18], and ruthenium.[8,19] This phenomena is attributed to the

[12] Lox, E. "Kinetics of the Fischer-Tropsch Reaction on a Precipitated Promoted Iron Catalyst, 2 Kinetics Modeling." *Ind. Eng. Chem. Res.* 32 (1993): p71-82

[13] Dry, M. "Catalytic aspects of industrial Fischer-Tropsch synthesis." *J. Mol. Catal.* 17 (1982): p133-144

[14] Sarup B. "Studies of the Fischer-Tropsch Synthesis on a cobalt catalyst. I. Evaluation of product distribution parameters from experimental data." *Canadian Journal Chemical Engr.* 66 (1988): p831-843

[15] Iglesia, E. "Transport-enhanced α -olefin re-adsorption pathways in ruthenium-catalyzed hydrocarbon synthesis." *Journal of Catal.*129 (1991): p238-256

[16] Rao, V. "Iron-based catalysts for slurry-phase Fischer-Tropsch process: Technology." *Fuel Process technology* 30 (1992): p83-107

[17] Dictor, R. "Fischer-Tropsch synthesis over reduced and unreduced iron oxide catalysts." *Journal of Catal.* 97 (1986): p121-136

[18] Madon, R. "Selectivity in Catalysis" (S.L. Suib and M.E Davis, eds.), *American Chemical Society*, Washington, DC, (1993): p382

[19] Inoue, M. "Simple criteria to differentiate a two-site model from a distributed-site model for Fischer-Tropsch synthesis." *Journal of Catal,*105 (1987): p266-269

occurrence of catalytic sites. Most of these deviations can be attributed to secondary reactions of α-olefins.[20]

2.3 FTS Reactors

Pichler discovered in 1936 that when pressure was increased from atmospheric to about 15 bar, the life of iron catalyst improved significantly.[21] The original German industrial rector of 1936 (Lamellenofen) had 10 m^3 of packed catalyst between 600 parallel metal plates spaced 7 mm apart with 600 tubes.[22] After the 2nd World War, Ruhrchemie and Lurgi formed Arbeitsgemeisnschaft (ARGE) and developed the fixed-bed reactor using a precipitated iron catalyst to produce high yields of wax.[5] The heat of the reaction was removed using water circulated through horizontal tubes which passed through the vertical plates. Due to low linear velocities of the gas, 100 hr^{-1}, the heat removal was not sufficient. This resulted in carbon deposition and disintegration of catalyst particles attributed to localized over-heating[3]. The next improvement was the development of the concentric tube reactor which had 2000 pairs of tubes with ID's of 21 and 24 mm and 4.5m long. Cooling water was circulated outside of outer tube and through the inside of the inner tube but still low space velocity was still an issue. BASF utilized the concept of high recycle ratio (100 to 1) in a single bed reactor of catalyst (3.8 m^3) to attempt to resolve the temperature rise within the FTS reactor.[23] However, overheating still occurred leading Lurgi to improve such a technique by splitting the bed into several sections with fresh feed split, i.e. feed between successive beds. The overall recycle to fresh feed gas ratio per bed was 20 to 1 and the temperature rise per bed was about 5°C.[4] The reactor was operated at 270°C, 20 bar and a

[20] Iglesia, E. "Design, synthesis, and use of cobalt-based Fischer-Tropsch synthesis catalyst." *Applied Catalysis A* 161(1997): p59-78
[21] Pichler, H. :ibid (1952) vol. 4
[22] Frohning, C. "Fischer-Tropsch Synthese." *Chemierohstoffe aus kohle (Falbe J., ed.)* (1977). Stuttagart: Thieme
[23] Ullmanns Encyklopadie d. techn. Chem. 9, 715 Munchen-Berlin: Urban and Schwarzenberg (1957)

fresh feed space velocity of about 200 hr^{-1}. A high conversion of 85% was obtained.[3] The use of a high gas linear velocity through the catalyst bed ensures that heat generated is removed along the length of the tubes and this results in a nearly isothermal reactor at the expense of compression cost.

2.3.1 Reactor Design

There are four types of FT reactor commercially used today,

- Tubular fixed-bed reactor
- Circulating fluidized-bed reactor
- Fluidized bed reactor
- Slurry phase reactor

A picture of these reactors is shown in Figure 2.

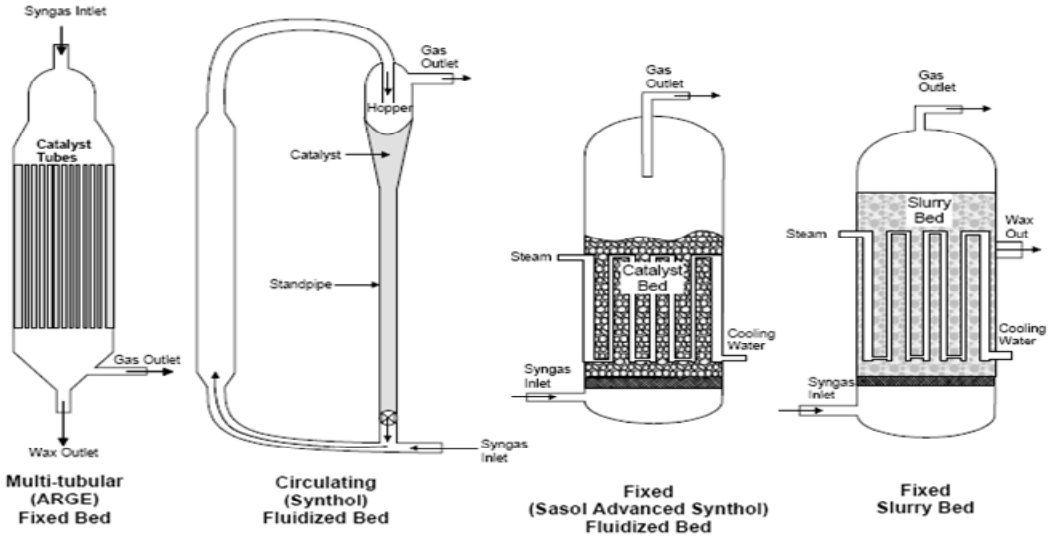

Figure 2 Types of Fischer-Tropsch Synthesis Reactors.[24]

Because of the strong exothermic nature of FT reaction, the control of temperature within the reactor is the most important issue for a safe and stable operation. Other important

[24]Steynberg, A. "Fischer Tropsch Reactors." *Studies in Surface Science and Catalysis* 152 (2004): p64-195

reasons for monitoring the temperature within the reactor include life of catalyst and product selectivity. In this regard, the industrial preference is to use a slurry reactor over fixed bed because of its high heat transfer characteristics.[25]

The slurry reactor operate within the range of 320°C to 350°C, hence the term high temperature Fischer Tropsch (HTFT) while that of the tubular fixed bed and slurry phase reactor operate within the 220°C to 250°C range and have been termed low temperature Fischer Tropsch (LTFT). Beyond the operating temperature range that differentiates between the HTFT and LTFT reactors is the fact that there isn't a liquid phase present outside the catalyst particles in the HTFT reactors. This is because of particle agglomeration and loss of fluidization.[26]

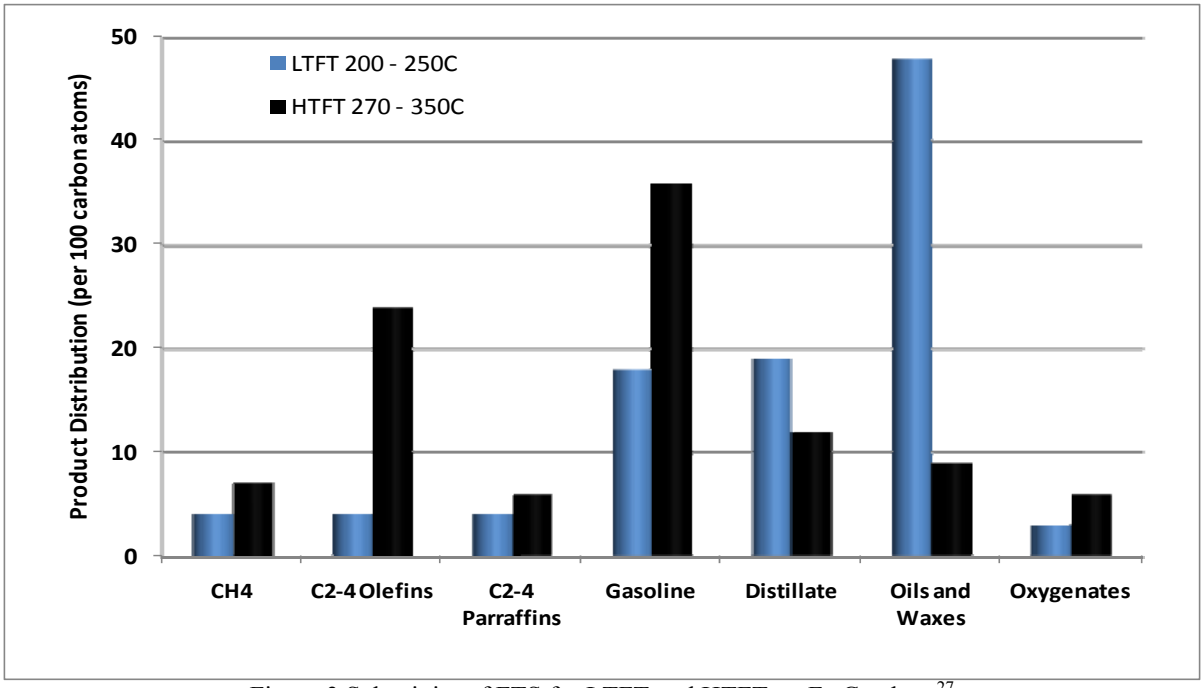

Figure 3 Selectivity of FTS for LTFT and HTFT on Fe Catalyst.[27]

[25]Song, H. "Operating Strategies for Fischer-Tropsch Reactors: A Model-Directed Study." *Journal of Chemical Engineering* 21(2004): p308-317.
[26] Baird, M. "FT Process investigated at the Pittsburgh Energy Technology Center since 1944." *Ind. Eng. Chem. Prod. Res. Dev.*, 19 (1980): p175-191
[27] Mulder, H. "From Syngas to clean fuels and chemicals via Fischer-Tropsch process." Presented at Gasification, the gateway to a cleaner future, Dresden Germany, Sept. 1998.

2.3.2 Fixed Bed Reactors

Fixed bed reactors are vertically spaced packed bed and radial flow reactors with cooling tubes between the beds. The multi-tubular reactor is packed with catalyst inside the tube walls (by using narrow tube diameters) and usually operates at high gas linear velocities to improve the transfer of the heat generated from the catalyst to the cooling medium. The use of narrow tubes ensures that the distance between the hot catalyst particles and heat exchanger surface is short and also ensures that the ratio of heat exchanger surface area to catalyst mass is high. There are radial as well as axial temperature gradients in these reactor tubes, about 2^{o}C to 4^{o}C (tube centre to wall) and an axial temperature difference of 15^{o}C to 20^{o}C (peak in upper section to exit)[28] with the high linear space velocities.

There are advantages to using a fixed bed reactor; these are; easy to operate. They can be used over wide range temperature ranges irrespective of whether the FT products are gaseous or liquid, or both, under reaction conditions. There are no problems with separating liquids products from the catalyst. However, fixed bed reactors are prone to pressure drop, however this can be reduced by working with a high catalyst bed voidage of about 90%.[29] Some more disadvantages include cost, expensive to construct. The FT reaction is diffusion controlled and so it would be advantageous to use small catalyst particles. Replacing the catalyst is labor intensive due to the narrow tubes. Typical fixed bed reactors operate at low temperature, but with iron catalyst a high temperature, 260^{o}C, with an operating pressure of 28 bar and a fresh space velocity of about 1000 hr^{-1} (recycle ratio of about 20) is commonly used.[30]

[28] Dry, M. "Practical and theoretical aspects of the catalytic Fischer-Tropsch Process." *Applied Catalysis A* 138 (1996): p319-344.
[29] Forney, A. "US Bur. Mines Rep." 5841ACS Div. Fuel 20 (1961)
[30] Fischer, F Roelen, O.:ibid.11,489 (1930)

2.3.3 Fluidized Bed

An alternative way of rapidly transferring heat is to move the particles to the heat exchanger which is what actually occurs in a two phase fluidized bed. The high gas velocity limits film diffusion at both the particle surfaces and the heat exchanger surfaces. The direct physical contact between hot catalyst particles and heat exchanger tube walls also contributes to heat exchange. The combination of these factors results in a much higher efficiency of heat exchange within the fluidized bed which means a smaller heat exchanger area is required. Another advantage of fluidized beds is that once catalyst particles are fluidized, the differential pressure across the reactor will not increase with further increase in gas velocity. The pressure drop is proportional to the mass of catalyst being used. Commercial fluidized beds operate in turbulent regimes and this result in a nearly isothermal reaction zone with differential temperatures across the bed of $2^{o}C$ or less. Fluidized beds do have a few disadvantages owing to their operational complexity. Separation of the catalyst from the exhaust gas is not simple. There is erosion of the tubes and fouling due to the abrasive iron carbide catalyst. This adds to cost and increases reactor down time.[31] Two-phase fluidized systems cannot be used when wax is to be produced and typical fluidized bed reactors operate at temperatures of $300^{o}C$ and above.

2.3.4 Slurry Bed Reactors

Gas can be bubbled through a suspension of finely divided catalyst particles (typically 10 -200μm) in a liquid which has a low vapor pressure. The heat generated is removed by circulating the slurry through external heat exchangers or immersing heat exchangers directly

[31] Jager, B. "Experience with a new type of reactor for Fischer-Tropsch synthesis." *Catalysis letters* 7 (1990): p293-301

into the slurry bed. The influence of internal mass transfer resistance is negligible and both optimal activity and selectivity are achieved. The Slurry reactor is a fixed fluidized bed. In FT applications, it is used for the production of high molecular waxes which are liquids under synthesis conditions and also why the liquid of choice is usually a cut from the product spectrum, e.g. high boiling wax. A slurry bed has a direct advantage over a fixed bed in the sense that it can be used easily for HTFS operations. Comparing this reactor to a "dry" fluidized bed, it has the advantage of operating with lower H_2/CO ratio. Disadvantages of the slurry bed include scalability and the separation of the solid catalyst. Advantages and disadvantages of both established reactor technologies are summarized in the table below.

Table 3. Advantages (+) and disadvantages (-) of established reactors for FTS.[2]

	Fixed bed reactor	Bubble column Reactor
Pore diffusion	-	+
Catalyst content in reactor	+	-
Gas-liquid mass transfer	+	-
Isothermal behavior	-	+
Catalyst exchange	-	+
Catalyst attrition	+	-
Need for liquid-solid separation	+	-
Scale up	+	-
Reactor cost	-	+

(+) Advantages and (-) Disadvantages

Both reactors technologies exhibit certain disadvantages: the fixed-bed multi-tubular reactor suffers from high pressure drop, low catalyst utilization and insufficient heat removal, whereas slurry bubble column reactor faces the need for catalyst separation, less ideal residence time behavior and highly demanding scale up. An ideal reactor would have the following characteristics:

- Fixed bed catalyst
- High catalyst efficiency due to short diffusion distances
- Highly efficient gas-liquid mass transfer

- Isothermal operation at the highest possible temperature

2.4 FT Polymerization Reaction

The overall reactions for an FT process are listed below:[32]

Main reactions

Paraffins	$(2n+1)H_2 + nCO \rightarrow C_nH_{2n+2} + nH_2O$
Olefins	$2nH_2 + nCO \rightarrow C_nH_{2n} + nH_2O$
WGS reaction	$CO + H_2O \leftrightarrow CO_2 + H_2$

Side reactions

Alcohols	$2nH_2 + nCO \rightarrow C_nH_{2n+2}O + (n-1)H_2O$
Catalyst Ox/Red	(a) $M_xO_y + yH_2 \leftrightarrow yH_2O + xM$ (b) $M_xO_y + yCO \leftrightarrow yCO_2 + xM$
Bulk carbide formation	$yC + xM \leftrightarrow M_xC_y$
Boudouard reaction	$2CO \rightarrow C + CO_2$

The FT synthesis product spectrum consists of a complex multi-component mixture of linear and branched hydrocarbons and oxygenated products. The main products are linear paraffins and alpha-olefins.

2.5 FT Mechanism/Kinetics

FTS kinetics has been studied extensively and many describe the rate using a power law model or certain mechanistic assumptions that are thermodynamically controlled. These empirical equations that describe the intrinsic rate of Fischer-Tropsch carbon monoxide hydrogenation have been proposed using a mechanism that highlights the rate of formation of monomer as the rate limiting step. Anderson et al. postulated a method to describe the

[32] Van der Laan, G. "Kinetics and Selectivity of the Fischer-Tropsch Synthesis: A Literature Review." *Catal. Rev. – Science Engineering* 41 (1999): p255-315

product formation by successive addition of C_1 units to growing chains on a catalyst surface.[33] He also postulated that the rate of consumption of carbon monoxide for cobalt catalyst was proportional to the rate of desorption of the hydrocarbon chains growing on the catalyst surface.[9] There are many general theories that have been postulated. Carbide theory was the first and describes how CO dissociates and forms surface metal carbide. The intermediate reacts to form a methlyene group which is said to polymerize into a hydrocarbon chain.

$$CO + 2* \xleftrightarrow{K_1} C* + O*$$

$$O* + H_2 \xleftrightarrow{K_2} H_2O + *$$

$$C* + H_2 \xrightarrow{k} CH_2*$$

The model derived from this theory describes how CO dissociates on the surface; adsorbed carbon reacts with hydrogen in the rate-determining step. This leads to a rate reaction of

$$-r_{FT} = \frac{kK_1K_2P_{CO}P_{H_2}^2}{1 + kK_1K_2P_{CO}P_{H_2} / P_{H_2O}} \qquad (4)$$

The Enolic theory is the second, where it is believed that adsorbed CO is hydrogenated to a hydroxylated species. The chain growth forms from the elimination of water via condensation.

$$CO + * \xleftrightarrow{K_1'} CO*$$

$$H_2O + * \xleftrightarrow{K_2'} H_2O + *$$

$$CO* + H_2 \xrightarrow{k'} COH_2*$$

This leads to an equation of

[33] Anderson, R. "Fischer-Tropsch Reaction Mechanism Involving Stepwise Growth of Carbon Chain" *J. of Chem. Phys.19* (1951): p313

$$-r_{FT} = \frac{k'(K_1'/K_2')P_{CO}P_{H_2}}{P_{H_2O} + (K_1'/K_2)P_{CO}} \quad (5)$$

Steen proves extensively that this is flawed because methane is the most abundant product and the polymerization character of FTS along with observed product distribution are never accounted for in the popularly postulated mechanisms.[34] The rate equation proposed by van Steen is based on the assumption that the rate of the reaction in FTS is governed by the rate of hydrogenation of surface carbon. The formation of organic compounds in FTS features a polymerization reaction with three classes of reactions: initiation, propagation and termination. Steen defines the reaction initiation as the formation of a chain starter from the reactants hydrogen and carbon monoxide. The propagation step is the incorporation of monomer units into growing chains which is the chain growth step in FTS. The monomer produced in situ on the catalyst surface. The termination is desorption of growing chains from the catalyst surface. The rate of carbon monoxide consumption is equal to the sum of the initiation rate, propagation and termination steps. Carbon is not involved in the termination reaction therefore the rate of consumption of carbon monoxide equals the rate of initiation plus propagation. This is also the rate of formation of chain starts plus the rate of incorporation of carbon into the growing chain (chain growth). In FTS the rate of incorporation is a function of the carbon number of the growing chain.

[34] Steen, van Eric. "Polymerization Kinetics of the Fischer-Tropsch CO hydrogenation using iron and cobalt based Catalyst." *Applied Catalysis A* 186 (1999): p309

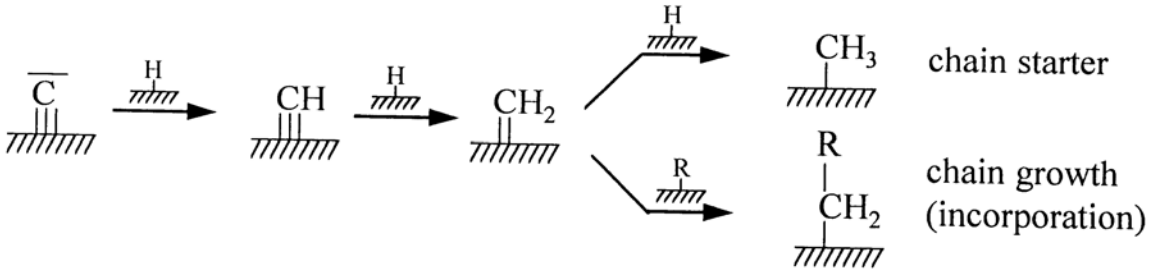

Figure 4 kinetic scheme of the successive hydrogenation of surface carbon.[34]

At steady state, the net rate of formation of CH_2 surface species equals zero. Therefore, the rate of formation of CH_2 surface species by hydrogenation of CH species ($r_{CH\rightarrow CH_2}$) equals the rate of incorporation. The rate of formation of CH_2 surface species is thus equal to the rate of carbon monoxide consumption for the formation of organic compounds.

$$r_{C,org} = r_{CH\rightarrow CH_2} = r_{CH3} + r_{incoporation_2}$$

The rate of consumption of monomer units is equal to the sum of the rates of incorporation into chains of all possible lengths. The net rate of formation of CH_2 surface species equals the net rate of formation of CH species. The rate of consumption of carbon monoxide for the formation of organic compounds is expressed as the rate of formation of CH surface species.

$$r_{C,org} = r_{C\rightarrow CH} = r_{CH\rightarrow CH_2}$$

Because the formation of CH surface species can be regarded as irreversible, the net rate of formation of surface species is proportional to the fractional coverage of surface carbon and the fractional coverage of surface hydrogen;

$$r_{C\rightarrow CH} = k_{C\rightarrow CH}\theta_C\theta_H$$

The rate of formation of organic compounds on a carbon basis can principally be derived by using steady state approximation of C, H, CO, O and OH surface species. For simplicity, the species are in equilibrium with the gas phase compounds.

$H_2 + 2* \leftrightarrow 2H*$ $\qquad K_H = \frac{\theta_H}{P_{H_2}^{0.5}\theta_*}$

$CO + * \leftrightarrow CO*$ $\qquad K_{CO} = \frac{\theta_{CO}}{P_{CO}\theta_*}$

$CO* + * \leftrightarrow C* + O*$ $\qquad K_C = \frac{\theta_C\theta_O}{\theta_{CO}\theta_*}$

$O* + 2H* \leftrightarrow H_2O + 3*$ $\qquad K_{H_2O} = \frac{p_{H_2O}\theta_*^3}{\theta_O\theta^2{}_H}$

The postulated equilibrium is assumed to occupy approximately the same geometric space. The rate of consumption of carbon monoxide can be now be expressed as

$$r_{C,org} = kc \rightarrow C_H K_H^3 K_{CO} K_C K_{H_2O} \frac{p_{H_2}^{3/2}}{p_{H_2O}} \theta_*^2$$

With a reasonable assumption that the surface is mainly covered with surface carbon under reaction conditions:

$$\theta_* + \theta_C = 1$$

Which gives the rate of organic compounds as

$$r_{C,org} = \frac{kc \rightarrow C_H K_H^3 K_{CO} K_C K_{H_2O} (p_{H_2}^{3/2} p_{CO} / p_{H_2O})}{\left(1 + K_H^2 K_{CO} K_C K_{H_2O} (p_{H_2} p_{CO} / p_{H_2O})^2\right)}$$

$$r_{C,org} = \frac{a(p_{H_2}^{3/2} p_{CO})}{p_{H_2O}\left[1 + b(p_{H_2} p_{CO} / p_{H_2O})\right]^2} \qquad (6)$$

2.5.2 Water-Gas Shift Reaction

The water-gas shift can increase or decrease the rate of FTS. This is because of the shared components of adsorption and desorption reactions as well as dissociation of H_2, H_2O

and CO_2. There are a few studies that have reported empirical kinetic expressions for the WGS reaction under FTS conditions using iron catalysts;[35]

$$r_{CO2} = k_w(P_{H_2O} p_{CO} - \frac{P_{CO_2} p_{H_2}}{K_P}) \quad (7)$$

Because WGS is an equilibrium reaction,[36] close at or close to under FTS conditions, the reverse reaction has to be taken into account;

$$\log Kp = (\frac{2073}{T} - 2.029) \quad (8)$$

It is believed that the reaction of WGS may take place on the same catalytic sites as those in FT.[36] The authors were not able to derive reliable kinetics equations for WGS under FT conditions and the question remains as to how WGS competes with FTS.

Taking full advantage of the above technology concept of combining the length-independent chain growth process with a selective chain length-dependent conversion process is a technology that will help meet the growing energy demand. Though there is still a need to reduce the investment required and improve operating efficiency in commercial FT process applications, GTL fuels offer very attractive options to the hydrocarbon industry to introduce clean fuels. The FT process can and will be tuned so as to yield JP-5 in the next chapters.

[35] Huff, G. "Intrinsic Kinetics of the Fischer-Tropsch Synthesis on a Reduced Fused-Magnetite Catalyst." *Ind. Eng. Chem. Process Des. Dev.* 23 (1984): p696-705
[36] Graaf, G. "Chemical equilibria in methanol synthesis." *Chem. Eng. Sci.* 41 (1986): p2883-2890

"Civilization is in a race between education and catastrophe. Let us learn the truth and spread it as far and wide as our circumstances allow. For the truth is the greatest weapon we have."
H.G Wells.

Chapter 3

FTS Catalyst Design for Jet Fuel

Abstract

This chapter focuses on the design of an optimal catalyst matrix to enhance JP-5 selectivity with the aid of a highly thermally conductive microfibrous material. A promoted iron catalyst, Fe/Cu/K-La-Al_2O_3, was ultimately chosen because of its high alpha value of 0.87 and high water gas shift activity. The effects of promoters and supporters, investigated by pioneers and their relationship towards iron catalysts, are highlighted in this chapter. Kinetics of different catalysts was used to calculate the catalyst bulk activity with promoted iron showing high promising values. In addition, the thermal conductivity for a packed bed was measured and compared with that of a microfibrous bed. The microfibrous material increased the effective bed thermal conductivity by 90%. The ability to improve the bed conductivity will allow for a more prominent JP-5 selective control in FTS.

3.1 Catalyst Design and Optimization

The interaction between the reaction kinetics and transport phenomena in a catalytic process takes place on a number of different levels; from the atomic site, to the catalyst size, and reactor operating conditions. Most FT studies and evaluations have separated catalyst development from reactor technology and development. A different design approach has been applied in this thesis, merging the two different paths, from the active site level of one's catalyst to modeling scale up facilities, in an iterative manner. The relationship is symbiotic because active sites lie within porous pellets which control the rates of diffusive processes that supply reactants and remove products while the reactor allows for convective transfer of mass and heat over the catalyst bed. The added advantage of working simultaneously on these two steps for a catalyst design for FT is to achieve high metal particle dispersion and catalytic conversions. This will ensure that potential losses are minimized and the labor required to design an overall process for FT is reduced. In order to achieve optimum process design and product selectivity for Fischer Tropsch Synthesis (FTS), the two different paths of design that have in the past been separated must be coupled.

Commercial catalyst screening was chosen as a logical starting point. After the new catalyst has been synthesized, its catalytic performance is tested and compared to that of conventional and commercial catalysts. This is known as catalyst screening. Catalyst synthesis, activations, pretreatments, evaluation of catalytic performance, and characterization are the next primary steps in the catalyst design. Comparisons of characterization data and results of catalyst testing allows for the nature of active sites to be characterized and catalyst synthetic routes to be optimized.

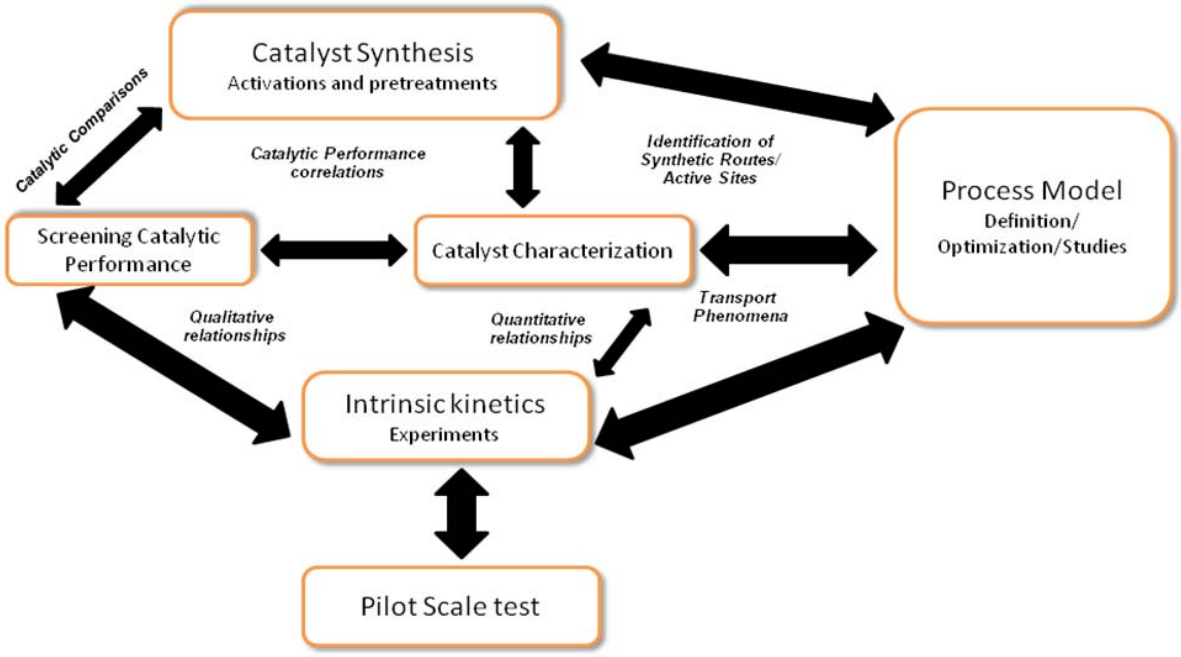

Figure 1 A Integrated Approach in FTS Catalyst Design Framework and Process Design for Balance of Plant.[1]

The next stage of the catalyst design is the generation of catalytic systems whose structure, composition, actives sites and catalytic performance have been qualitatively defined by characterization and screening as well as the development of a molecular simulation. Kinetic studies then provide a quantitative relationship between the intrinsic reaction rates and composition of fluid around the catalyst. Developing the intrinsic kinetic model of the catalytic reaction will lead to the next step which would be linked to molecular simulations and thus modeling and evaluation of a pilot reactor testing.

JP-5 is composed of C_9-C_{16}, linear hydrocarbons with no aromatics. It should come as no surprise that to design such a catalyst for FTS, the first step should focus on the catalyst, α, chain growth probability value and, by employing the Anderson-Schulz-Flory[2] distribution; such values should be around 0.86 to achieve the maximum C_9-C_{16} selectivity.

[1] Khodakov, A. "Advances in the Development of Novel Cobalt Fischer Tropsch for Synthesis of Long Chain Hydrocarbon and Clear fuels." *Chemical Reviews* 107 N5 (2007): p1692-1744
[2] Anderson, R. "Catalyst for the Fischer-Tropsch Synthesis." *Van Nostrand Reinhold* 4 (1956) New York

Figure 2 shows the weight distribution of FTS. The product selectivity can be achieved by optimizing the syngas ratio, operating conditions of the FT reactor and with the use of an efficient heat removal technique with an appropriate catalyst that has been promoted.

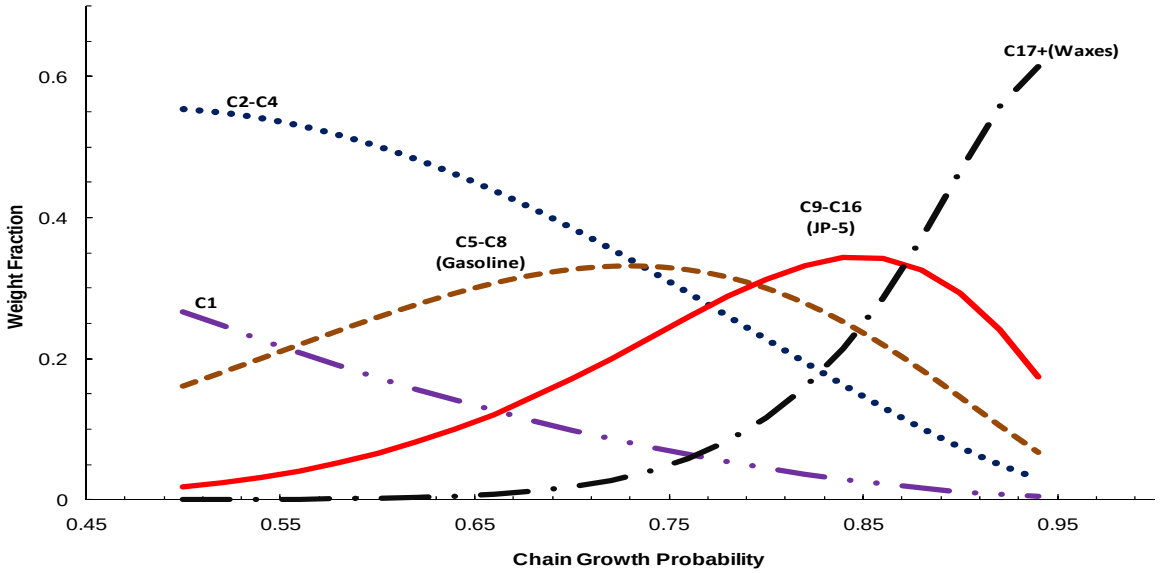

Figure 2 ASF Weight distributions as a function of chain growth probability

The objective of this work is to design an appropriate catalyst structure that will achieve an optimum performance with the aid of a microfibrous material. Microfibrous materials provide a mechanical and electrical entrapment of a particle/fibrous solid such as sorbents or catalysts within a sinter-locked network of a secondary fibrous matrix such as a metal or polymer fiber (MFEC). With MFEC, there are certain advantages over a conventional packed bed reactor or a reactor packed with monolithic catalyst structures such as high heat transfer removal rates due to a high thermal conductive reactor bed.[3]

[3] Kalluri, R. "Microfibrous Supported Sorbents/Catalysts - Micro-Structured Systems with Enhanced Contacting Efficiency." Presented at AIChE Annual Meeting. (2005)

3.2 Catalyst Matrix

Ruthenium is a very active catalyst and studies have reported its ability to have high alpha values in FTS.[4] However, it is relatively expensive as a catalyst when compared to cobalt and iron catalysts, and consequently commercial reactors typically avoid this catalyst.[5] In addition, ruthenium is highly selective toward producing large amounts of methane at low pressures and at low temperatures; a shift towards high amounts of waxes is seen.[6] Co and Ru catalysts promoted with Zr, Ti or Cr are widely used to for the production of waxes which can be cracked to diesel fuels and olefins.[5] Conventional catalysts used to make various premium products are summarized in Table 1.

Table 1. Summary of Premium Products, Catalyst and Technology Used.[7]

Premium product	Catalyst	Reactors
Gasoline	Fused Fe/K	Fluid-bed
	$Co/ThO_2/Al_2O_3$/Silicalite	Fixed-bed
	Fe/K/ZSM-5, Co/ZSM-5	Slurry/Fixed-bed
	Ru/ZSM-5	
	Fe/Cu/K and ZSM-5	
Diesel Fuel	Fe/K, $Ru/V/TiO_2$	Fixed-bed (low *T*)
	Co/Zr, Ti or Cr/Al_2O_3	Slurry bed (low *T*)
	$Co/Zr/TiO_2$	
	$Co\text{-}Ru/Al_2O_3$	
Waxes	Fe/K, Fe/Fe/Cu/K	Slurry-bed (low *T*)
	Co/Zr, Ti or Cr/Al_2O_3	Fixed bed (low *T)*
	$Co/R/Al_2O_3$, Fe/Ru	

The three key properties for FT catalysts that many have optimized are product selectivity, activity and lifetime. Each one of these properties can be affected by a variety of

[4] Dry, M. "Catalytic aspects of industrial Fischer-Tropsch synthesis." *J. Mol. Catal.* 17 (1982): p133-144
[5] Rao, V. "Iron-based catalysts for slurry-phase Fischer-Tropsch process: Technology." *Fuel Process technology* 30 (1992): p83-107
[6] Dry, M. "The Fischer Tropsch Synthesis." *Catalysis: Science and Technology* v1 (1981): p159-225
[7] Bartholomew, C. H. "Recent technological developments in Fischer-Tropsch catalysis." *Catalysis Letters* 7 (1990): p303-314

strategies including the use of promoters, catalyst preparation and formulation, pretreatment and reduction, and shape selectivity.

Early precipitated iron catalysts were promoted with potassium salts and thus, to improve the stability of these catalysts towards thermal sintering, supports like zinc oxide, kieselguhr, and alumina were added. The influence of varying SiO_2 on the total area and pore structure of Fe_2O_3 is apparent in the following figures, figure 3 and 4. It is believed that SiO_2 increases the area and stabilizes the presence of larger pores.[6]

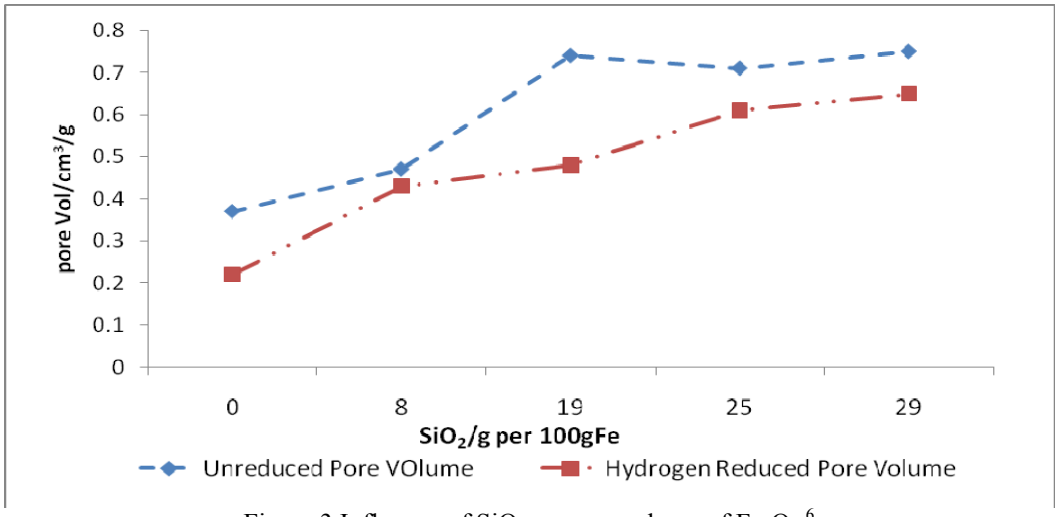

Figure 3 Influence of SiO_2 on pore volume of Fe_2O_3.[6]

.

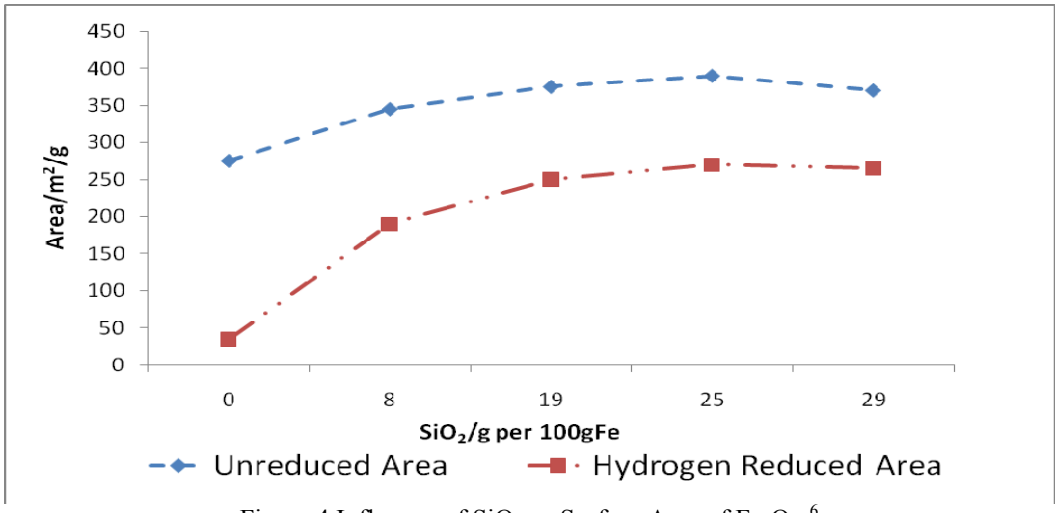

Figure 4 Influence of SiO_2 on Surface Area of Fe_2O_3.[6]

There are a large number of different recipes used for the preparation of heterogeneous catalysts for FT. The inherent compositional and structural inhomogenity of these supported systems make selecting the right catalyst extremely difficult. Preparation, techniques involving impregnations, controlled pH precipitations, and decomposition of metal carbonyl on dehydrated supports all affect the activity of the catalyst, and thus alpha value during FT.[8,9] The activity of a catalyst and the product selectivity are also influenced by the reducing temperature with which the catalyst is reduced. When a catalyst is reduced in H_2 at 220^{o}C for example, it allows for higher molecules such as waxes to be formed as opposed to another catalyst when reduced at 280^{o}C.[9] While preparation techniques are important in the determination of the pore structure of a catalyst and its activity, it is not the focus of this research.

3.2.1 Catalyst for Jet Fuel Production

Fe/Cu/K has been chosen as the desired catalyst for JP-5 production because of its related high activity as a catalyst, its ability to achieve high alpha values, and subsequently high fractions of C_9-C_{16} paraffin and waxes. In addition, a high water-gas shift activity makes a promoted iron also a favorable catalyst for FTS. The effects of potassium promoters on iron catalysts have being well documented by pioneers such as: Anderson et. 1952[10]/1956;[11] Dry and Oosthuizen, 1968,[12] Bonzel and Krebs, 1981,[13] Dry 1981,[4] Arakawa and Bell, 1983,[14]

[8] Bukur, D. "Pretreatment effect studies with a precipitated iron Fischer-Tropsch catalyst." *Applied Catalysis A* 126 (1995): p85-113
[9] O'Brien, R.J and Davis, B.H. "Activation of Precipitated Iron Fischer Tropsch Catalyst." *Energy & Fuels* 10 (1996) : p921-926
[10] Anderson, R. "Fischer-Tropsch Synthesis, Some important variables of the synthesis on iron catalyst." *Ind. Eng. Chem.* 44 (1952): p391-397
[11] Anderson, R. "Catalyst for the Fischer-Tropsch Synthesis." *Van Nostrand Reinhold* 4 (1956) New York
[12] Dry, M. "Heat of Chemisorptions on Promoted Iron Surfaces and the Role of Alkali in Fischer-Tropsch Synthesis." *Journal of Catalysis* 15 (1969): p190-199

Dictor and Bell, 1986,[15] Donnelly and Satterfield, 1989.[16] With respect to promoting iron with potassium and copper, Bukur studied the effects of these specific promoters on iron's alpha values, product selectivity as well as catalyst activity for different catalyst compositions in a fixed bed at temperatures of 235-365^{o}C and 15 bar (Bukur, 1990).[17] Bukur reported that both potassium and copper increased the catalytic alpha distribution and activity for FTS and water gas shift, suppressing the secondary reactions (olefin hydrogenation and isomerization of 1-alkenes to 2-alkenes). The reported alpha values for the two different regimes normally seen in FT[18] are shown in Table 2.

Table 2. Chain Growth Probability factors for different Catalyst[17].

Catalyst	α_1	α_2
100 Fe	0.56 ± 0.11	-
100 Fe/0.2 K	0.61 ± 0.08	0.84 ± 0.04
100 Fe/0.5 K	0.68 ± 0.02	0.94 ± 0.03
100 Fe/1 K	0.66 ± 0.02	0.88 ± 0.02
100 Fe/3 Cu	0.63 ± 0.03	0.91 ± 0.03
100 Fe/3 Cu/0.2 K	0.62 ± 0.09	0.79 ± 0.01
100 Fe/3 Cu/0.5 K	0.69 ± 0.02	0.93 ± 0.06

Three different catalysts were tested and evaluated, Fe/Cu/K/La-Al_2O_3, the second as Fe/Al_2O_3 and Fe/SiO_2/Al_2O_3 were tested under FT conditions at 20 bars and H_2/CO ratio of

[13] Bonzel, H. P. "Enhanced Rate of Carbon Deposition during Fischer-Tropsch Synthesis on K Promoted Fe." Surface Science Letters 109 (1981): pL527-531
[14] Arakawa, H. "Effect of potassium promotion on the activity and selectivity of iron Fischer-Tropsch Catalyst." *Ing. Eng. Chem. Process Des. Dev*. 22 (1983): p97-103
[15] Dictor, R. "Fischer-Tropsch synthesis over reduced and unreduced iron oxide catalysts." *Journal of Catal.* 97 (1986): p121-136
[16] Donnelly, T. J. "Product Distributions of the Fischer-Tropsch Synthesis on Precipitated Iron Catalysts." *Applied Catalysis* 52 (1989): p93-114
[17] Bukur, D. "Promoter Effects on Precipitated Iron Catalyst for Fischer Tropsch Synthesis." *Ind. Eng. Chem. Res.* 29 (1990): p194-204
[18] Huff, G. "Evidence for two chain growth probabilities on Iron Catalysts in Fischer Tropsch Synthesis." *Journal of Catalysis* 85 (1984) p370-379

2. Figure 5 was constructed from the collected data and the calculated values of alpha from the product distribution with respect to operating temperature.[19]

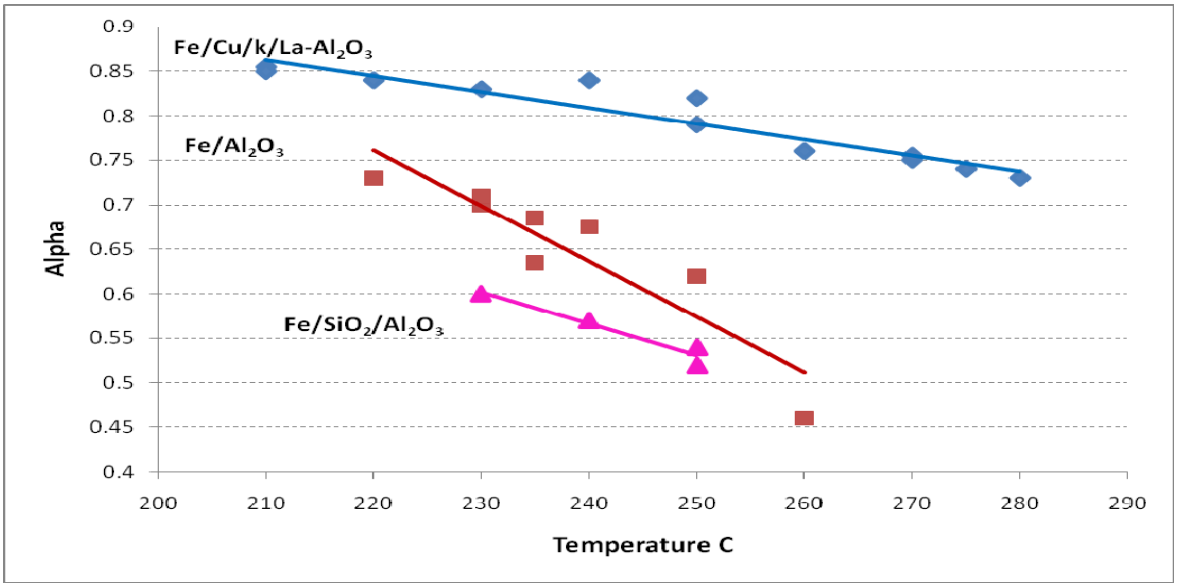

Figure 5 Alpha for Fe/Cu/K, Fe/Al_2O_3 and Fe/ Al_2O_2/SiO_2 (20bars and H_2/CO ~2)

With increasing hydrogen concentration and temperature, an empirical equation was developed for α;[20,21] one that takes into account both the H_2/CO ratio and temperature relationship. This means that the potential product distribution could be obtained with respect to temperature and concentration at any point in the reactor.

$$\alpha = A\frac{y_{CO}}{y_{CO} + y_{H_2}} + B[1 - 0.0039(T - 260)] \qquad (1)$$

Tables 3 show the values of A and B that were obtained from a Non-Linear regression analysis on the data in Figure 5. Figure 6 show the influence of Syngas ratio on alpha.

[19] IntraMicron, Inc/Cerametec Topic N07-T027, Proposal Number N2-2578 (2009)
[20] Yermakova, A. "Thermodynamica Calculations in the Modeling of Multiphase Processes and Reactors." *Ind. Eng. Chem. Res.* 39 (2000): p1453-1472
[21] Lox, E. "Kinetics of the Fischer Tropsch Reaction on a Precipitated Promoted Iron Catalyst, 2. Kinetic Modeling." *Ing. Eng. Chem. Res.* 32 (1991): p71-82

Table 3 Estimated constants A and B

Catalyst	A	B
Fe/Cu/K/La-Al_2O_3	0.984 ± 0.34	0.46 ± 0.11
Fe/Al_2O_3	-3.41 ± 2.46	1.59 ± 0.72
Fe/SiO_2/Al_2O_3	-1.29 ± 2.32	0.91 ± 0.69

See Appendix V for non linear analysis.

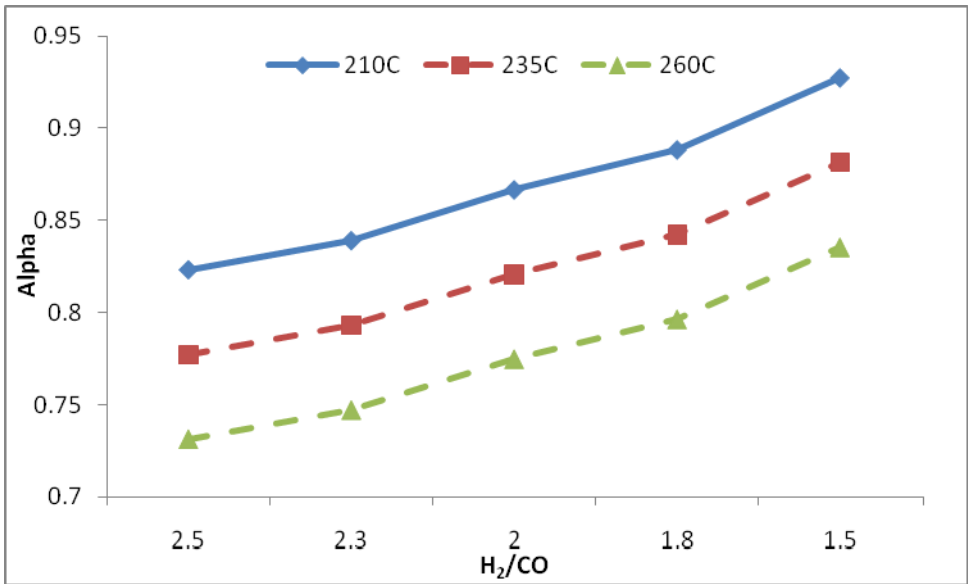

Figure 6 Alpha as a function of H_2/CO on Fe/Cu/K/La- Al_2O_3 Catalyst.

A low-temperature Fischer-Tropsch (LTFT) reaction would be appropriate for achieving this high alpha and JP5 selectivity. There is also the advantage of operating within this region to avoid the formation of fouling "coke". LTFT would extend the life of a catalyst as opposed to operating within a high-temperature Fischer Tropsch (HTFT) regime and dealing with the issues of associated phase changes of the Iron catalyst.[7] In addition, at high temperatures, the Boudouard reaction becomes more prominent[22], resulting in a continuous increase in elemental carbon content at the surface of the catalyst. Carbon deposition becomes apparent on the catalyst, directly affecting the decline of the catalyst and fouling the tubes.

[22] Dry, M. "The Fischer-Tropsch (FT) synthesis processes." *Handbook of heterogeneous catalysis.* 6 (2008)**:** p2965-2994

Kolbel et al.[23] concluded that potassium when used as a promoter stabilizes the surface area of precipitated iron oxy-hydrides and protects against re-crystallization during calcinations. In addition, there were more active sites found than in an un-promoted catalyst. However, using higher concentrations of potassium as a promoter will cover active sites, resulting in a decrease in catalyst activity. While there are no proven theories, an increase in the overall activity of a catalyst in the presence of copper has been observed. Dry reports that copper facilitates the reduction of iron thus decreasing the total surface area of the catalyst.[7]

The effects of the promoters, supports, additives, pretreatments and preparation are only meaningful in the comparison of baseline catalytic properties in the absence of these effects. In order to calculate the activity (or turnover frequency), a proposed reaction mechanism is needed. A few related mechanisms have been reported as well as the associated rate formula derived for such mechanisms. Eliason reported rate data and proposed a power law expression based on such data for unsupported Fe and Fe/K catalysts which was then used to calculate a bulk activity (Eliason and Bartholomew, 1999[24]). Atwood (Atwood and Bennett, 1979[25]) reported intrinsic kinetics over a commercial promoted fused iron catalyst, $Fe/Al_2O_3/K_2O_3/SiO_2$. Liu (Liu and Li, 1995[26]), and Leib (Leib and Kuo, 1984[27]) reported Langmuir-Hinshelwood (LHHW) expression for our proposed catalyst, Fe/Cu/K, which was derived through the Carbide theory.

[23] Knobel, H. "Beitrag zur Fischer-tropsch Synthese on Eisenkontakten." *Chem. Ing. Tech.* 23 (1951): p153
[24] Eliason, S. A. "Reaction and deactivation kinetics for Fischer-Tropsch synthesis on unpromoted and potassium-promoted iron catalysts." *App. Catalysis A* 186 (1999): p229-243
[25] Atwood, H. "Kinetics of the Fischer-Tropsch reaction over iron." *Ind. Eng. Chem. Process Des. Dev.* 18 (1979): p163-170
[26] Liu, Z. "Intrinsic kinetics of Fischer-Tropsch Synthesis over Fe-Cu-K Catalyst." *J. Chem. Soc. Faraday Trans.* 91 (1995): p3255-3261
[27] Leib, T. "Modeling the Fischer-Tropsch Synthesis in Slurry Bubble-Column Reactors." Paper presented at the AIChE Annual Meet., San Francisco, California (Nov. 25-30, 1984)

Table 4.
Summary of FT Kinetics and Parameter Values from Literature.

Source	Catalyst	Rate	T(C)	*Ko*	*a*
Atwood and Bennett (1979)	CCI fused Iron	$r_{FT} = \frac{k_o P_{CO} P_{H_2}}{P_{CO} + a P_{H_2O}}$	250	0.0017 (mols/gcat-s-Mpa)	0.028
				E (kJ/mol) 85	-8.8
Leib and Kuo (1984)	Fe/Cu/K	$r_{FT} = \frac{k_o P_{CO} P_{H_2}}{P_{CO} + a P_{H_2O}}$	265	0.062 (mols/gcat-s-Mpa)	0.58
				E (kJ/mol) 85	-8.8
Liu and Li (1995)	Fe/Cu/K	$r_{FT} = \frac{k_o P_{CO} P_{H_2}}{P_{CO} + a P_{H_2O}}$	210	7.83E-6 (mols/cm3-s-Mpa)	1.9E-5
				E (kJ/mol) 66.5	E (kJ/mol) 65.4
Eliason and Bartholomew (1999)	Unpromoted Fe	$r_{FT} = k_o P_{CO}^{-0.46} P_{H_2}^{0.68}$	265	3.77E+6 (mols/kg-Cat-s-atm ^0.98)	
				E (kJ/mol) 101	
	Fe/K	$r_{FT} = k_o P_{CO}^{-0.08} P_{H_2}^{0.6}$	265	3.77E+6 (mols/kg-Cat-s-atm ^0.55)	
				E (kJ/mol) 92	

Turnover frequency, is the number of revolutions of the catalytic cycle per unit time, generally second.[28] As a measure of the activity of a catalyst, turnover frequency is the number of molecules of CO converted per catalytic site per second. This has been calculated for different catalyst structures for FTS operating temperature 210^{o}C (LHFT), 260^{o}C (HTFT) and pressure of 20 bars. The turnover frequencies were calculated based on the assumption of 10% dispersion and a constant loading. Figures 7 and 8 show this comparison between the estimated turnover frequencies of promoted iron catalyst.

[28] Boudart, M. "Kinetics of Heterogeneous Catalytic Reactions" Princeton University Press: Princeton, NJ, 1984

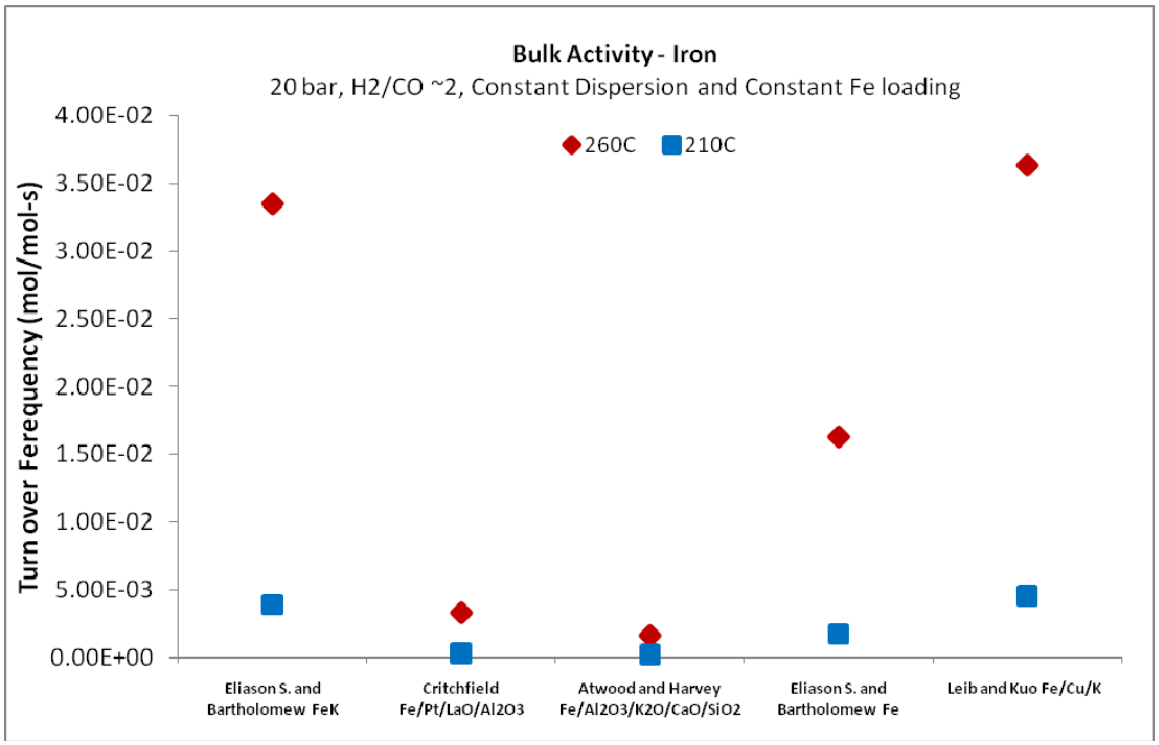

Figure 7 CO hydrogenation activities

As seen in Figure 8, Fe/Cu/K gives a high turnover frequency. At high temperatures a higher extent of activity is seen because these rates occur faster.

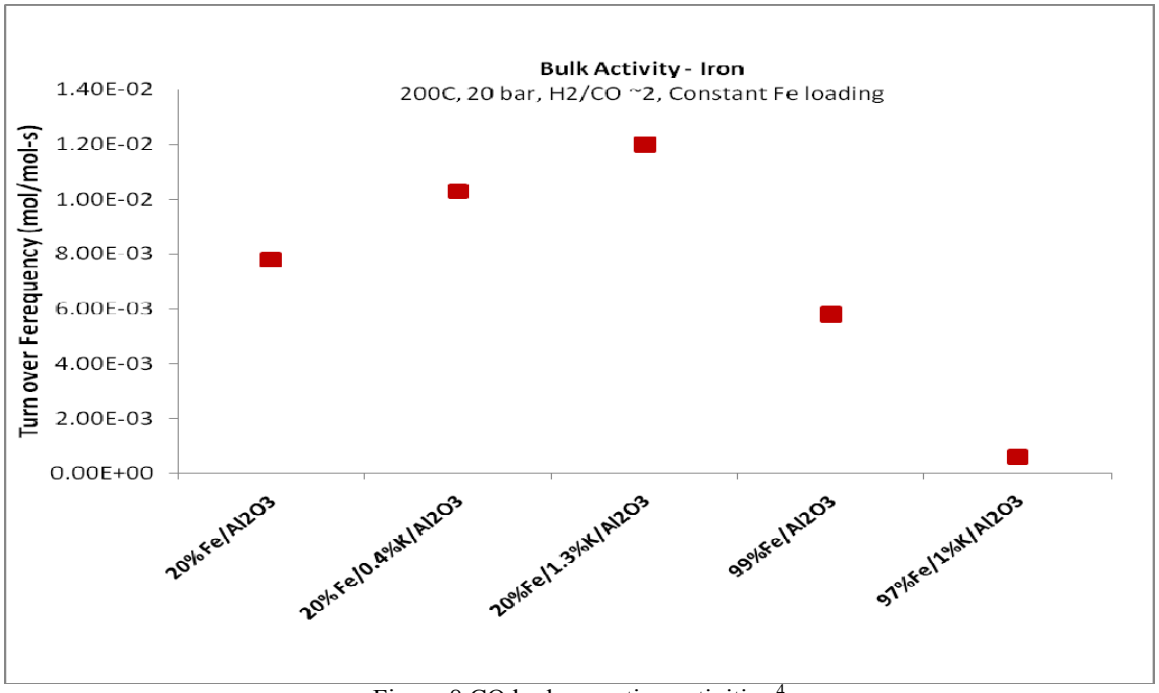

Figure 8 CO hydrogenation activities.[4]

In a study conducted by Jam,[29] $Fe/Cu/La/SiO_2$ was compared with Co/Al_2O_3. Cobalt was revealed to have a smaller particle diameter size. The table below shows average particle size and BET surface area of the catalyst.

Table 5. Characterization data of Catalyst[29].

Catalyst	Bet Specific Area (m^2/g)	Particle Diameter (XRD)
Co	154	14.4(nm)
Fe	47	60(um)

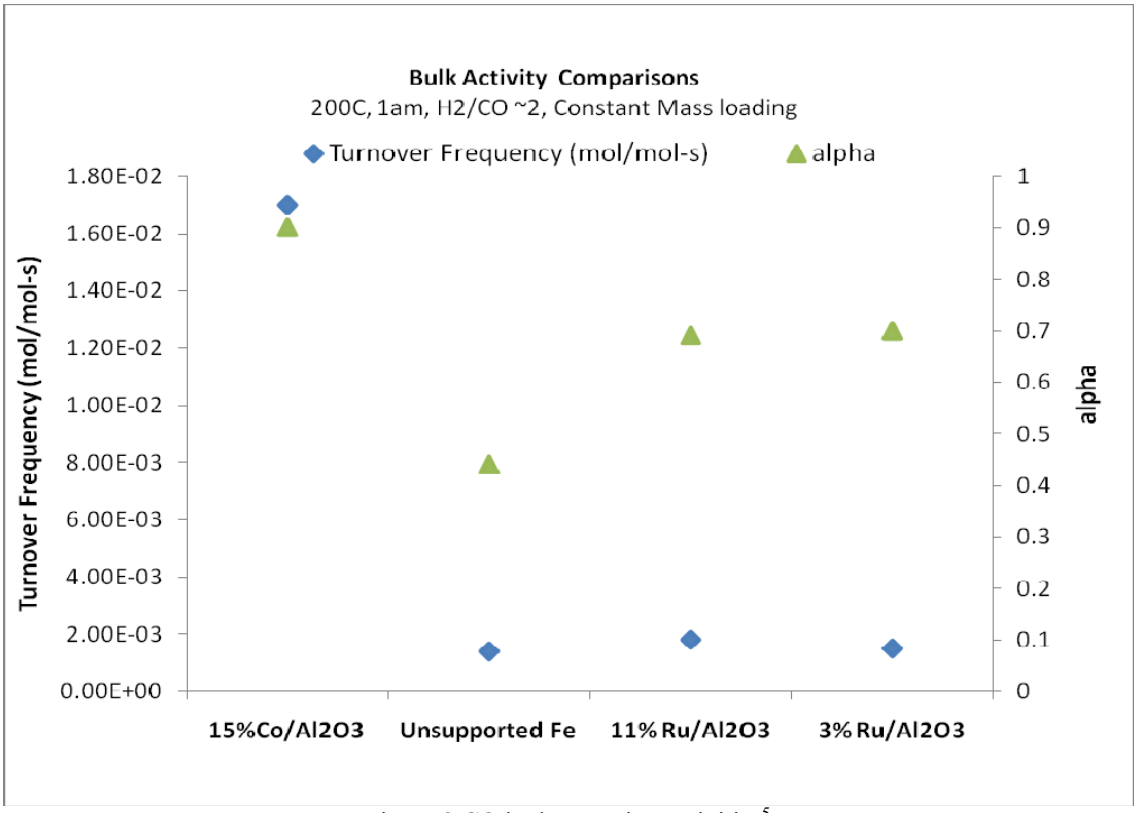

Figure 9 CO hydrogenation activities[5]

It can be inferred from figure 9 and table 5 above that at a cobalt catalyst would be a better choice for FTS to make JP-5 given its high activity and surface area, making it easier to achieve higher per pass conversions over an iron catalyst. However, more research needs to be conducted on the use of cobalt as a catalyst because it is difficult to obtain consistent

[29] Jam, S. "Enhancement of Distillate Selectivity in Fischer Tropsch Synthesis by Using Iron and Cobalt Catalyst in a Novel-Dual Bed Reactor." *Reaction Kinetics and Catalysis Letters* 89(2006): p71-79

literature data for the rate conversion of CO. Many reports highlight certain short comings for cobalt catalysts, for example, its rapid decline in activity due to the buildup of long chain waxes in the pores.[30,31] It has also been found that for a Co/Al_2O_3 catalyst, the presence of water in the syngas results in surface oxidation of the cobalt, causing permanent loss in activity.[32,33] In addition, Kogelbauer and coworkers report that with Co/silica, an increase in amount of silicates is formed with time under FT conditions, causing cobalt to lose its activity.[34] In spite of these reports, however, defining a catalyst activity is subjective. Under proper conditions and depending on operating regimes, both catalysts have the potential to operate six months or longer.[35] The following table summarizes a desired catalytic function for FT reactions.

Table 6. Optimization of Fe Catalyst Design.

Desired Catalytic Functions	Proven Catalyst Components/ Structural Features	Key Aspects of Preparation and Pretreatment
High Structure Integrity with MFEC	Dense alumina, silica and titania carriers stabilized with Ba, La, or Zr oxides.	Modify Al_2O_3 surface with promoter like La
Extent of Reduction	addition of Cu, Pt, Pd, or Ru;	Dope Fe precursors with promoted metal, K, Pt, Pd
High resistance to fouling by carbon and heavy waxes	Relatively large mesopores (d_{pore} = 12-16 nm); additives such as Cu, Ru and Pt which gasify carbon	Choose γ–Al_2O_3 with d_{pore} = 12-16 nm; uniform dispersion of additives like Cu

[30] Van Berge, P.J. "Cobalt as an alternative Fischer-Tropsch catalyst to iron for the production of middle distillates." *Studies in Surface Science and Catalysis* 107 (1997): p207-212

[31] Niemela, M.K "The long-term performance of Co/SiO2 catalysts in CO hydrogenation." *Catal. Letters* (1996) v42, p161-166

[32] Schanke, D. **"**Study of the deactivation mechanism of Al2O3-supported cobalt Fischer-Tropsch catalysts" *Catalysis Letters* 34 (1995):, p269-284

[33] Hilmen, A. "Study of the effect of water on alumina supported cobalt Fischer-Tropsch catalysts. *Applied Catalysis. A* 186 (1999), v186, p169 -188

[34] Kogelbauer, A. "The formation of cobalt silicates on Co/SiO2 under hydrothermal conditions." *Catalysis. Letters.* (1995) v34 p259-267

[35] Davis, B.H. "Fischer-Tropsch Synthesis: Comparison of Performances of Iron and Cobalt Catalysts." *Ind. Eng. Chem. Res.* 47 (2007): p8938-8945

High activity High C_{9-16} selectivity	High surface area High Fe loading and site density; large mesopores (d_{pore} = 12-16 nm); High dispersion (10-15%); add Cu, or Ru to enhance Fe reduction; add K to increase C_{9+} selectivity	Inert support; uniform catalyst distribution; drying, calcination and reduction at low heating rate and high SV; uniform dispersion of additives

3.2.2 Phase Changes during Synthesis

There can be many changes within the phase composition when using an iron catalyst. This is due to the ease with which iron can be oxidized as well as the formation of iron carbides. The metallic iron phase is not stable under normal FT conditions. Below is a plot of the phase diagram of iron magnetite with time during an FT operation.

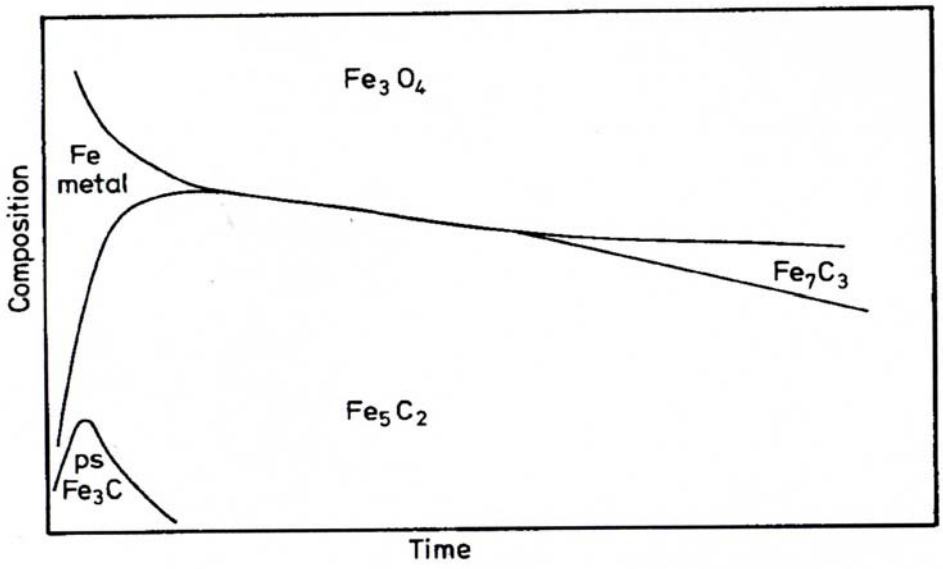

Figure 10 The change in composition of iron catalyst during FT reaction 300C.[6]

Figure 10 represents an illustration of a possible phase change with time at 300^{o}C for an iron catalyst in FT. The phases are those which are present according to X-ray diffraction analysis. At time equals zero, the catalyst is 100% metallic iron. The units are undefined since the rates of the phase changes depend on the amount of alkali present. A phase diagram is shown in Appendix III for iron magnetite with respect to temperature and pressure.

3.2.3 Influence of Promoters on Physical Properties and Synthesis

Fe catalysts are significantly affected by the chemical nature of promoters and/or supports. The promotion with an optimal amount of alkali materials, such as potassium salts, affects the FT activity as well as the required selectivity.[6]

The first concern is the influence of promoters on the physical properties of iron. Using pure iron oxide as the host, the influence of various cations has been studied extensively. Al^{3+}, Li^{+} and Mg^{2+} have a decreasing effect in the Fe_3O_4 unit cell as the promoters are increased. For larger cations like Ca^{2+}, Mn^{2+}, Ti^{3+} and Na^{+}, the unit cell size increases as these promoters are increased.[36] K^{+} ions do not have any effect on the unit cell because they are too large to replace the Fe ions in Fe_3O_4. Arakawa et. al[13] in his studies showed that potassium promotion on an alumina supported iron catalyst causes a decrease in the Fe dispersion, however, it increased the strength of CO chemisorptions on reduced Fe. The presence of the promoters inhibits crystal growth of the α-Fe and thus results in a high surface area of the reduced catalyst.[37] This promotional effect has been described by Dry and it is due the ratio of the ionic charge to ionic radius of the cations. Therefore, the more "acidic" the cation, the larger the surface area of your catalyst. In a nutshell, Al_2O_3 and TiO_2 strongly increase the area while CaO and MnO have little effect.

[36] Dry, M. "The distribution of promoters in magnetite catalysts." *Journal of Catalysis* 7 (1967): p352-358
[37] Dry, M. "The influence of structural promoters on the surface properties of reduced magnetite catalysts." *Journal of Catalysis* 6 (1966): p194-199

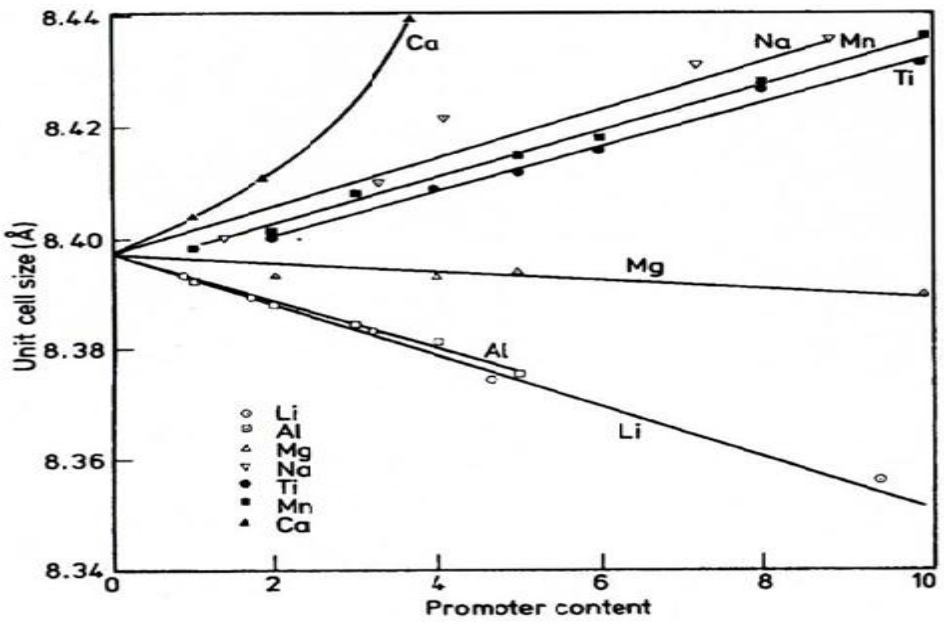

Figure 11 Influence on the unit cell size of magnetite (in Am) of various promoters in solid solution with magnetite.[6]

See Figure 11 and 12 for the influence of the unit cell size of magnetite and typical results of the influence of promoters on area. If the catalyst were operated at high temperatures, the associated reaction rates appear to be diffusion controlled and thus an increase in internal surface area will show some benefit.

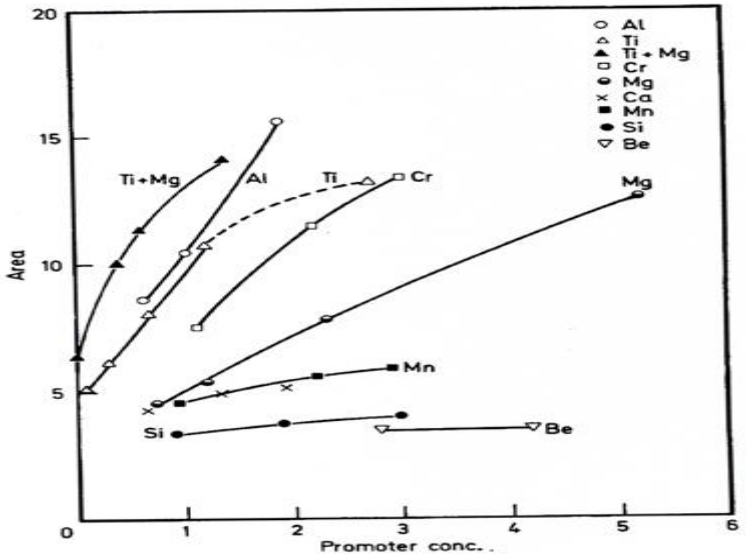

Figure 12 The surface area of fully reduced catalyst in m2 (g unreduced sample)-1 as function of promoter content (g atom promoter cation per 100 g atom Fe). [6]

It is important to promote the iron catalyst with strong alkali metals of Group 1, (i.e. K_2O). This is because precipitated catalysts are unstable and thus need to have their available active surface area increased and stabilized to a level required for high conversions during FTS. The higher the level of alkali, the greater the relative activity as shown in Table 7.

Table 7. Influence of alkali content on synthesis performance of precipitated iron catalyst[6].

Unsupported Fe_2O_3		Silica Supported Fe_2O_3	
K_2O level[a]	Activity[a]	K_2O level[a]	Activity[a]
0	26	12	112
1	47	16	109
1.6	50	21	85
2	53	24	83
3	40	32	75

[a] relative quantities

3.2.4 Catalyst Size and Shape

The effect of the catalyst size can be seen in Figure 14. CO conversion increases when particle sized is reduced from 0.3mm to 0.154mm, highlighting the point that intra-particle diffusion is eliminated when particle size is reduced. This is a simulation study that was obtained using Aspen™. It can be verified experimentally.

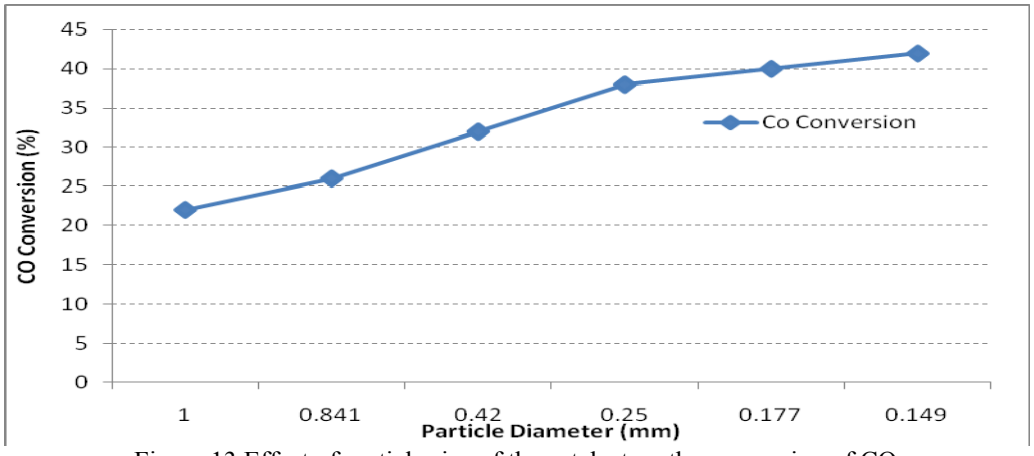

Figure 13 Effect of particle size of the catalyst on the conversion of CO
(Conditions: T = 210C, 20bars, H/CO = 2, L = 100mm GHSV = 600hr^{-1})

The effictiveness facor can be calculated; certain assumption such as a pseudo first-order reaction rate, $k=0.06s^{-1}$ and diffusivity of H_2.[38] Utilization of smaller catalyst particles improves selectivity toward larger molecular weight hydrocarbons promoting intra-particle mass transport. This will allow reeducation of the catalyst loading while maintaining the same or higher volumetric reactivity. Higher effectiveness factors and smaller particles provide greater surface to volume ratios and better activity maintenance. These are represented in Figure 13 and 14.

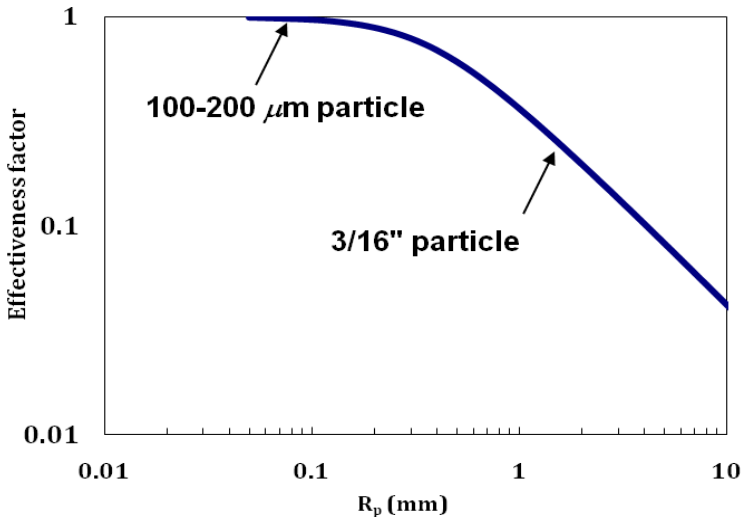

Figure 14 Catalyst Effectiveness Factor

Table 8. Some common catalyst shape.[39]

Shape	*Comments*
Spheres	Low manufacturing cost. Some granulated material can be weak, and cementing agents are frequently used to increase strength. Packed beds of spheres produce relative high pressure drop
Irregular Granules	Not a common catalyst shape. Consequence of restricted methods of manufacture. Used for low surface area catalyst such as bulk metal

[38] Post, M.F.M. "Diffusion Limitation in Fischer-Tropsch Catalyst." *AIChE Journal* 35 (1989): p1107-1114
[39] Twigg, M. V "The Catalyst: Preparation, Properties and Behavior in Use." *Catalysis and Chemical Process* (1981) R. Pearce and W.R Patterson p11

Pellets	Highly regular shape, good strength. Although expensive to produce, the most common catalyst shape.
Extrudate	Low bulk density and low pressure drop. Often poor strength.
	Some formulations can be extruded which are difficult to pellet.
	Extrusion aids (additives) and cementing agents are
	frequently used. Production cost is much less than pelleting
Rings	Impregnation of preformed rings can produce very high strength catalyst.
	Low pressure drop, and so used in tubular reactors. Manufactured by pressing or extrusion Pressed rings have superior physical properties but costly to produce.

3.3 Thermal Conductivity

Thermal conductivity is key to the idea of using a metal micro-fibrous entrapped catalyst to improve the rate of heat transfer. The adiabatic temperature rise in FTS is about 1750^{o}C, and conventional reactors for fixed beds have use recycle gas/diluents such as nitrogen with high space velocity, monolithic catalyst structures[40] or a slurry reactor to solve this problem. Since weight and volume is a constraint for this operation, it is important to limit the size of this reactor, therefore the use of a bubble column is not an option. It is imperative that heat removal is performed efficiently to avoid a loss in product selectivity.

To determine the thermal conductivity of the packed bed for comparison with an MFEC bed, a steady-state temperature profile inside a heated tube with flow through a homogeneous material was measured on a packed bed of alumina powder and a micro-fibrous copper sample. A segregated 2-D heat balance for the gas, catalyst and fiber phases were written to model the tube heat up. PDEs describing the heat transfer inside the bed were discretized using central finite differences with radial averaging. These equations

[40] Mesheryakov, V.D. "A multifunctional reactor with a regular catalyst packing for Fischer-Tropsch synthesis." *Chemical Engineering Science* 54(1999): p1565-1570

describing the transient heat transfer were integrated into steady-state using a line implicit Euler method in the axial direction. The simulation was programmed using the Euphoria interpreter. The derivation of the segregated 2-D model is given in the Appendix II.

Two materials were tested for this comparison. One with a bed of 80x100 mesh alumina powder. The other with a sintered mesh consisting of equal amounts of 4 and 12 micron copper fibers and the same alumina powder. A two inch section of a 1 ½" O.D. stainless steel tube was filled with the media to be evaluated. The tube was sealed with five thermocouples inside during the first set of tests.

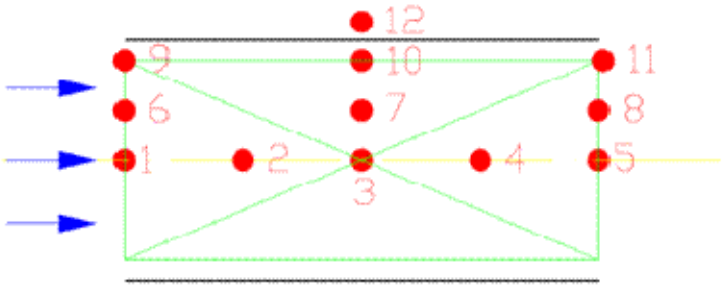

Figure 15 Diagram of thermocouple locations in the packed tube heat-up test.

In a second set of heat-up tests, eleven thermocouples were used. A diagram of the location of the thermocouples in the packed bed heat-up test is shown in Figure 15 above. More results of this work, including temperature profiles and calculations can be seen in a work which is currently being developed.[41] The temperature profile obtained and a fitted profile is shown in Figure 16 and 17.

[41]Sheng M. "Effective Thermal Conductivity of Metal Microfiber Entrapped Catalyst." (2010) *Auburn University* Unpublished

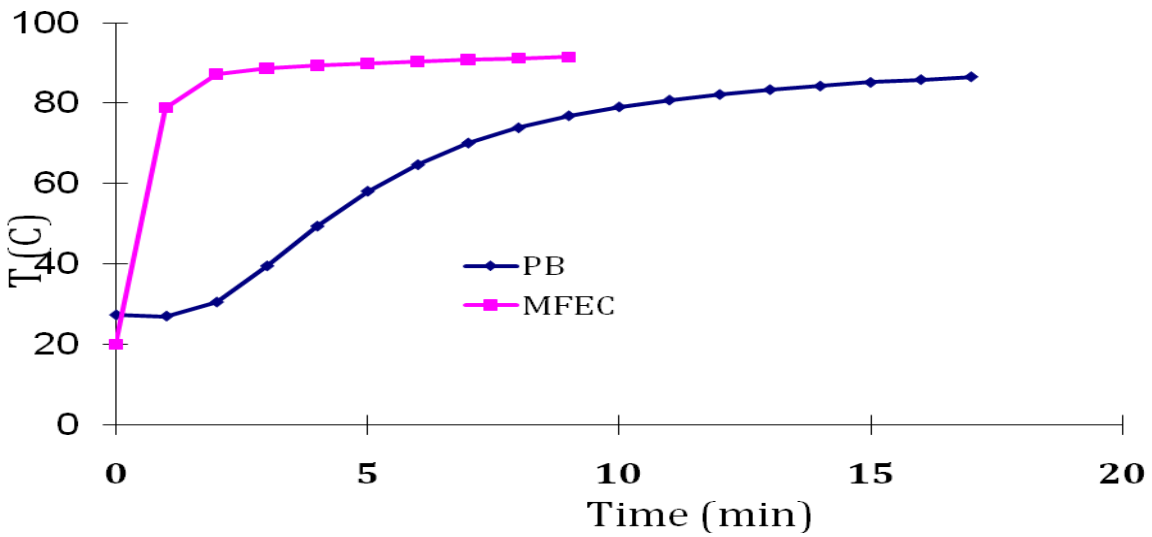

Figure 16. Temperature Bed comparisons between Packed Bed and MFEC (Copper fibers and alumina powder-80x100).

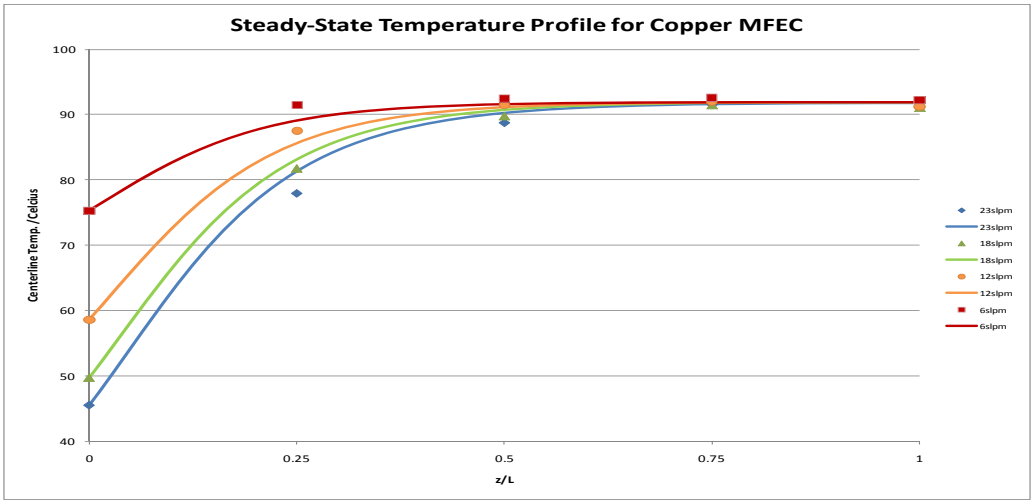

Figure 17. Segregated 2-D simulation result for heat-up of a tube packed with MFEC (Copper fibers and alumina powder-80x100).

Table 9. Thermal Conductivity and Wall heat transfer coefficients

	Packed bed	MFEC
k(W/mK)	0.16 ± 0.35	9.05 ± 0.21
h(W/m^{2}K)	22.7 ± 10.2	235±30.5

Adding mass balances and heat generation in the catalyst phase to a segregated 2-D model would be a simulation of the FTS reaction with uniform velocity at any cross section. This would be a further development on the work already done and will allow the

determination of an effective thermal conductivity measurement during FT conditions. There are radial and axial temperature profiles that need to be considered also. These profiles could produce a limitation in the performance of iron kinetics because of the fixed bed characteristics. All possible scenarios should be explored.

Conclusion

The ideal Fe catalyst will be supported on a relatively inert support. It's ability to be well reduced with the addition of a noble metal makes such a catalyst very good choice for FTS. Such a catalyst will contain Cu/K as a promoter that enhances Fe reduction and limits carbon formation. Hypothetical compositions include $Fe/Cu/K/Al_2O_3$ or $Fe/Pt/K/La_2O_3/Al_2O_3$. With the use of a micro-fibrous entrapped catalyst, intra-bed heat transfer can be enhanced which will able to maintain the temperature profile within the reactor. This in turn will improve the product selectivity for JP-5 within the FT reactor.

"It isn't that they can't see the solution.
It is that they can't see the problem."
G.K. Chesterson

Chapter 4

FTS Process Design for Jet Fuel

Abstract

The feasibility of using Micro-Fibrous Entrapped Catalysts (MFEC) in Fischer-Tropsch Synthesis (FTS) for selective JP-5 production as well as overall balance of plant reductions (BOP) will be addressed in this chapter. Three different simulation case studies based on a minimized weight by volume analysis of a Gas-To-Liquid (GTL) process under optimum reaction conditions of, 210^{o}C and 20 bars, were carried out using an iron promoted catalyst, (Fe/Cu/K) entrapped in 8 vol.% copper microfibers for the benefit of a mobile skid unit. The use of MFEC significantly enhanced the selectivity to JP-5 (33wt%), reduced the balance of plant (BOP), 20 to 30% and improved the utilization of natural gas (14%) while maintaining the same production capacity when compared to a conventional GTL plant with a packed bed reactor. By greatly reducing the size of process equipment, this in turn will reduce the cost; these are achievements that are attractive for a GTL offshore plant design.

4.1 Introduction

GTL is a promising method of converting syngas to fuel products. The conversions of natural gas to synthetic fuel has attracted significant attention due to current economic uncertainties surrounding crude oil prices, low margins on crude refining and, more importantly the need to become less dependent on foreign crude oil supplies.[1] Currently, the major source of energy in the United States is petroleum, as seen in Figure 1; with 37% of this source being crude oil and, 20% of crude oil imported from Canada.[2]

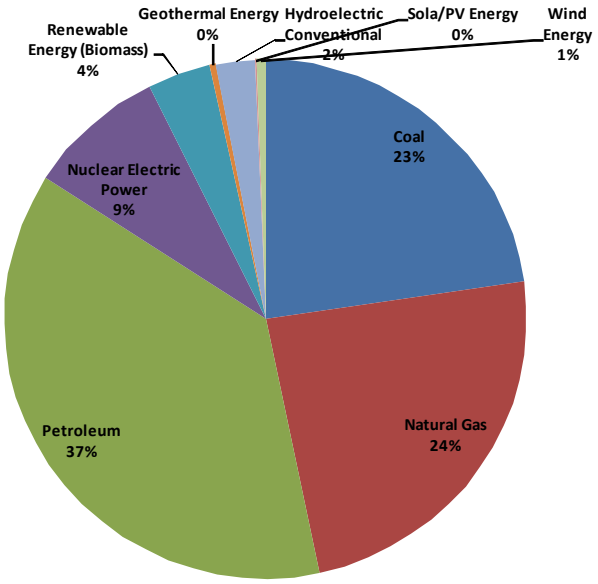

Figure 1 U.S Energy Consumption.[2]

Natural gas without access to the world market is known as "stranded gas." This includes large reserves in remote places and associated gas that is co-produced with crude-oil. There are an estimated 900 to 3,000 trillion cubic feet in volume of available natural gas; which includes stranded gas.[3] Natural gas is either co-produced with petroleum or rests on

[1] Speight, J. "Liquid Fuels from Natural Gas." *Handbook of Alternative Fuel Technologies.* (2007): p153-170
[2] U.S Energy Information Administration – Independent Statistics and Analysis.
< http://tonto.eia.doe.gov/energy_in_brief/foreign_oil_dependence.cfm> May 2010.
[3] Petroconsultants-MIA and Zeus International "Remote Gas Development Strategies." HIS Energy Services (1999)

top of petroleum reservoirs. With no local market for this gas, oil production is not possible without venting, flaring, or reinjection of the gas back into the reservoir. Venting is not an option as the global warming potential of methane is about 21 times that of CO_2. Gas flaring is also not desirable because of stringent environmental policies in effect in a large number of countries. The current cost of reinjection is about $13 per equivalent barrel, with offshore gas reinjection being more expensive, thus making this option economically infeasible.[3]

GTL synthetic fuels play a significant role in the environment as their use results in low emissions of CO, and NO_x.[4] Although coal is another major source of energy and its role in Fischer-Tropsch Synthesis (FTS) is resurging in the United States,[5] it has a number of disadvantages to overcome such as considerable amounts of CO_2, SO_x, NO_x and pollution-causing particulate matter (PM) being formed. Coal-to-Liquid (CTL) technology will be a vital source of energy supply when an acceptable and efficient way of CO_2 sequestration is found.

Synthetic fuels produced from FTS range from light gases, which fall into the category of LPG to middle distillates, which comprise of mainly C_7-C_{22} hydrocarbon chains such as jet fuel, kerosene, and diesel, to the heavies, C_{20+}, known as "wax." Figure 2 shows a descriptive comparison of products obtained from an FTS process and those produced via conventional crude oil refineries.

[4] Li, X. "Particle size distribution from a GTL engine." *Sci. Total Environment.*382 (2007): p295-303
[5] Eilers, J. "The Shell Middle Distillate Synthesis Process (SMDS)." *Catalysis Letters* 7 (1990): p253-269

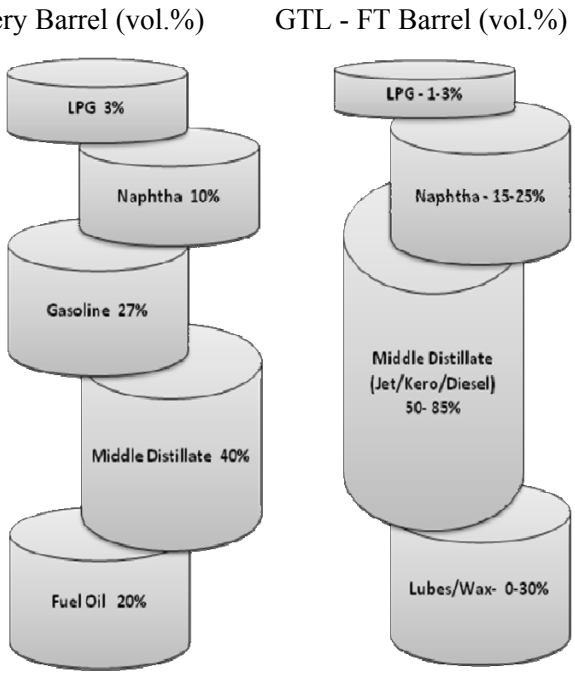

Figure 2 Comparison of FT Products with conventional Refinery barrel.[6]

The United States Department of Defense (DoD) specifically the Navy, has several reasons for an interest in JP-5 fuel produced from alternative energy resources and processes, such as FTS.[7] Most of these reasons are similar to those discussed earlier with others worth mentioning; supply chain vulnerability and fuel supply continuity. In the case of a natural disaster, there is a concern related to acquiring fuel because of the heavily reliance upon crude oil imports, and the majority of crude-oil refineries are located on the East, Gulf and West coast, which are vulnerable to attack.

Another attractive reason is that FTS technology has the ability to manufacture fuel near or within remote locations not easily accessible for pipelines to be built. This would seem vital as there is a high cost associated with transporting fuel to battlefield endured by the Military. GTL plants can be mounted on barges or ships in order to be moved from one site to another as needed. This enables monetization of many smaller fields where reserves

[6] Ronald, M. "New developments in Gas to Liquid Technology." CERI 2004 Petrochemical Conference, Alberta, Canada. (2004).
[7] Forest, C. "Fischer-Tropsch Fuels: Why are they of interest to the United States Military?" *SAE Tech. Pap. Ser.* (2005)

are smaller or rapid depletion is indicated, as constructing a gas pipeline would present a large financial risk. Many drivers for use of any technology offshore are safety, size, reliability and cost. When one considers each of these factors, a floating or air based GTL technology is suitable for offshore use.

The DoD currently uses a single kerosene-type fuel for all its gas-turbine and diesel applications which comply with Jet-Propulsion 8 (JP-8), specifications. JP-8 is similar to commercial aviation turbine fuel but with required additives such as corrosion inhibitors, icing inhibitors and static dissipator additives.[8] JP-8 is a kerosene type fuel whereas diesel fuels are generally a distillate blend, a distillate and kerosene blend, or a kerosene blend depending on the grade of diesel which differ from state to state. There are additives in JP-8 such as lubrication improvers, biocides, antioxidants, and thermal stability improvers are also used in specified amounts as governed by military specifications.[9] JP-5 is used on aircraft carriers which is similar to JP-8 but with a higher flash point of 60^{o}C. A higher flash point provides an additional degree of safety for handling fuels.[10] JP-5 is a complex mixture of hydrocarbons and naphthalene's consisting of C_9-C_{16} linear alkanes.

Synthetic jet fuels produced from alternative energy sources have to comply with the MIL-DTL-5624T specification. This specifies the fuel's physical and chemical properties such as freezing point, flash point, density, heating value, hydrogen content and smoke point.[11] A comparison between the specifications of diesel fuel and FTS JP-5, as JP-5 is the focus of this work, is seen in Table 1.

---

[8] Muzzell, P. "Composition of Syntroleum S-5 and Conformance to JP5 Specification." *Prepr. Pap.-Am. Chem Soc., Div., Pet. Chem.* 49 (2004): p411-413

[9] DOD JP-5 and JP-8(1992). <http://www.atsdr.cdc.gov/toxprofiles/tp121-c3.pdf > May 2010

[10] Lamrecht, D. "Fischer Tropsch Fuel for Use by the U.S. Military as Battlefield-use Fuel of the Future." *Energy & Fuels* 21 (2007): p1448-1453

[11] MIL-DTL-5624U Detail Specification, Turbine Fuel, Aviation, Grades JP-4 and JP-5 < http://www.desc.dla.mil/DCM/Files/5624t.pdf> May 2010

Table 1. Selected Fuel Properties for Jet Fuel and Diesel

	Units	MIL-DTL-5624T (JP-5)[11]	Diesel (ASTM D975)[12]	S-5 (JP-5 from FTS)[13]
Density at 15°C	kg/L	0.788 - 0.845	0.810 - 0.95	0.767
IBP 10%	°C	206	~130	182
FBP	°C	300	360	195
Flash Point	°C	60	52	62
Viscosity	cSt	8.5@-20°C	4.1 @38°C	7.0 @-20°C
Freezing Point	°C	-46	<0	<50
Heating Value	MJ/kg	42.6	43-49	44.1
Cetane No.		-	40	62
Smoke Point	mm	19	-	>43
Aromaticity	% vol., max	25	35	-

Before GTL conversion can become an investment of the future, certain technological challenges must be addressed, specifically for a mobile skid unit. The theoretical maximum thermal efficiency for the conversion of coal to paraffin is 60%, while that of natural gas is approximately 75%. The efficiency attainable in practice is lower, which is why proper heat integration must be performed so that heat generated onsite is reused in the process while minimizing external cooling and heating requirements. Furthermore, capital investment for installation is a limiting factor; with reports of Sasol's capital cost for a 34,000 bpd costing $25,000 bpd.[14] The hydrocarbon condensates and wax produced by an FTS process are usually seen as value added fuels, however, it will require additional energy and capital investment to hydrogenate the olefins and oxygenates formed as well as the use of a hydro-cracking unit in order to break down higher chain molecules into shorter chains. Other challenges facing GTL facilities involve syngas production: justifying the economy of scale when choosing among steam methane reforming (SMR), partial-oxidation (POX) and auto-

[12] Diesel Fuel Spec. Sheet ASTM D975
< http://xtremefueltreatmentdenver.com/ASTM_D975_TEST.pdf> May 2010

[13] Freerks, R. "Production and Characterization of Synthetic Jet fuel Produced From Fischer Tropsch Hydrocarbons." *Prepr. Pap.-Am. Chem. Soc., Div. Pet. Chem.* 49 (2004): p407

[14] Thacheray, F. "GTL in 2007." *Petroleum Reviews* (2003) p18-19

thermal reforming (ATR). The DoD also must be concerned with introducing FTS fuels into its military fleet which currently runs on crude-oil derived fuels which contain aromatics.

There is a fundamental need for applied innovative research into catalytic materials as well as structural architectures that enable FTS to be transformed into a modular, flexible and inexpensive technology. Due to the exothermic nature of FTS, fully packaged catalyst structures are required which possess high inherent heat transfer rates offering the opportunity for a better control on intra-bed hot spots and product selectivity. A high selectivity towards JP-5 would reduce the BOP requirements for post processing operations. High inherent heat transfer rates also permit fundamental changes and simplifications in the form factor and geometry of the FTS reactor with respect to the number of individual reactor tubes. The design of this plant should be easily transported in modular fashion by ship and operated with quick startup properties; these are traits that are highly desirable for the Navy.

The objective of this chapter is to assess the possibilities of reducing the BOP by developing and utilizing a process simulation analysis on a steady state performance with the use of micro-fibrous entrapped catalyst (MFEC) in a fixed bed reactor with the goal of producing JP-5. The use of an MFEC reactor will not be subjected to drawbacks that conventional fixed bed reactors face, (e.g. hot spots and high gas compression cost). Process operating conditions such as temperature and reactant partial pressures as well as syngas composition are addressed in order to enhance the selectivity of JP-5. A preliminary Phase 1 engineering design and evaluation is performed on the possibilities of making the FTS reactor smaller and thus its effect on the overall BOP. An analysis based on weight and volume for the skid unit was evaluated for 3 different operations.

4.2 Integrated Simulated Designs

Aspen Plus™ was used as the process simulator with material and energy balances solved for all process units. It was assumed that the system operates at steady-state and natural gas feed was held constant. A heterogeneous model was used to model this problem. The formation of olefins and alcohols were ignored for simplifications. The physical properties of reaction medium were calculated by the Peng-Robinson equation of state. The NTRL equation of state was applied for a three phase system; a situation where separations of liquid-liquid-vapor mixture was needed. The following compounds have been selected from Aspens databank: O_2, N_2, CO, CO_2, H_2, and paraffins from CH_4-$C_{30}H_{62}$ with a minimum number of other heavy hydrocarbons introduced into Aspen because of its lack of property definitions for higher chain alkanes greater than C_{31+}. The properties added for higher chain alkanes were vapor pressure, density, molecular weight and boiling point from API and ASTM tables. Linear and saturated hydrocarbons are selected to describe gasoline (C_5-C_{11}), JP-5 (C_9-C_{16}) and waxes (C_{20+}). A plug flow model is used to model the FTS reaction in Aspen using a promoted iron catalyst, Fe/Cu/K on alumina. A flow scheme of a typical FTS system is presented in figure 3.

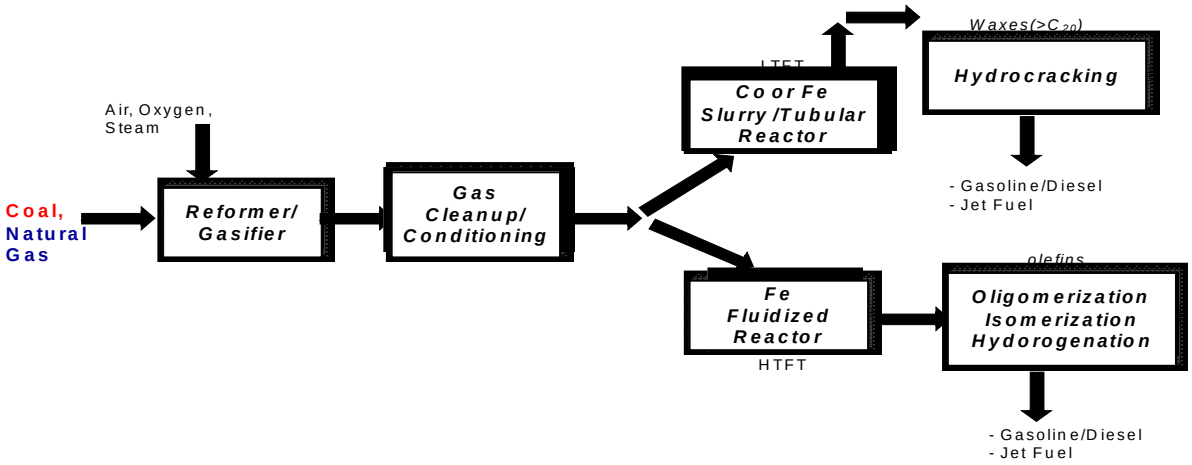

Figure 3 Flow Scheme of an FTS Process

An FTS system consists of at least 4 stages; upstream, (where syngas is produced and purified), Fischer-Tropsch Synthesis (FTS) reactor, separations of products, hydro-cracking, and water/product treatment and recycling.

4.2.1 Upstream

The manner in which syngas is produced is influenced by many factors, which in turn impacts many aspects of the rest of a GTL design. Some of these factors include plant size and location, the need for an oxygen plant, gas compression, heat integration and gas recycle options as well as configuration of power generation alternatives.

One can calculate the thermal efficiencies from the syngas producing facilities through the ratio of enthalpy of syngas to that of the feed (methane and/or oxygen) used, as written in Equation 1. Tables 2 and 3 compare syngas generating facilities to one another.

$$ThermalEfficiency\% = \frac{SyngasEnthalpy}{FeedEnthalpy} \quad (1)$$

Table 2. Comparison of Syngas generation technologies (Natural Gas Feed) I[15]

Technology	Advantages	Disadvantages
SMR	- Most extensive Industrial experience	- H_2/CO ratio often higher than required when CO also is to be produced
	- Oxygen not required	- Highest air emissions
	- Lowest process temperature requirement	- Highest air emissions
	- Best H_2/CO ratio for hydrogen production applications	
POX	- Feedstock desulfization not required	- Can be a disadvantage when requiring H_2/CO ratio >2
	- Absence of catalyst permits carbon formation and therefore, operation without steam significantly lowering syngas CO_2 content	- Very high process operating temperatures
	- Low methane slip	- Usually requires Oxygen

[15] Tindal, A. "Natural gas reforming technologies." Gas-to-Liquids Processing; Bringing Clean Fuels to market, San Antonio, TX, March 18-20 1998

	- Low natural H_2/CO ratio is an advantage for applications	- High temperature heat recovery and soot formation/handling adds process complexity
	- Low natural H_2/CO ratio is an advantage for applications	- Syngas methane content is inherently low and not easily modified to meet downstream processing requirements
ATR	- Natural H_2/CO ratio often is favorable	Limited commercial experience
	- Lower process temperature requirement than POX	- Usually requires oxygen
	- Low methane slip	
	- Syngas methane content can be tailored by adjusting reformer outlet temperature	

Table 3. Comparison of Syngas generation technologies II.

	SMR	POX	ATR
Operating Temperature, ^oC	900	1500	1100
Pressure, bars	25	25	25
Thermal Efficiency, %	75	79	82
		CO/H_2 Ratio	
Normal	3.5	2	2.5
Recycle CO_2	1.9	1.6	1.6
Increase Steam	>5.0	>1.8	>2.65

Auto-thermal (ATR) proves to be more thermally efficient due to the fact that it is a combination of partial oxidation (POX) with a catalytic steam reforming (SMR). However, SMR results in a higher production of hydrogen compared to carbon monoxide in the product syngas and therefore, will be the preferred technological route for this facility because of this very reason. Another attractive reason for choosing SMR as the favorite syngas producing technology is an oxygen plant is not required. This will be one less unit which minimizes the weight and volume design for a mobile GTL facility. It has been well advised that steam methane reforming by itself is not the preferred technology for syngas production for large

scales (>10,000bpd) GTL facilities because of the economics but this technology is sufficient for a 500 bpd plant.[16]

Synthesis gas for low temperature Fischer Tropsch (LTFT) operations has an optimum H_2/CO ratio slightly greater than 2 with low CO_2 concentration.[17] However, a hydrogen starved syngas increases chain growth probability, and thus selectivity hence, a target ratio of H_2/CO of 1.9 from the SMR unit will be set (See Chapter 3 for effects of syngas composition on alpha). A flowsheet of the upstream process is shown in Figure 4.

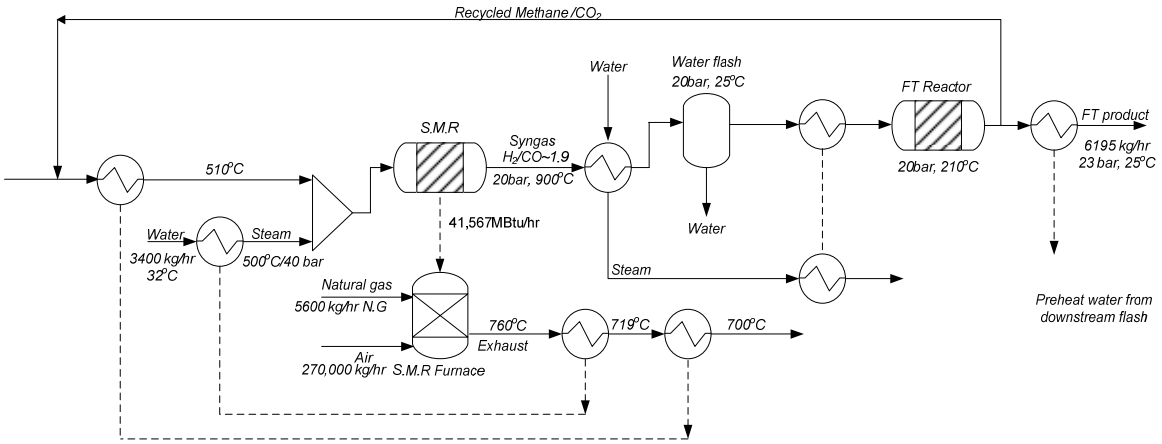

Figure 4 Process Flow Diagram of FTS - Upstream.

The key reactions in steam methane reforming are;

$$CH_4 + H_2O \rightarrow CO + 3H_2O \quad (2)$$

$$CH_4 + CO_2 \rightarrow 2CO + 2H_2O \quad (3)$$

$$CO + H_2O \leftrightarrow CO_2 + H_2 \quad (4)$$

It has been assumed most content of sulfur in the natural gas stream has been stripped, thus leaving a mole fraction composition of 1% N_2, 96% CH_4, 1.5% C_2H_6 and 0.5% C_{3+} (by mole fraction).[15] The furnace is modeled as two blocks in Aspen, with one being the reactor

[16] Aasberg-Perterson, K. "Synthesis gas production for FT synthesis." *Studies in surface science and catalysis.* 152 (2004): p258

[17] Lu, Yijun. "Influence of the Feed Gas Composition on the Fischer-Tropsch Synthesis in Commercial Operations." *Journal of Natural Gas Chemistry* 16 (2007): p329-341

(SMR) and the other furnace. The heat from the SMR is used to determine the heat duty of the furnace that is needed. Two design specs were used to obtain the correct amount of air and natural gas feed needed to set the outlet temperature of the SMR at 900ºC. The effluent gas from the furnace is used to heat various other streams in the plant before it is vented into the atmosphere.

Water is converted to pressurized steam at 500ºC and natural gas (stream NGAS1) is preheated to 500ºC at 20 bars using the heat from the furnace. These streams heat up to just slightly above 500ºC, the minimum temperature suggested by IEA,[18] and react through the 900ºC reactor which is assumed to achieve equilibrium concentrations. One benefit of this design is that all of the required steam is produced within the plant. With CO_2 being recycled back into the SMR, we are able to achieve the desired hydrogen to carbon monoxide ratio of 1.9:1 with over 65% conversion of methane. The addition of recycled CO_2, causes a water gas shift reaction to occur, reducing the ratio of H_2/CO ratio for desirable LTFT conditions.

A sensitivity analysis was performed by varying the steam/natural gas ratio and temperature in the feed stream to maximize the energy efficiency and H_2/CO ratio of 1.9 of the SMR unit (results displayed in table 4). The variation of the steam to natural gas volume ratio and natural gas feed temperature are expected to improve the energy efficiency of the SMR. Decreasing the ratio of steam to natural gas with a constant CO_2 recycle favors the desired ratio of H_2/CO but does not increase the thermal efficiency. This is can be attributed to the effect of the recycled CO_2. The natural gas temperature was varied with a constant steam to volume ratio of 30%. High natural gas feed temperature increases the thermal efficiency of the SMR.

[18] Precombusion Decarburization, IEA Greenhouse Gas Program, Report #PH2/19, p22

Table 4. Sensitivity Analysis of steam to methane ratio and N.G temperature on GTL Performance.

Steam/N.G (vol.%)	Thermal Efficiency %	H_2/CO ratio	N.G temperature ^oC	Thermal Efficiency %
20	73.48	1.71	400	73.60
30	73.64	1.92	510	76.25
50	75.01	2.36	600	79.42

After the syngas exits the steam reformer, it is cooled down to 70^{o}C in a heater. This heat is used to produce 9,000kg/hr of pressurized steam that can be used as feed, operate a turbine engine or, as indicated in this simulation, to operate steam heated bottoms reboiler for the distillation columns. The separation of CO_2 from the syngas stream can be achieved with the use of methanol via the Rectisol process as cold methanol absorbs carbon dioxide between 25-30 bars. The Rectisol process requires more electrical energy for refrigeration to maintain the low temperatures required (-44^{o}C) but also requires less steam energy for regeneration.[19,20] Another method for removing CO_2 is through the use of N-methyl-diethanolamine (MDEA), removal of CO_2 is achieved by condensation and drying and through a pressure swing adsorption unit, other contaminants can be removed. MDEA is preferred as it is less energy intensive and operates at a favorable temperature of 57^{o}C.[21] These processes are more complicated and require a complex model of their own for complete representation and would not be address in this thesis but for the purpose of the overall modeling effort, a black box model have been utilized for simplicity.

After the syngas is cooled, the water is separated out in a flash in order to reduce reactor size and to prevent condensation. This is also performed in order to prevent a competing water-gas shift reaction that would reduce the selectivity of JP-5. Almost 1700kg/hr of water is being removed and reused as a coolant or raw feed.

[19] Liu, J. "The Rectisol process for natural gas purification." *Natural Gas Chemistry* 32 (2007): p47-50
[20] Kohl, A. "Gas Purification" (5th ed.), Gulf Publishing, Houston, TX (1997).
[21] Aliabad, Z "Removal of CO_2 and H_2S using Aqueous Alkanolamine Solution." *World Academy of Science, Engr. And Technology.* 49 (2009): p194-203

4.2.2 FTS Reactor

The FTS reaction is highly exothermic and has an adiabatic temperature rise of up to 1750^{o}C. The problem of heat removal which many are faced with is most efficiently solved by using a slurry reactor. This in practices provides isothermal operation. There are a number of advantages besides temperature control for the use of a slurry reactor: high extent of catalyst use, design simplicity, ability of on-line catalyst regeneration and lower operation expenses. There are a few distinct disadvantages associated with this type of reactor such as the need for separating the liquid-catalyst phase from the product stream and for scale up purposes, this unit will not be ideal for a mobile FTS skid unit because of its size. With a fixed bed reactor, heat removal from the catalyst particles is done conventionally through high gas velocities of the reaction mixture flow and with diluents such as nitrogen. This results in additional energy expenditures to overcome hydraulic resistance of the catalyst bed. Attempting to use large particles to reduce the hydraulic resistance of the catalyst bed will only result in a decrease in the effectiveness factor of the catalyst as the process then is controlled by intra-particle diffusion. There has been a recent growing interest in monolith reactors,[22] but there are problems associated with these as well, such as low volumetric reactivity and flow distribution. Micro-fibrous entrapped catalyst (MFEC) reactors combine the advantages of a fixed and a slurry reactor without their corresponding disadvantages assuming operating equipments are properly maintained. Table 5 summarizes the advantages and disadvantages of each of these reactors and highlights the benefits of a MFEC reactor.

[22] Mesheryakov, V.D. "A multifunctional reactor with a regular catalyst packing for Fischer-Tropsch synthesis." *Chemical Engineering Science* 54(1999): p1565-1570

Table 5. MFEC Reactors versus Fixed and Slurry Reactors.

	Fixed bed reactor	MFEC bed reactor	Bubble Column reactor
Pore diffusion	-	-	+
Catalyst content in reactor	+	+	-
Gas-liquid mass transfer	+	+	-
Isothermal behavior	-	+	+
Catalyst attrition	+	+	-
Need for liquid-solid separation	+	+	-
Scale up	+	+	-
Reactor cost	-	-	+

(+) Advantages and (-) Disadvantages

In order to determine the overall heat transfer coefficient and model a bed temperature profile, one needs to be able to calculate the wall heat transfer coefficients; specifically for wall-to-fluid and wall-to-solids. Dixon's detailed works on effective heat transfer in a packed bed[23] provides the theoretical background necessary to calculate these coefficients. The effective axial and radial thermal conductivities are known and as such, an effective intra-bed thermal conductivity and overall heat transfer coefficient can be calculated. The Nusselt number relationship for a packed bed is defined:

$$Nu = 4\beta(\frac{D_p}{R}) + Nu_{fw}(1 + \beta\frac{Pe_{RF}}{\mathrm{Re}\,\mathrm{Pr}}) \qquad (5)$$

The wall heat transfer coefficient with respect to fluid and solid respectively;

$$h_{wf} = \frac{K_{rg} * Nu}{d_p};\ h_{ws} = \frac{K_{rs} * 2.12}{d_p} \qquad (6)$$

The effective radial thermal conductivity is calculated and used in solving an overall heat transfer coefficient.

[23] Dixon, A. "Theoretical Prediction of Effective Heat Transfer Parameters in packed Beds." *AIChE Journal* 25 (1979): p663-676

$$k_r = k_{rg} + k_{rs}\left(\frac{1+\frac{8k_{rg}}{h_{wf}d_t}}{1+\frac{\frac{16}{3}k_{rs}\left(\frac{1}{h_{fs}d_p}+\frac{0.1}{k_{rs}}\right)}{(1-\varepsilon)\left(\frac{d_t}{d_p}\right)^2}}\right) \quad (7)$$

The Overall Heat transfer coefficient[24]

$$*\frac{1}{U} = \frac{1}{h_w} + \frac{R_t}{3k_r}\frac{Bi+3}{Bi+4} \quad (8)$$

The relationship for concentration and temperature dependence in a 1D heterogeneous model are listed below;[25]

$$-u_s\frac{dC_A}{dz} = \rho_B r_A \quad (9)$$

$$u_s\rho_B C_p\frac{dT}{dz} = (-\Delta H)\rho_B r_A - 4\frac{U}{d_t}(T-T_w) \quad (10)$$

Pressure drop[19]

$$\frac{\partial P}{\partial z} = -\left(150\frac{(1-\varepsilon_B)^2}{\varepsilon_B{}^3(d_p\phi_p)^2}\eta_G\mu_G + 1.75\frac{(1-\varepsilon_B)^2}{\varepsilon_B{}^3(d_p\phi_p)}\rho_G\mu_G{}^2\right) \quad (11)$$

More details can be found in Appendix IV.

A recent kinetic study by Liu[26] allows for the use of intrinsic kinetics for FT synthesis over the design catalyst of choice, Fe-Cu-K. The lumped reaction kinetics are listed below.

$$-R_{CO+H_2} = \frac{1.2178*10^2\ \exp(-66{,}520/RT)P_{CO}P_{H_2}}{P_{CO} + 1.8973*10^{-5}\ \exp(65{,}412/RT)P_{H_2O}} \quad (12)$$

The effectiveness factor on the Fe-Cu-K catalyst has been reported by Wen Jie[27]

[24] Dixon, A. "An improved equation for the overall heat transfer coefficient in Packed beds." *Chemical Engineering and Processing* 35 (1996): p323-331
[25] Froment, G. "Chemical Reactor Analysis and Design." John Wiley & Sons (1979) New York
[26] Liu, Z. "Intrinsic kinetics of Fischer-Tropsch Synthesis over Fe-Cu-K Catalyst." *J. Chem. Soc. Faraday Trans.* 91 (1995): p3255-3261

$$\eta = 5.33 * 10^{-3} \exp(18900/RT) \frac{1 + 4.52 * 10^{-5} \exp(-59900/RT) \frac{P_{H_2O}}{P_{CO}}}{1 + 6.28 * 10^{-8} \exp(-73600/RT) \frac{P_{H_2O}}{P_{CO}}} \quad (13)$$

An FT WGS kinetic equation is also incorporated into this model of the FT reactor.

$$r_{CO2} = k_w (P_{H_2O} p_{CO} - \frac{P_{CO_2} p_{H_2}}{K_P}) \quad (14)$$

The conversion of CO can be seen in Figure 5 for different promoted iron catalysts that were based on different mechanism (See Chapter 3).

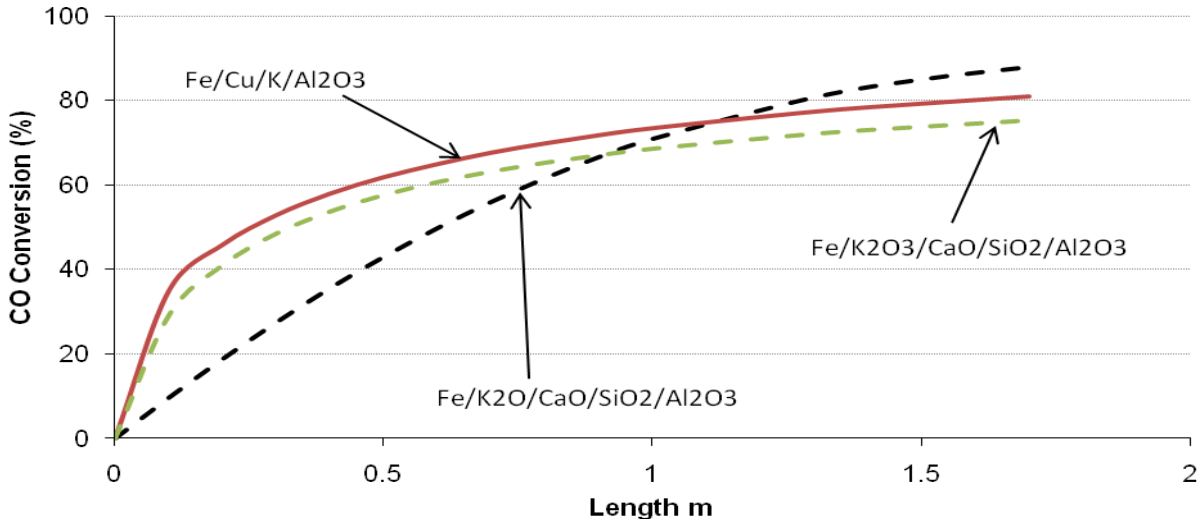

Figure 5 CO Conversion in FTS reactor.
0.042l/min, 232C, 20bars H_2/CO~2 on 40mm I.D

Several studies were first conducted on a single tube, varying tube diameter to determine the effects of conversion and temperature rise down the reactor bed. The comparison of a MFEC bed is compared with that of a packed bed. With a constant space velocity and constant flowrate respectively, the temperature & conversion profile between a packed bed and MFEC is shown in Figure 6 & 7 for a tube with constant cooling of 225°C, and constant particle size of 165um. The packed bed has a temperature rise of 20°C while

[27] Quan-Sheng, L. "Steady-State and Dynamic Behavior of fixed Bed Catalytic Reactor for Fischer Tropsch Synthesis II. Steady State and Dynamic Simulation Results." *Journal of Nat. Gas Chem.* 8 (1999): p238-248

that of a MFEC bed is less than 5°C. With this benefit of MFEC, the tube diameter can be increased and reactor length reduced to achieve the same conversion of CO. This will allow an FTS reactor to be much smaller than conventional reactors.

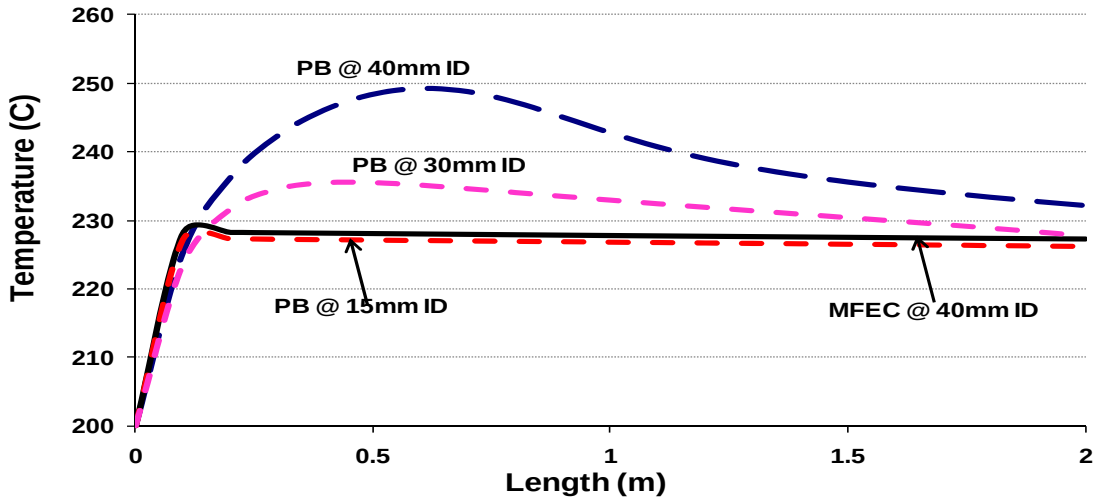

Figure 6 Temperature profile in FTS reactor.
Packed bed and MFEC bed contain 165*um* diameter particle

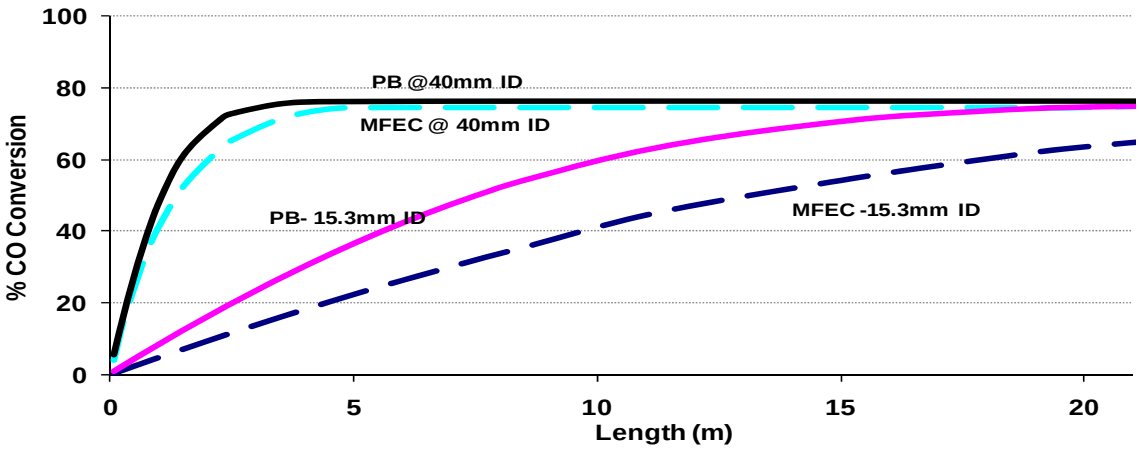

Figure 7 CO Conversion profile in FTS reactor for Packed Bed and MFEC.
Packed bed and MFEC bed contain 165μm diameter particles.

The next set of studies where to compare a conventional packed bed to MFEC reactor where particles sizes were changed to determine the effect of temperature and pressure drop distribution to meet a constant CO conversion. A constant space velocity of 100/hr was enforced. These results are shown in the Table below.

Table 6. Conventional Packed Bed Reactors vs. MFEC

	70% Conversion CO					
	Packed Bed, 3mm Dp			MFEC 165um		
Tube Diameter, mm	15.3	30	40	15.3	30	40
Length, m	20	16	1	20	13	6
Overall Heat Transfer Coefficient, W/m^2K	299.96	159.86	121.49	4642.40	2407.20	1880.50
ΔT / C	31	100	150	2	4	5
Pressure Drop, bar	2	1	-	15	11	6

The following equations, as well as an alpha-temperature relationship shown in chapter 3 allows for simulating and calculating with respect to CO conversion the product distribution in the PFR reactor. A 7 m multi-tubular reactor of 900 tubes with a 2 in I.D is modeled in Aspen to achieve a high pass conversion of 80% for MFEC. With a MFEC bed voidage of 75% and a particle density 1774kg/m^3, the pressure drop of 7 bar is seen across the reactor. The product distribution of a packed bed and MFEC are shown in figure 8.

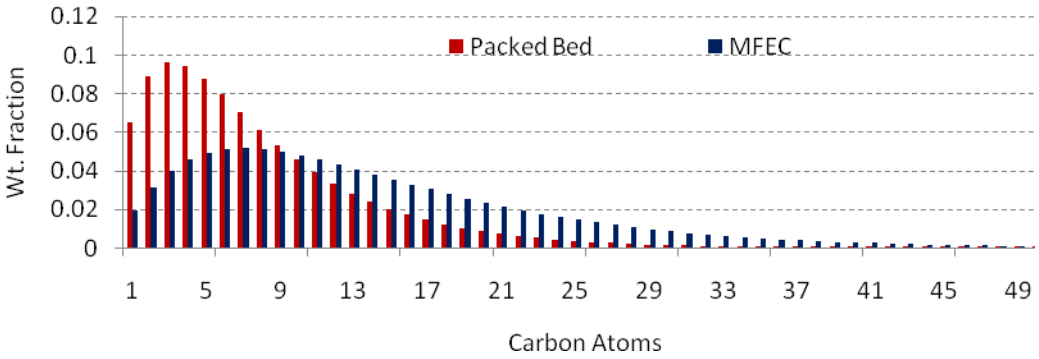

Figure 8 Product Selectivity Comparisons between Paced Bed and MFEC.

A significant improvement is seen with the MFEC in terms of C_{9+}. This is because the FTS reactor operates under optimum conditions necessary to yield the highest JP5 selectivity. The packed bed produces more light gases due to the temperature hotspots. The uniformity in temperature is essential to achieving such high C_9-C_{16} selectivity. The advantages can be seen in using MFEC reactor as the reactors yielded higher selectivity to jet fuel and heavier hydrocarbons C_{17+} which will be further broken down into smaller chained hydrocarbons via

a hydrocracker. FTS reactors provided lower selectivity to light hydrocarbons (C_{1-8}). Un-reacted CO, about 30 mol%, can be recovered from the light gas product stream and recycled back into the reactor after a gas-liquid separation by reacting the gas stream with a lower alkyl-alcohol to form an alkyl-formate. The formate is separated from the fuel gas easily and carbon monoxide is regenerated by decomposition of the formate.[28]

Water exiting the FT reactor amounts to about 49 wt.% of all products and contains number of other products that are not modeled; such as organic acids and alcohols. Heavy paraffin conversion process through the use of a hydro-cracking unit is necessary to improve the yield of JP-5. To achieve a high selectivity through this process; the right catalysts and operating conditions have to be selected, so that heavy molecules display much higher reactivity than light components, which will prevent over cracking of materials of C_9 or smaller into light gases. Hydro-cracking catalysts are characterized by the presence of two types of active sites that operate simultaneously; acidic sites, which provides the isomerization/cracking and the metal sites which is responsible for hydrogenation/de-hydrogenation.[29] Common catalysts on amorphous silica-alumina supports are platinum, palladium or bi metallic systems (i.e., Ni/Mo, Ni/W or Co/Mo). Catalysts loaded with a noble metal (particular Pt) show better performances in terms of selectivity for hydroisomerization and product distribution.[30,31] Temperatures of 350-385^{o}C have shown to favor cracking of heavy hydrocarbons chains in diesel.[32,33] The hydro-cracking unit is operated at a pressure of

[28] James, L. "Recovering carbon monoxide from fuel gas." *U.S Patent* -3716619 (1971)
[29] Archibadld, R.C "Catalytic hydro-cracking of aliphatic hydrocarbons." *Industrial & Engineering Chemistry* 52 (1960)**:** p745-750
[30] Gibson, J.W "The use of dual function catalyst in isomerization of high molecular weight n-paraffin." *Industrial & Engineering Chemistry* 52(1960): p113-116
[31] Weitkamp, J. "Factors influencing the selectivity of hydro-cracking in zeolites." In: Barthomeuf, D.,, Guidelines for Mastering the Properties of Molecular Sieves. (1990): p343. Plenum Press, New York.
[32] Sturtevant, P. et al., "Fischer-Tropsch Wax Characterization and Upgrading: Final Report." *DOE Report,* DE88014638 **(**1988).

50 bars and 1-2 LHSV.[34] The products of the hydro-cracking unit are diesel (80 wt.%), gasoline (15 wt.%) and minimal light gases such as ethane, propane and butane (5 wt.%).[32] It is important to note that diesel and gasoline both contain C_9-C_{16} hydrocarbon chains. For simplicity, the hydrocracker is modeled with a yield reactor, "RYield," in AspenPlus™. Product yields are calculated assuming an 80% conversion of heavy feed (waxes) and the hydrogen consumed in this section is 65% of this heavy feed. The product distributions are shown in figure 9.

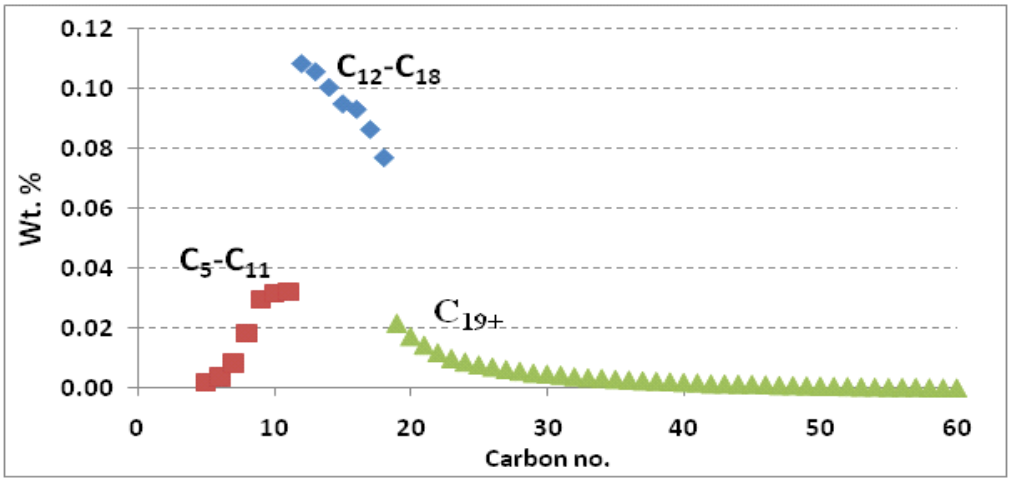

Figure 9 Products Yield from hydro-cracking.

The following table, Table 7, shows the overall yield of JP-5, an improvement is seen when a hydro-cracking unit is included in the process.

Table 7 Overall Product Yield of JP-5

	Packed Bed wt.%	MFEC wt.%	Packed bed + Hydro-cracker wt.%	MFEC+ Hydrocracker wt.%
C_1-C_8	0.54	0.34	0.6	0.46
C_9-C_{16}	0.3	0.34	0.4	0.54
C_{17+}	0.16	0.32	-	-

[33] Fernandes, F. "Modeling and optimization of Fischer-Tropsch products hydro-cracking." *Fuel Processing Technology* 88 (2007): p207-214
[34] Walas, Personal Communications (1985)

In a further research study, the hydro-cracking unit can be designed to operate with a micro-fiber catalyst, as this should help with the removal as the process is exothermic. The following parameters are suggestions that can be optimized to improve product yield for JP-5 in a hydro-cracking unit; a process configuration layout; the need for a single-stage or two stage reactor or just once-through in order to determine a maximum systematic conversion. In addition to the configuration, the need for and an optimal feed/recycle ratio should be determined as well as the fractional cut point and conversion level in combination with kinetic studies to accurately model this unit. A flowsheet of the downstream process is shown in Figure 10.

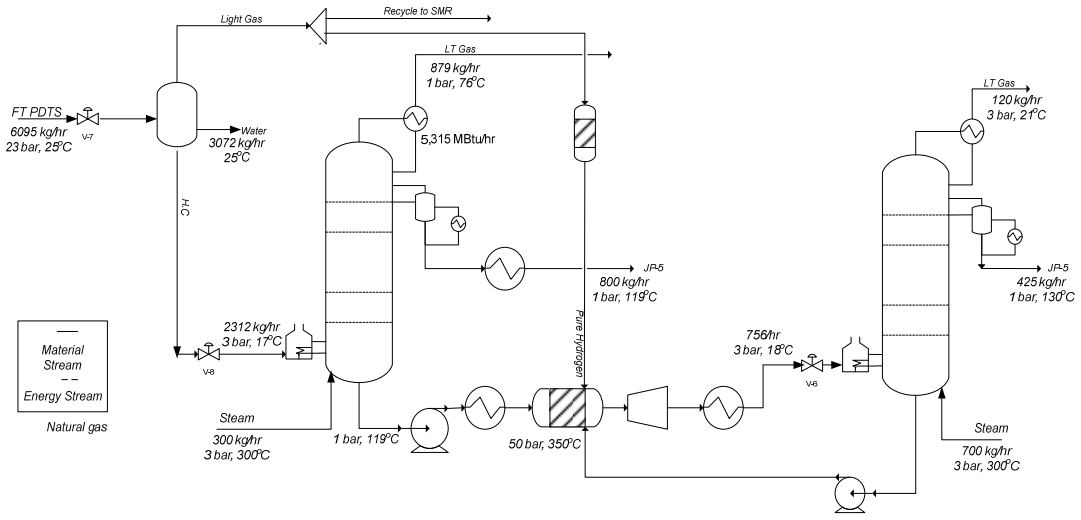

Figure 10 Process Flow Sheet of FTS - Downstream.

4.2.3 Downstream

The fuel and wax is cooled in a series of heat exchangers and a post flash drum is needed to separate light gases and water from the FT reactor products. The stream contains un-reacted CO, CO_2 and $C_2 – C_8$ with a heating value of 3.81MMBtu/hr which can be used in the furnace. 2 steam operated distillation columns with 18 stages are used to obtain the

96wt% purity of JP-5 at 470 bpd. The waxes are then transported to the hydro-cracking unit. Hydro-treatment of the product is necessary to remove reactive species such as olefins and alcohols that interfere with the hydro-cracking process however; this is beyond the scope of this work. The desire to use one major distillation column to separate and achieve high purity from feeds originating from the hydro-cracking unit and post flash drum will come at a cost of having a high heat duty and a very tall column with 32 stages.

4.3 Weight/Volume BOP Analysis

The weight by volume analysis is a unique way at looking at a specific plant design case and this is an important design criterion for a mobile-skid unit. Available space limits how much process equipment one can have. This is why it is important to optimize reactor conditions and have an efficient heat removal system for the FTS reactor to attain a high single pass conversion along the reactor without recycle while maintaining selectivity, resulting in decreased demand on downstream separations. There is however, the need to increase carbon efficiency for larger production units which is achieved through recycling. Piping layout, with isometric drawings and piping and instrumentation diagrams (P&ID) will be the next developmental phase for the skid unit.

There are numerous possibilities with regards to FT design, and product slates. However, with regards to only focusing on JP-5, while maintaining minimal volume and weight of the designed plant, three possible case scenarios were developed based on pilot scale-up needs (Case A) and the need for a larger facility capable of producing 500 bpd JP5 (Cases B and C).

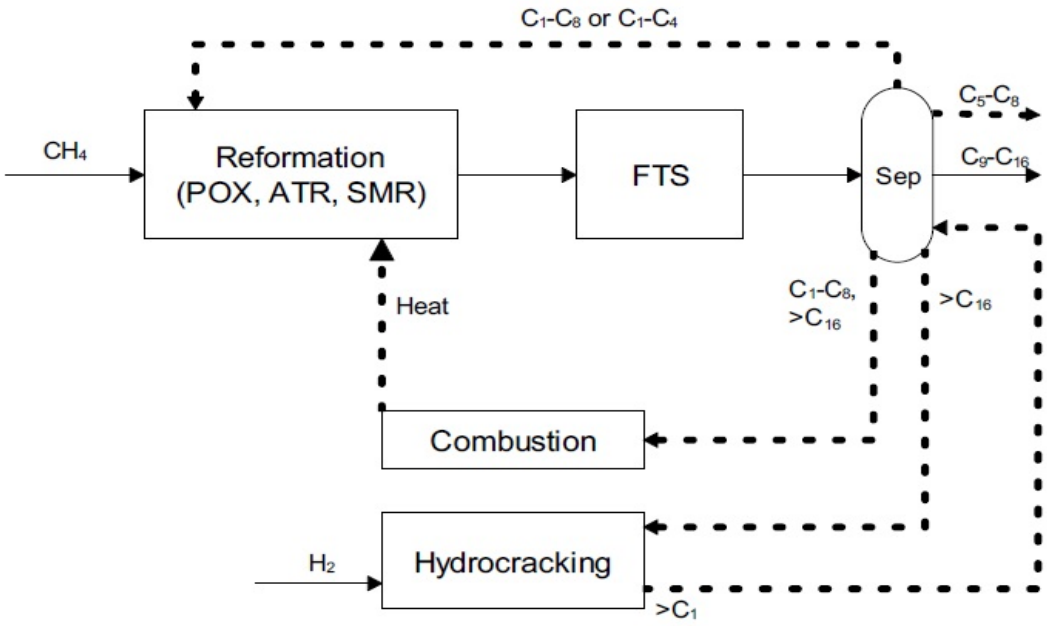

Figure 11 Fischer Tropsch Possibilities for Mobile Skid Unit.

Case A, the once through pass within the FT reactor, is first designed to meet a production target of 2L/12hr day of JP-5 without any recycle. This design is the first stage in a pilot developmental process. A POX, ATR or SMR unit can be used to produce syngas for these cases but the SMR was selected over the others because of overall syngas production output, an oxygen plant is not needed for this design, and the lowest process temperature requirement is used for this process. Case A was enhanced further to meet a target of 500 bpd of JP-5 for a basis of comparisons. This was done assuming that undesirable products, C_1-C_8 and C_{16+}, will be burned in the SMR furnace. This is the smallest possible unit that can be designed as there is no need for a hydro-cracking unit. One would not ideally put this design into practice because of the loss of valuable fuel (C_{16+}) associated with this design and its thermal efficiency. Cases B and C, model a more realistic GTL operating plant with the need to recycle lights gases to be burned as fuels in the SMR furnace or reformed to make syngas. Case B models a plant which only focuses on JP-5 as single product produced while Case C

allows for the production of JP-5 and light naphtha (C_5-C_7) as its two only products. Both plants have onsite steam producing facilities and a hydro-cracking unit.

A simulation model was created to optimize JP5 production for 2 L per 12 hr day with no recycling in a 1.64" I.D tube with a length of 2 m, and this case is illustrated in Figure 12.

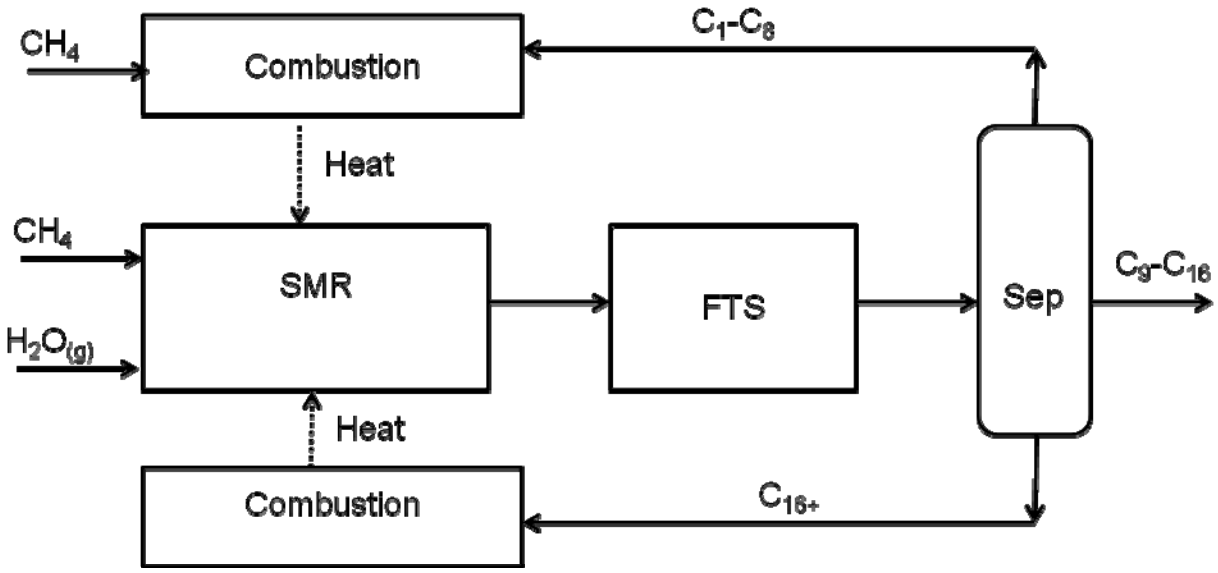

Figure 12 Process Flow Diagram for Case A (Single Pass).

Using a detailed kinetic model in Aspen, the operating temperature was varied, with a constant pressure of 20 bars to find an optimum operating regime to meet the targeted production of 2 L/12-hour day. The major advantage of the use of an MFEC reactor bed in this particular operation is seen with the temperature rise and, selectivity as shown previously in Figure 6. The highest production of JP-5 was achieved at 255^{o}C with a selectivity of 27wt%. The rate of conversion is much higher within this temperature range. There are disadvantages, however, with performing FT at such high temperatures. The rate of catalyst deactivation is much higher due to carbon deposition from a catalyst phase changes and a possible "Boudouard" reaction; where carbon monoxide reduces into carbon dioxide and

elemental carbon.[35] The temperature rise results in a low α value and thus, selectivity for C_9-C_{16} hydrocarbons, and an increase in lighter products (C_1-C_9) are seen. As seen in Table 8 and figure 13, JP-5 has a low selectivity of 27wt.%, but the rate of conversion is much higher.

Table 8 Case A: Overall Product Yield of JP-5 - HTFT

	Temp, deg C					
	235	250	260	270	275	280
Alpha	0.807	0.780	0.762	0.743	0.734	0.725
CO conversion, %	50.2	65.5	73.5	79.6	82.0	83.9
C9-C16 prod., L/12 h day	1.251	1.431	1.478	1.419	1.405	1.323
C17+ prod., L/12 h day	0.442	0.336	0.262	0.220	0.171	0.148
C9-C16 selectivity, %	33.4	29.0	26.6	23.3	22.5	20.7

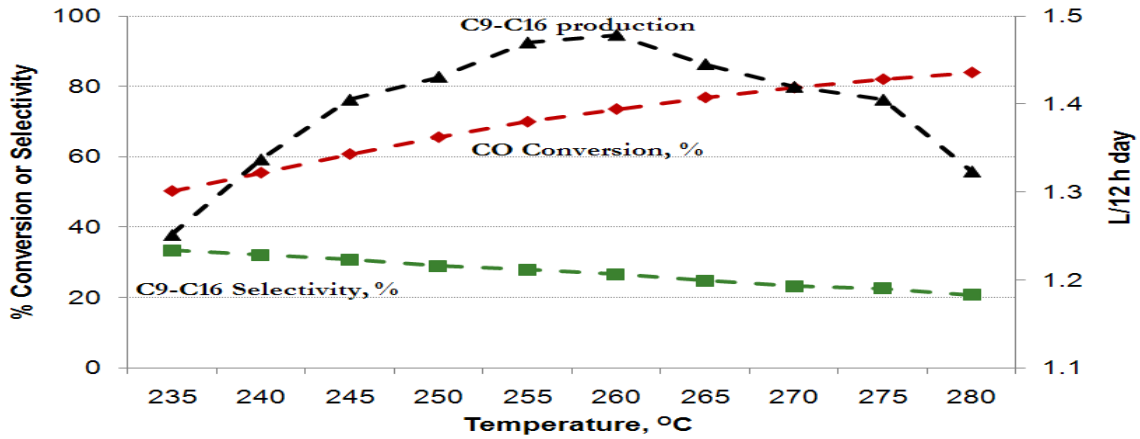

Figure 13 High Temperature Fischer Tropsch for Case A (Single Pass).

To validate our simulation model, it was compared to experimental data that was gathered by Cerametec, an independent R&D group who also have research interests in Fischer-Tropsch catalysis. Figure 14 compares the conversion and selectivity for Case A, where 2L/12 hr day of JP5 is being produced, with that of an iron catalyst at similar experimental conditions.

[35] Bohlbro, H. "An Investigation on the Kinetics of the Conversion of Carbon Monoxide with Water Vapor over Iron Oxide Based Catalysts." *Gjellerup, Copenhagen* (1969)

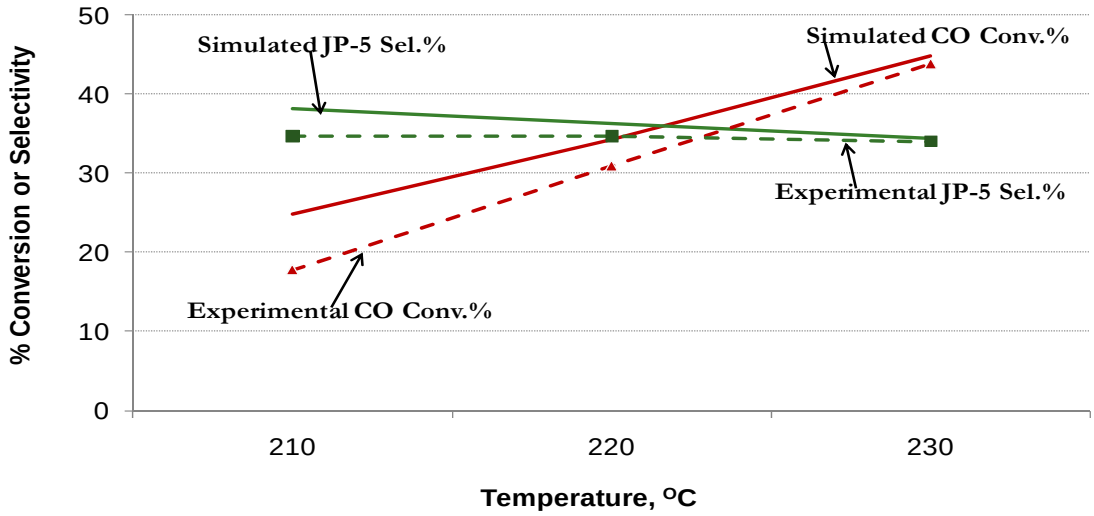

Figure 11 Case A (Single Pass)
Simulation validation with experimental results.

In an effort to model a low temperature Fischer Tropsch (LTFT) to meet the targeted production of 2 L/12 hour day, it was observed that more syngas is needed in the feed stream to meet the production target. Tables 9 and figure 15 illustrate the effects of temperature variation on JP5 production and selectivity for both LTFT reaction regimes.

Table 9 Case A: Overall Product Yield of JP-5 - LTFT

	Temp, deg C				
	200	205	210	215	220
Alpha	0.872	0.863	0.853	0.844	0.835
CO conversion, %	17.5	20.9	24.9	29.4	34.2
C9-C16 production, L/12 h day	0.506	0.603	0.712	0.821	0.928
C17+ production, L/12 h day	0.275	0.292	0.318	0.342	0.296
C9-C16 selectivity, %	39.1	38.8	38.1	37.4	36.3

With a constant flowrate of $1.4x10^{-4}$ SCMM which is used for the HTFT, a significant amount of JP-5 is not produced, 48% on average, due to low conversion of CO and overall FT reaction rates. However, improved selectivity is maintained at 40 wt.%, which counteracts the reduced reaction rate.

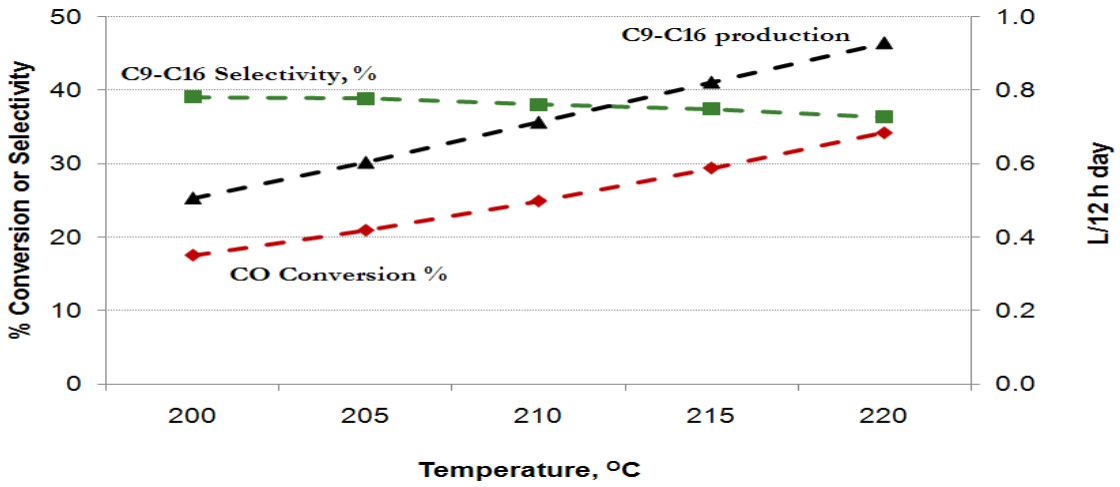

Figure 15 Low Temperature Fischer Tropsch for Case A (Single Pass).

There are several advantages of running a LTFT for case A: the increased selectivity to JP5 due to operating near optimal α, reduced soot formation risk compared to high temperature and also a reduced risk of temperature runaway. However, a low single-pass conversion dictates the need for recycle and/or increased feed flowrate.

Cases B and C have light gases recycled in order to be burned as fuel in the SMR furnace. There is the addition of a hydro-cracking unit to break down all heavy waxes so as to increase the product yield of JP5. Figures 16 and 17 show block flow diagrams of different case studies for JP-5 production.

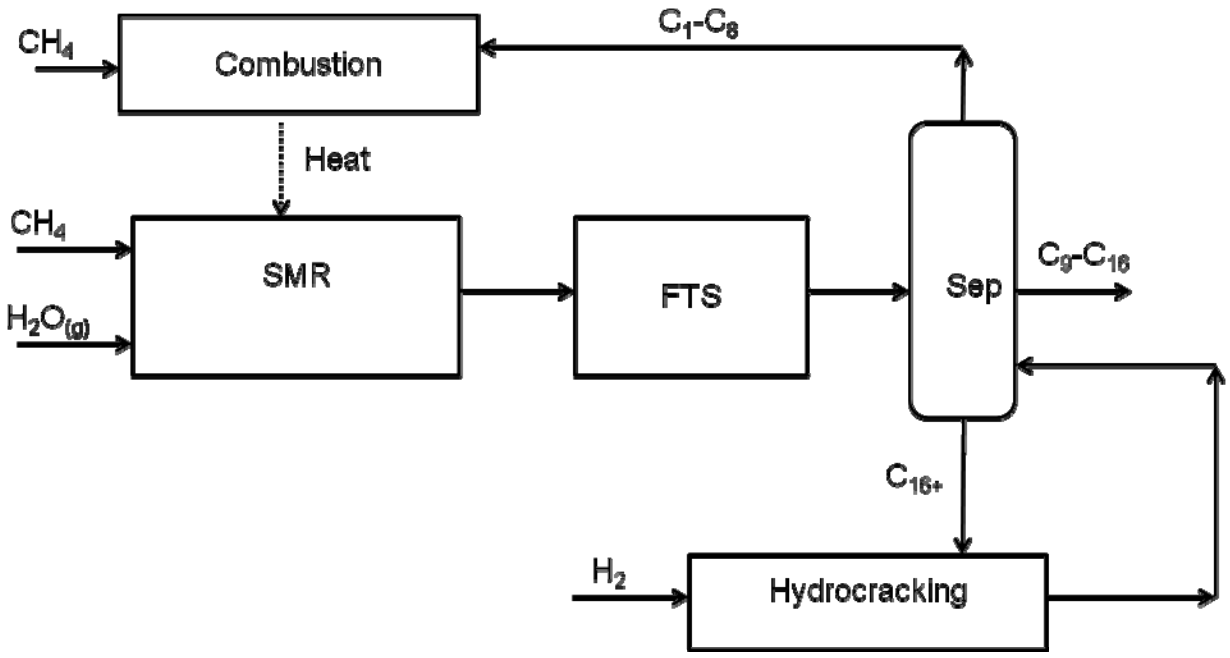

Figure 16 Process Flow diagram for Case B (Single Pass with Hydro-Cracking Unit).

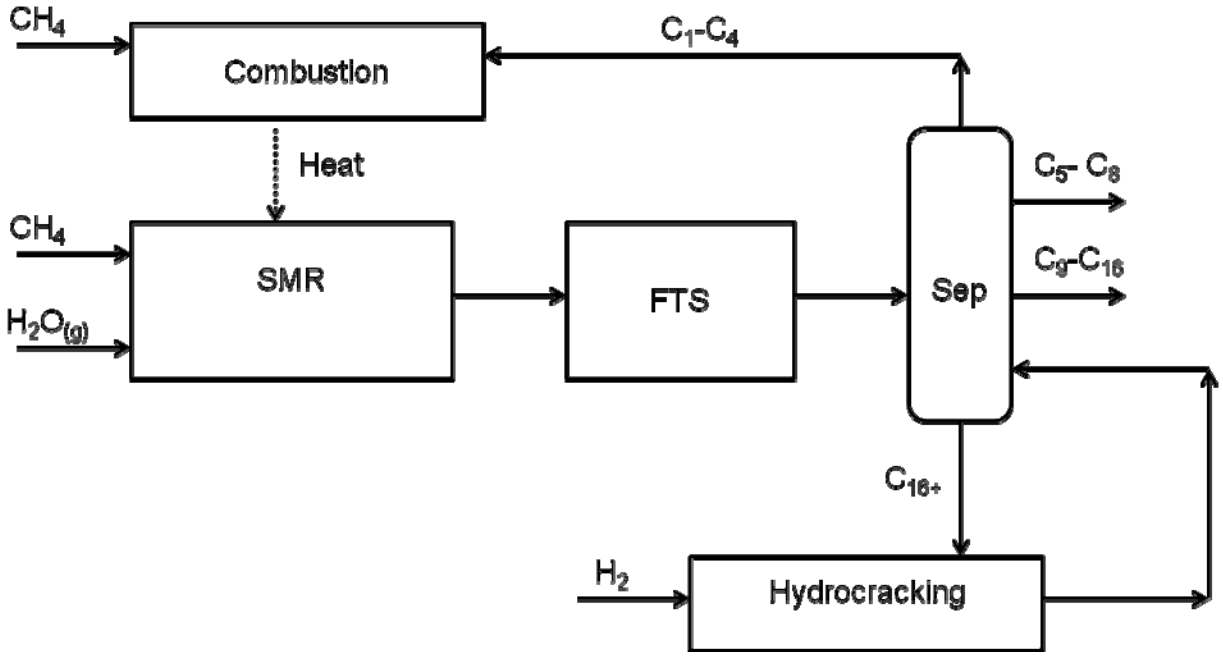

Figure 17 Process flow diagram for Case C (Single Pass with Hydro-Cracking Unit/Lt naphtha).

Equipment Sizing

In reality, the SMR unit and furnace is a single unit, called heat exchanger reformers, and the heated streams run through piping in the reformer furnace to be heated.[36] A high alloy steel tubes will be used, (25 Cr 35 Ni Nb Ti),[37] known as "mircoalloys" because of their ability to withstand high temperature and maintain its strength. The shell thickness and tube thickness are 50 mm and 8 mm respectively, which results in a very heavy unit. Assuming a nickel catalyst on zirconia is used for SMR operations which will have WHSV of 1.25 Ibs NGas/hr/Ibcat and catalyst density of 54 Ibs/ft^3.[38] Detailed kinetics are not included in the model for the SMR unit in Aspen. More details on the mechanical design of steam reformers are available in literature.[39,40]

Assuming a liquid hold up of 4 min,[41] the flash drums and distillation columns can be sized. The heat exchangers are sized by calculating the required surface area of heat exchanger from a known heat duty using the overall heat transfer coefficient and log mean temperature difference.

$$Q = UFA(\Delta T)_m \tag{14}$$

$$(\Delta T)_m = (\Delta T)_{\log mean} = \frac{\Delta T_2 - \Delta T_1}{lm[(\Delta T_2 / \Delta T_1)]} \tag{15}$$

With a shell-and-tube exchanger with multiple-tube passes, a correction factor, F, is applied to compensate for flow direction.[41] Based on a 1.25" square pitch for a 1" tube and two pass

[36] Dybkjaer, I. "Advanced reforming technologies for hydrogen production." *International Journal of Hyrdrocarbon Engineering* 3 (1998): p56-58
[37] Mohri, T. "Application of advanced material for catalyst tubes for steam reformers." *Ammonia Plant Safety* 33(1993): p86-100
[38] Walas, S. "Chemical Process Equipment Selection and design." (1988) Butterworth Publishers
[39] Dybkjaer, I. "Tubular reforming and autothermal reforming of natural gas — an overview of available processes." *Fuel Processing Technology* 42 (1995): p85-107
[40] Rostrup-Nielen, J.R *Catalysis, Science and Technology*, (1984) Springer-Verlag, Berlin.
[41] Seider, W.D. and Lewin, D.R. "Process Design Principles." (2004) 2nd Ed. John Wiley and Sons Inc. New York.

heat exchangers of 16 ft, the total number of tubes is estimated from a heat exchanger tube sheet layout count table[19] and with the shell I.D known from the required surface area, each exchanger's weight and volume can be calculated with an assumed carbon-steel material that has a shell I.D and tube thickness of 0.375" and 0.07" respectively. A more detailed analysis will involve calculating the pressure drop within these exchanger units. All calculations are included in Appendix IV.

Table 10, 11 and 12 give a summary of results obtained from Case A, Case B and C. The catalyst bed packing density is 0.98 g/cc for $Fe/Cu/K/Al_2O_3$ and MFEC (8 vol.% Cu fiber-15 vol.% catalyst-75 vol.% void) is 0.653 g/cc.

Table 10. Products for Case Scenarios

	Case A Single Pass JP-5 Only		Case B Single Pass + HCC JP-5 Only		Case C Single Pass + HCC JP-5+Naptha	
	Packed Bed	MFEC	Packed Bed	MFEC	Packed Bed	MFEC
Jet Fuel Fraction (wt.%)	100	100	100	100	60	69
Naphta Fraction (wt %)	-	-	-	-	40	31

Case A, no hydro-cracking unit and all off spec. products are burned. Case B, JP-5 only. Case C, JP-5 and light naphtha are products and recycling of lights are burned as fuel. There is the addition of a hydro-cracking unit.

Table 11. Weight and Volume of Major Process Equipments for Case A

Unit		Case A Single Pass JP-5 Only	
		Packed Bed	MFEC
SMR	Weight (tonne)	292	285
	Volume (m^3)	29	17
FTS	Weight (tonne)	495	310
	Volume	57	49

	(m^3)		
Heat Exchanger	Weight (tonne)	710	710
	Volume (m^3)	63	63
Column	Weight (tonne)	18.7	16.3
	Volume (m^3)	13.9	17.4

Table 12. Weight and Volume of Major Process Equipments for Case B and C

Unit		Case B Single Pass + HCC JP-5 Only		Case C Single Pass + HCC JP-5+Lt. Naphtha	
		Packed Bed	MFEC	Packed Bed	MFEC
SMR	Weight (tonne)	269	256	261	256
	Volume (m^3)	10	9	10	9
FTS	Weight (tonne)	375	128	351	116
	Volume (m^3)	42	17	21	13
Hydro-Cracking	Weight (tonne)	92	90	85	79
	Volume (m^3)	12	10	9	8.4
Heat Exchanger	Weight (tonne)	1247	1021	1247	1021
	Volume (m^3)	158	130	158	130
Column	Weight (tonne)	18.7	16.5	18.7	18.7
	Volume (m^3)	13.9	11.4	8.6	8.6

Compressors, valves, condensers, pumps, Membrane separator, Hydrotreaters, pipes are not included

The effect is drastically seen with the FTS reactor weight and volume. The MFEC reactor tube diameter was scaled up to 50 mm I.D, tube counts for the reactors were varied, and reactor lengths were reduced to 9 m in order to meet a CO conversion of 80% for a single pass. The most significant amount of tubes was seen in the MFEC reactor was for Case A, which had 1500 tubes, compared to MFEC cases B and C with 1100 each. The packed Bed reactors had a tube count of 2050 tubes for each case.

At equivalent production rates, MFEC requires much lower flow rates through the steam reformer and the FTS reactor. Smaller heat exchangers are needed and thus smaller reactor sizes. When light gases are recycled to be burned in the SMR, significant improvements can be seen in the reduction of the weight and volume of the overall BOP when compared to a packed bed reactor. Case B offers a reduction in FTS reactor size and an overall 25% reduction is seen when compared to a packed bed. It is important to remove the CO_2, from the FT tail gas recycle which will improve the thermal efficiency of this process. With light naphtha being produced that can be blended for gasoline production, there is a reduction in light gases that will be burned, and the overall weight and volume of the FTS are significantly reduced. A 30% reduction is seen in Case C.

Table 13. General Comparison Cases for 500 bpd of JP-5 for MFEC Cases

	Case A Single Pass JP-5 Only	Case B Single Pass + HCC JP-5 Only	Case C Single Pass + HCC JP-5+Lt. Naphtha	Packed Bed Single Pass + HCC JP-5+Lt. Naphtha
Natural Gas (MMCF/hr)	13.1	6.2	6.2	7.6
Steam (kg/hr)	6200	3400	3400	4200
Weight (tonne)	310	128	116	351
Volume (m3)	49	17	13	21
Lt. Naphtha	-	-	+	+

Table 14 compares the recycled streams and SMR duty for each case. Case A provides an added advantage of being able to supply heat to the SMR from the off-spec products.

Table 14. Composition of Recycled Streams for MFEC Cases

	Case A Single Pass JP-5 Only	Case B Single Pass + HCC JP-5 Only	Case C Single Pass + HCC JP-5+Lt. Naphtha	Packed Bed Single Pass + HCC JP-5+Lt. Naphtha
Natural Gas (MMCF/hr)	0.075	0.3	0.4	0.4
C_1-C_4 (vol.%)	64.6	34.9	32.7	62
C_5-C_8 (vol.%)	25.5	22.1	-	-
C_{16+} (vol.%)	99	-	-	-
Heating Value[MMBtu/hr]	7.9	3.81	1.32	4.2
SMR Duty [MMBtu/hr]	49.8	31.3	31.3	35

MFEC bed reactor operates with small particles that greatly improve heat and mass transfer. This allows for a high effectiveness factor for catalyst, maximizing activity and life. This will lead to far high reactor productivity as seen in figure 18.

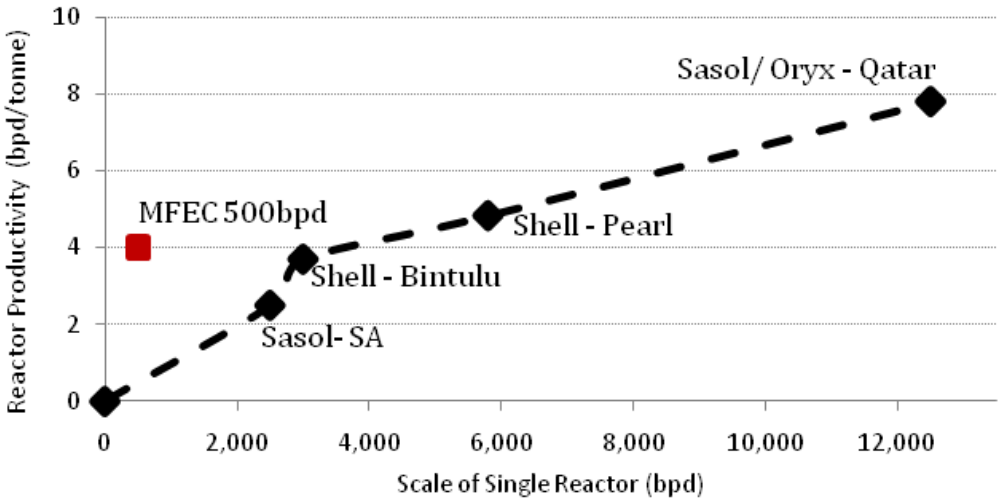

Figure 18 Reactor Productivity.

The process by which MFEC is made is by wet lay process, an inexpensive and environmentally friendly paper-based manufacturing process. MFEC FT achieves the

economy of scales at much smaller size (500 bpd) than conventional technology (5000 bpd). This advantage allows MFEC-FT to be feasible for GTL applications because of the reduction in its weight and volume.

Conclusion

A GTL process was modeled and simulated to produce 500 bpd of JP-5. The feasibility of using MFEC for FTS has been verified for a phase I evaluation. Due to the high thermal conductivity of metal fibrous media, MFEC significantly improves the temperature profile in the fixed bed reactor, and allows the FTS take place at lower temperatures. Product selectivity was attributed to maintaining the temperature profile and as a result, JP-5 selectivity was enhanced. The use of a hydrocracker in an FTS process can enhance the selectivity by 30wt.%. It was found that the use of MFEC can significantly reduced the BOP (20 to 30%) and improved the utilization of natural resources (14%) while maintaining the same production capacity.

"Nothing in life is to be feared.
It is only to be understood."
Marie Curie

Chapter 5

Accomplishments and Future Directions

5.1 Accomplishments

The promoted iron catalyst has shown it can have an alpha value of 0.86; high enough to achieve the maximum selectivity towards JP-5 from an FTS reaction. With the use of a micro-fibrous entrapped catalyst, we are able to enhance intra-bed heat transfer by 90%, reducing the temperature rise within the reactor tube, which damages the catalyst. The reduction in temperature rise will ensure a high JP-5 product selectivity in this process.

A detailed kinetics has been modeled efficiently with the integration of Matlab and Aspen^{TM} to accurately predict the thermal conductivity of the bed, overall heat transfer coefficient and temperature profile under FTS conditions. This allowed us to accurately model the FTS reactor needed to achieve a conversion of 80%. An overall GTL process was modeled and simulated to produce 2L/12hr day for a small scale pilot plant. The experimental results marched very well with simulated data for 2L/12hr-day for a 1.67 inch, 2 m tube. A larger producing plant, 500 bpd of JP-5, was also simulated.

The feasibility of using MFEC for FTS has been verified for a phase I evaluation. Due to the high thermal conductivity of metal fibrous media, MFEC significantly improves

the temperature profile in the fixed bed reactor, and allowed the FTS to take place at a low temperature level. Product selectivity was attributed to maintaining the temperature profile; JP-5 selectivity was enhanced. The use of a hydrocracker, allowed us to increase the selectivity of JP-5 by 30wt.%.

5.2 Future Directions

There is still a lot of work that can be done on the simulation efforts. First, a pinch analysis could be done to improve heat integration of overall plant system. This could have the potential of reducing the required number of heat exchangers and increase thermal efficiency.

Further work needs to be done on modeling hydro-cracking unit with an ideal kinetics. This is an exothermic process where the use of a micro-fibrous material can improve the intra-bed thermal conductivity, thereby allowing one to achieve the same producing capacity with a smaller reactor.

An ideal piping layout and P&ID should be constructed with the aid of process control integrations.

The next phase of this work involves development of additional process models for the generation of performance metrics, specifically information on conversion, yield, and production cost for economic metrics. This would be analyzed based on recent and future predictions of crude oil and natural gas prices. Although the case study illustrated previously demonstrates real world usage of this methodology, many simplifications have been made, and over time the simplifying assumptions will be further reduced in order to increase the realism and rigor of the framework as an evaluation tool.

Bibliography

Aasberg-Perterson, K. "Synthesis gas production for FT synthesis." *Studies in surface science and catalysis.* 152 (2004): p258

Aliabad, Z "Removal of CO_2 and H_2S using Aqueous Alkanolamine Solution." *World Academy of Science, Engr. And Technology.* 49 (2009): p194-203

Anderson, R. "Fischer-Tropsch Reaction Mechanism Involving Stepwise Growth of Carbon Chain" *J. of Chem. Phys.19* (1951): p313

Anderson, R. "Fischer-Tropsch Synthesis, Some important variables of the synthesis on iron catalyst." *Ind. Eng. Chem.* 44 (1952): p391-397

Anderson, R. "Catalyst for the Fischer-Tropsch Synthesis." *Van Nostrand Reinhold* 4 (1956) New York

Arakawa, H. "Effect of potassium promotion on the activity and selectivity of iron Fischer-Tropsch Catalyst." *Ing. Eng. Chem. Process Des. Dev.* 22 (1983): p97-103

Archibadld, R.C "Catalytic hydro-cracking of aliphatic hydrocarbons." *Industrial & Engineering Chemistry* 52 (1960)**:** p745-750

Atwood, H. "Kinetics of the Fischer-Tropsch reaction over iron." *Ind. Eng. Chem. Process Des. Dev.* 18 (1979): p163-170

Baird, M. "FT Process investigated at the Pittsburgh Energy Technology Center since 1944." *Ind. Eng. Chem. Prod. Res. Dev.,* 19 (1980): p175-191

Bartholomew, C. H. "Recent technological developments in Fischer-Tropsch catalysis." *Catalysis Letters* 7 (1990): p303-314

Bohlbro, H. "An Investigation on the Kinetics of the Conversion of Carbon Monoxide with Water Vapor over Iron Oxide Based Catalysts." *Gjellerup, Copenhagen* (1969)

Bonzel, H. P. "Enhanced Rate of Carbon Deposition during Fischer-Tropsch Synthesis on K Promoted Fe." *Surface Science Letters* 109 (1981): pL527-531

Boudart, M. “Kinetics of Heterogeneous Catalytic Reactions” Princeton University Press: Princeton, NJ, 1984

Bukur, D. “Promoter Effects on Precipitated Iron Catalyst for Fischer Tropsch Synthesis.” *Ind. Eng. Chem. Res.* 29 (1990): p194-204

Bukur, D. “Pretreatment effect studies with a precipitated iron Fischer-Tropsch catalyst.” *Applied Catalysis A* 126 (1995): p85-113

Chaumette, P. “Higher alcohol and paraffin synthesis on cobalt based catalyst: comparisons of mechanistic aspects.” *Topics in Catalysis* 2 (1995): p117-126

Davis, B.H. “Fischer-Tropsch Synthesis: Comparison of Performances of Iron and Cobalt Catalysts.” *Ind. Eng. Chem. Res.* 47 (2007): p8938-8945

Dictor, R. “Fischer-Tropsch synthesis over reduced and unreduced iron oxide catalysts.” *Journal of Catal.* 97 (1986): p121-136

Diesel Fuel Spec. Sheet ASTM D975 < http://xtremefueltreatmentdenver.com/ASTM_D975_TEST.pdf> May 2010

Dixon, A. “Theoretical Prediction of Effective Heat Transfer Parameters in packed Beds.” *AIChE Journal* 25 (1979): p663-676

Dixon, A. “An improved equation for the overall heat transfer coefficient in Packed beds.” *Chemical Engineering and Processing* 35 (1996): p323-331

DOD JP-5 and JP-8(1992). <http://www.atsdr.cdc.gov/toxprofiles/tp121-c3.pdf > May 2010

Donnelly, T.J. “Analysis and Prediction of Product Distributions of the Fischer-Tropsch Synthesis.” *Energy & Fuels* 2 (1988): p734-739

Donnelly, T. J. “Product Distributions of the Fischer-Tropsch Synthesis on Precipitated Iron Catalysts.” *Applied Catalysis* 52 (1989): p93-114

Dry, M. “The influence of structural promoters on the surface properties of reduced magnetite catalysts.” *Journal of Catalysis* 6 (1966): p194-199

Dry, M. “The distribution of promoters in magnetite catalysts.” *Journal of Catalysis* 7 (1967): p352-358

Dry, M. “Heat of Chemisorptions on Promoted Iron Surfaces and the Role of Alkali in Fischer-Tropsch Synthesis.” *Journal of Catalysis* 15 (1969): p190-199

Dry, M. “The Fischer Tropsch Synthesis.” *Catalysis: Science and Technology* 1 (1981): p159-225

Dry, M. “Catalytic aspects of industrial Fischer-Tropsch synthesis.” *J. Mol. Catal.* 17 (1982): p133-144

Dry, M. “FT synthesis over iron catalyst.” *Catalysis Letters* 7 (1990): p241-252

Dry M. “Practical and theoretical aspects of the catalytic Fischer-Tropsch Process.” *Applied Catalysis A* 138 (1996): p319-344.

Dry, M. “The Fischer Tropsch Process: 1950-2000.” *Catalysis Today* 71 (2002): p227-41

Dry, M. “The Fischer-Tropsch (FT) synthesis processes.” *Handbook of heterogeneous catalysis.* 6 (2008)**:** p2965-2994

Dybjaer, I. “Tubular reforming and autothermal reforming of natural gas – an overview of available processes.” *Fuel Processing Technology* 42 (1995):p85-107

Dybkjaer, I. “Advanced reforming technologies for hydrogen production.” *International Journal of Hyrdrocarbon Engineering* 3 (1998): p56-58

Eilers, J. “The Shell Middle Distillate Synthesis Process (SMDS).” *Catalysis Letters* 7 (1990): p253-269

Eliason, S. A. “Reaction and deactivation kinetics for Fischer-Tropsch synthesis on unpromoted and potassium-promoted iron catalysts.” *App. Catalysis A* 186 (1999): p229-243

Espinoza, R.L. “Low-Temperature Fischer Tropsch synthesis from a Sasol Perspective. *Applied Catalysis A* 186 (1999): p13-26

Fernandes, F. “Modeling and optimization of Fischer-Tropsch products hydro-cracking.” *Fuel Processing Technology* 88 (2007): p207-214

Fischer, F Roelen, O.:ibid.11,489 (1930)

Forney, A. “US Bur. Mines Rep.” 5841ACS Div. Fuel 20 (1961)

Forest, C. “Fischer-Tropsch Fuels: Why are they of interest to the United States Military?” SAE Tech. Pap. Ser. (2005)

Freerks, R. “Production and Characterization of Synthetic Jet fuel Produced From Fischer Tropsch Hydrocarbons.” *Prepr. Pap.-Am. Chem. Soc., Div. Pet. Chem.* 49 (2004): p407

Frohning, C. “Fischer-Tropsch Synthese.” *Chemierohstoffe aus kohle (Falbe J., ed.)* (1977). Stuttagart: Thieme Ullmanns Encyklopadie d. techn. Chem. 9, 715 Munchen-Berlin: Urban and Schwarzenberg (1957)

Froment, G. “Chemical Reactor Analysis and Design.” John Wiley & Sons (1979) New York.

Graaf, G. “Chemical equilibria in methanol synthesis.” *Chem. Eng. Sci.* 41 (1986): p2883-2890

Gibson, J.W “The use of dual function catalyst in isomerization of high molecular weight n-paraffin.” *Industrial & Engineering Chemistry* 52(1960): p113-116

Guettel, R. “Reactors for Fischer Tropsch Synthesis.” *Chem. Eng. Tech.* 31 (2008): p746-54

Hilmen, A. “Study of the effect of water on alumina supported cobalt Fischer-Tropsch catalysts. *Applied Catalysis. A* 186 (1999), v186, p169 -188

Huff, G. “Intrinsic Kinetics of the Fischer-Tropsch Synthesis on a Reduced Fused-Magnetite Catalyst.” *Ind. Eng. Chem. Process Des. Dev*. 23 (1984): p696-705

Huff, G. “Evidence for two chain growth probabilities on Iron Catalysts in Fischer Tropsch Synthesis.” *Journal of Catalysis* 85 (1984) p370-379

Iglesia, E. “Transport-enhanced α -olefin re-adsorption pathways in ruthenium-catalyzed hydrocarbon synthesis.” *Journal of Catal.*129 (1991): p238-256

Iglesia, E. “Selectivity Control and Catalyst Design in the Fischer-Tropsch Synthesis: Sites, Pellet, and Reactors.” *Advances in Catalysis* 39 (1993): p221-298

Iglesia, E. “Design, synthesis, and use of cobalt-based Fischer-Tropsch synthesis catalyst.” *Applied Catalysis A* 161(1997): p59-78

Inoue, M. “Simple criteria to differentiate a two-site model from a distributed-site model for Fischer-Tropsch synthesis.” *Journal of Catal,*105 (1987): p266-269

Jager, B. “Experience with a new type of reactor for Fischer-Tropsch synthesis.” *Catalysis letters* 7 (1990): p293-301

Jager, B. “Advances in low temperature Fischer-Tropsch synthesis.” *Catalysis Today* 23 (1995): p17-28

Jam, S. “Enhancement of Distillate Selectivity in Fischer Tropsch Synthesis by Using Iron and Cobalt Catalyst in a Novel-Dual Bed Reactor.” *Reaction Kinetics and Catalysis Letters* 89 (2006): p71-79

Kalluri, R. “Microfibrous Supported Sorbents/Catalysts - Micro-Structured Systems with Enhanced Contacting Efficiency.” Presented at AIChE Annual Meeting. (2005)

Khodakov, A. “Advances in the Development of Novel Cobalt Fischer Tropsch for Synthesis of Long Chain Hydrocarbon and Clear fuels.” *Chemical Reviews* 107 N5 (2007): p1692-1744

Knobel, H. “Beitrag zur Fischer-tropsch Synthese on Eisenkontakten.” *Chem. Ing. Tech.* 23 (1951): p153

Kogelbauer, A. "The formation of cobalt silicates on Co/SiO2 under hydrothermal conditions." *Catalysis. Letters.* (1995) v34 p259-267

Kohl, A. "Gas Purification" (5th ed.), Gulf Publishing, Houston, TX (1997).

Lamrecht, D. "Fischer Tropsch Fuel for Use by the U.S. Military as Battlefield-use Fuel of the Future." *Energy & Fuels* 21 (2007): p1448-1453

Leib, T. "Modeling the Fischer-Tropsch Synthesis in Slurry Bubble-Column Reactors." Paper presented at the AIChE Annual Meet., San Francisco, California (Nov. 25-30, 1984)

Li, X. "Particle size distribution from a GTL engine." *Sci. Total Environment.*382 (2007): p295-303

Liu, J. "The Rectisol process for natural gas purification." *Natural Gas Chemistry* 32 (2007): p47-50

Liu, Z. "Intrinsic kinetics of Fischer-Tropsch Synthesis over Fe-Cu-K Catalyst." *J. Chem. Soc. Faraday Trans.* 91 (1995): p3255-3261

Lox, E. "Kinetics of the Fischer-Tropsch Reaction on a Precipitated Promoted Iron Catalyst, 2 Kinetics Modeling."

Lu, Yijun. "Influence of the Feed Gas Composition on the Fischer-Tropsch Synthesis in Commercial Operations." *Journal of Natural Gas Chemistry* 16 (2007): p329-341

Madon, R. "Selectivity in Catalysis" (S.L. Suib and M.E Davis, eds.), *American Chemical Society*, Washington, DC, (1993): p382

Mesheryakov, V.D. "A multifunctional reactor with a regular catalyst packing for Fischer-Tropsch synthesis." *Chemical Engineering Science* 54(1999): p1565-1570

MIL-DTL-5624U Detail Specification, Turbine Fuel, Aviation, Grades JP-4 and JP-5 < http://www.desc.dla.mil/DCM/Files/5624t.pdf> May 2010

Mohri, T. "Application of advanced material for catalyst tubes for steam reformers." *Ammonia Plant Safety* 33(1993): p86-100

Mulder H. "From Syngas to clean fuels and chemicals via Fischer-Tropsch process." Presented at Gasification, the gateway to a cleaner future, Dresden Germany, Sept. 1998.

Muzzell, P. "Composition of Syntroleum S-5 and Conformance to JP5 Specification." *Prepr. Pap.-Am. Chem Soc., Div., Pet. Chem.* 49 (2004): p411-413

Muan A. “Phase Equilibria at high temperatures in Oxide Systems involving Changes in Oxidation States.” *American Journal of Science* 256 (1958): p171-207

Niemela, M.K “The long-term performance of Co/SiO2 catalysts in CO hydrogenation.” *Catal. Letters* 42 (1996): p161-166

IntraMicron, Inc/Cerametec Topic N07-T027, Proposal Number N2-2578 (2009)

O’Brien, R.J and Davis, B.H. “Activation of Precipitated Iron Fischer Tropsch Catalyst.” *Energy & Fuels* 10 (1996): p921-926

Petroconsultants-MIA and Zeus International “Remote Gas Development Strategies.” HIS Energy Services (1999)

Pichler, H. :ibid (1952) vol. 4

Post M.F.M. “Diffusion Limitation in Fischer-Tropsch Catalyst.” *AIChE Journal* 35 (1989): p1107-1114

Precombusion Decarburization, IEA Greenhouse Gas Program, Report #PH2/19, p22

Quan-Sheng, L. “Steady-State and Dynamic Behavior of fixed Bed Catalytic Reactor for Fischer Tropsch Synthesis II. Steady State and Dynamic Simulation Results.” *J. of Nat. Gas Chem.* 8 (1999): p238-248

James L. “Recovering carbon monoxide from fuel gas.” *U.S Patent* -3716619 (1971)

Rao, V. “Iron-based catalysts for slurry-phase Fischer-Tropsch process: Technology.” *Fuel Process technology* 30 (1992): p83-107

Ronald, M. “New developments in Gas to Liquid Technology.” CERI 2004 Petrochemical Conference, Alberta, Canada. (2004).

Rostrup-Nielen, J.R *Catalysis, Science and Technology*, (1984) Springer-Verlag, Berlin.

Sarup, B. “Studies of the Fischer-Tropsch Synthesis on a cobalt catalyst. I. Evaluation of product distribution parameters from experimental data.” *Canadian Journal Chemical Engr.* 66 (1988): p831-843

Schanke, D. **“**Study of the deactivation mechanism of Al2O3-supported cobalt Fischer-Tropsch catalysts” *Catalysis Letters* 34 (1995): p269-284

Seider, W.D. and Lewin, D.R. “Process Design Principles.” (2004) 2nd Ed. John Wiley and Sons Inc. NY.

Sheng, M. “Measuring thermal Conductivity with MFEC.” (2010) (Auburn University-Unpublished)

Song, H. “Operating Strategies for Fischer-Tropsch Reactors: A Model-Directed Study.” *Journal of Chemical Engineering* 21(2004): p308-317.

Speight, J. "Liquid Fuels from Natural Gas." *Handbook of Alternative Fuel Technologies.* (2007): p153-170

Steen, van Eric. "Polymerization Kinetics of the Fischer-Tropsch CO hydrogenation using iron and cobalt based Catalyst." *Applied Catalysis A* 186 (1999): p309

Steynberg, A. "Introduction to Fischer Tropsch Technology." *Studies in Surface Science and Catalysis* 152 (2004): p1-63

Steynberg, A. "Fischer Tropsch Reactors." *Studies in Surface Science and Catalysis* 152 (2004): p64-195

Sturtevant, P. "Fischer-Tropsch Wax Characterization and Upgrading: Final Report." *DOE Report,* DE88014638 **(**1988).

Thacheray, F. "GTL in 2007." *Petroleum Reviews* (2003) p18-19

Tindal, A. "Natural gas reforming technologies." Gas-to-Liquids Processing; Bringing Clean Fuels to market, San Antonio, TX, March 18-20 1998

Twigg, M. V "The Catalyst: Preparation, Properties and Behavior in Use." *Catalysis and Chemical Process* (1981) R. Pearce and W.R Patterson p11

U.S Energy Information Administration – Independent Statistics and Analysis. < http://tonto.eia.doe.gov/energy_in_brief/foreign_oil_dependence.cfm> May 2010.

Van Berge, P.J. "Cobalt as an alternative Fischer-Tropsch catalyst to iron for the production of middle distillates." *Studies in Surface Science and Catalysis* 107 (1997): p207-212

Van der Laan, G. "Kinetics and Selectivity of the Fischer-Tropsch Synthesis: A Literature Review." *Catal. Rev. Science Engineering* 41 (1999): p255-315

Walas, Personal Communications (1985)

Walas, S. "Chemical Process Equipment Selection and design." 2nd Ed. Butterworth Publishers (1988) Newton

Weitkamp, J. "Factors influencing the selectivity of hydro-cracking in zeolites." In: Barthomeuf, D.,, Guidelines for Mastering the Properties of Molecular Sieves. (1990): p343. Plenum Press, NY.

Yermakova, A. "Thermodynamica Calculations in the Modeling of Multiphase Processes and Reactors." *Ind. Eng. Chem. Res.* 39 (2000): p1453-1472

Appendix I

Tapped density is easily measured by placing a powder sample in a volumetric flask and weighing it. The sample is tapped to settle the particles as much as possible. Bulk density is the density of the material without any pore volume. This data is usually available in the literature, handbooks etc. It can be measured by immersing a known weight of sample in a fluid that wets the sample. The bulk density can then be calculated from the increase in volume. Particle density can be calculated from pore volume and bulk density as follows.

$$\frac{1}{\rho_{particle}} = v_p + \frac{1}{\rho_{bulk}} \qquad \text{[AP1.1]}$$

The tap density, bed voidage and particle density are related as follows:

$$\rho_{tap} = (1-\varepsilon)\rho_{particle} \qquad \text{[AP1.2]}$$

Bed voidage can be estimated from the tap density as follows:

$$1-\varepsilon = \frac{\rho_{tap}}{\rho_{particle}} \qquad \text{[AP1.3]}$$

If catalyst or sorbent is loaded on the particles then the total volume of the particles does not change but the weight increases. The formula above can be modified to account for this increased weight.

$$\frac{1}{\rho_{particle}} = v_p + \frac{1}{\rho_{bulk}(1+L)} \qquad \text{[AP1.4]}$$

Appendix II

Derivation of a Segregated 2-D Model for Heat-up of a Packed Tube with Flowing Gas.

The partial differential equations describing the heat balance between gas, catalyst and fibers inside the tube are as follows:

$$\psi\rho_g C_{pg}\frac{\partial \mathrm{T_g}}{\partial \mathrm{t}} = k_g\frac{1}{\mathrm{r}}\frac{\partial}{\partial r}\left(\mathrm{r}\frac{\partial \mathrm{T_g}}{\partial r}\right) + \mathrm{k_g}\frac{\partial^2 \mathrm{T_g}}{\partial \mathrm{z}^2} - \rho_f C_{pf} v_z \frac{\partial \mathrm{T_g}}{\partial \mathrm{z}} - \mathrm{x_c}(1-\psi)\mathrm{a_c h_{gc}}\left(\mathrm{T_g}-\mathrm{T_c}\right)$$

$$-\mathrm{x_f}(1-\psi)\mathrm{a_f h_{gf}}\left(\mathrm{T_g}-\mathrm{T_f}\right) \qquad \text{[Ap2.1]}$$

$$\mathrm{x_c}(1-\psi)\rho_c C_{pc}\frac{\partial \mathrm{T_c}}{\partial \mathrm{t}} = k_c\frac{1}{\mathrm{r}}\frac{\partial}{\partial r}\left(\mathrm{r}\frac{\partial \mathrm{T_c}}{\partial r}\right) + \mathrm{k_c}\frac{\partial^2 \mathrm{T_c}}{\partial \mathrm{z}^2} - \mathrm{x_c}(1-\psi)\mathrm{a_c h_{gc}}\left(\mathrm{T_c}-\mathrm{T_g}\right) \qquad \text{[AP2.2]}$$

$$\mathrm{x_f}(1-\psi)\rho_f C_{pf}\frac{\partial \mathrm{T_f}}{\partial \mathrm{t}} = k_f\frac{1}{\mathrm{r}}\frac{\partial}{\partial r}\left(\mathrm{r}\frac{\partial \mathrm{T_f}}{\partial r}\right) + \mathrm{k_f}\frac{\partial^2 \mathrm{T_f}}{\partial \mathrm{z}^2} - \mathrm{x_f}(1-\psi)\mathrm{a_f h_{gf}}\left(\mathrm{T_f}-\mathrm{T_g}\right) \qquad \text{[AP2.3]}$$

With boundary conditions: $T=T_0$ at z=0. And $T=T_{bath}$ at the outside of the tube. x_c and x_f are the volume fraction of the solid phases occupied by the catalyst and fiber phases ($x_c + x_f=1$). The specific surface areas of the catalyst and fibers are designated by a_c and a_f. The bed voidage is represented by ψ.

Define:, $\lambda_c = \frac{\mathrm{a_c h_{gc}}}{\rho_c C_{pc}}$, $\lambda_f = \frac{\mathrm{a_f h_{gf}}}{\rho_f C_{pf}}$, $\alpha_g = \frac{k_g}{\rho_g C_{pg}}$, $\alpha_g = \frac{k_f}{\rho_f C_{pf}}$, x=z/L and ξ=r/R.

A heat transfer coefficient is applied at the interface of the tube wall and the gas, catalyst and fiber phases.

$$-k_g\frac{\partial \mathrm{T_g}}{\partial r} = h_{gw}\left(T_g - T_w\right) \ , -k_g\frac{\partial \mathrm{T_g}}{\partial r} = h_{gw}\left(T_g - T_w\right) \ -k_g\frac{\partial \mathrm{T_g}}{\partial r} = h_{gw}\left(T_g - T_w\right) \qquad \text{[AP2.4]}$$

Also, the total heat transferred into the gas, catalyst and fiber phases is equal to that coming through the wall of the tube.

$$k_w \frac{\partial T_w}{\partial r} = k_g \frac{\partial T_g}{\partial r} + k_c \frac{\partial T_c}{\partial r} + k_f \frac{\partial T_f}{\partial r} \quad \text{at r=R} \qquad \text{[AP2.5]}$$

A pseudo steady-state assumption for the temperature in the tube wall allows for the effect of the limitation of the thermal conductivity of the tube material to be included in the heat transfer model.

$$0 = \frac{1}{r}\frac{\partial}{\partial r}\left(r\frac{\partial T_w}{\partial r}\right) \qquad \text{[AP2.6]}$$

Given $T_w=T_\infty$ at r=R+W and T_w at r=R, estimate $\frac{\partial T_w}{\partial r}$ at r=R and combine this value in Equation 2. W is the wall thickness.

$$\frac{\partial T_g}{\partial t} = \frac{\alpha_g}{\psi R^2}\frac{1}{\xi}\frac{\partial}{\partial \xi}\left(\xi\frac{\partial T_g}{\partial \xi}\right) + \frac{\alpha_g}{\psi L^2}\frac{\partial^2 T_g}{\partial x^2} - \frac{v_z}{\psi L}\frac{\partial T_g}{\partial x} - \frac{x_c(1-\psi)\lambda_c}{\psi}\left(T_g - T_c\right) - \frac{x_f(1-\psi)\lambda_f}{\psi}\left(T_g - T_f\right)$$

[AP2.7]

$$\frac{\partial T_c}{\partial t} = \frac{\alpha_c}{(1-\psi)R^2}\frac{1}{\xi}\frac{\partial}{\partial \xi}\left(\xi\frac{\partial T_c}{\partial \xi}\right) + \frac{\alpha_c}{(1-\psi)L^2}\frac{\partial^2 T_g}{\partial x^2} - \lambda_c\left(T_c - T_g\right) \qquad \text{[AP2.8]}$$

$$\frac{\partial T_f}{\partial t} = \frac{\alpha_f}{(1-\psi)R^2}\frac{1}{\xi}\frac{\partial}{\partial \xi}\left(\xi\frac{\partial T_f}{\partial \xi}\right) + \frac{\alpha_f}{(1-\psi)L^2}\frac{\partial^2 T_f}{\partial x^2} - \lambda_f\left(T_f - T_g\right) \qquad \text{[AP2.9]}$$

$\left(T_w - T_g\right) = \frac{k_g}{h_{gw}R}\frac{\partial T_g}{\partial \xi}$,

$(T_w - T_c) = \frac{k_c}{h_{cw}R}\frac{\partial T_c}{\partial \xi}$ and

$\left(T_w - T_f\right) = \frac{k_c}{h_{cw}R}\frac{\partial T_f}{\partial \xi}$ at ξ=1 [AP2.10]

$$-k_w \frac{\partial T_w}{\partial \xi} = h_g\left(T_g - T_w\right) + h_c(T_c - T_w) + h_f(T_f - T_w) \quad \text{at } \xi=1, \qquad \text{[AP2.11]}$$

$0 = \frac{1}{\xi}\frac{\partial}{\partial \xi}\left(\xi\frac{\partial T_w}{\partial \xi}\right)$ with $T_w=T_{bath}$ at r=R+W [AP2.12]

Integrating Equation 12 and applying the boundary conditions results in the following expression for the radial derivative of temperature in the tube wall:

$$\frac{dT_w}{dr} = \frac{1}{R}\frac{T_\infty - T_w}{\ln\left(1+{}^{W}/_{R}\right)} \qquad \text{[AP2.13]}$$

Combining Equations 11 and 13 gives an expression for the wall temperature as a function of the temperatures of the outer wall and the segregated phases:

$$T_w = \frac{T_\infty + (h_{gw}T_g + h_{cw}T_c + h_{fw}T_f)\frac{R}{k_w}\ln(1+{}^{W}/_{R})}{1+(h_{gw}+h_{cw}+h_{fw})\frac{R}{k_w}\ln(1+{}^{W}/_{R})} \quad \text{at } \xi=1. \qquad \text{[AP2.14]}$$

Discretization of the Segregated Energy Balances in Cylindrical Coordinates

The radial coordinate is expressed as □$_i$ =(i-1)*□□and the axial coordinate as x_j=(j-1)*□x. A radial average can be obtained by volume averaging from point i-1 to point i+1 as follows:

$$\langle y\rangle_i = \frac{\int_{\xi_{i-1}}^{\xi_i} \xi\frac{(y_{i-1}+y_i)}{2}d\xi + \int_{\xi_i}^{\xi_{i+1}} \xi\frac{(y_{i-1}+y_i)}{2}d\xi}{\int_{\xi_{i-1}}^{\xi_{i+1}} \xi d\xi}$$

The resulting formula is: $\langle y\rangle_i = \frac{(2i-3)T_{i-1}+4(i-1)T_i+(2i-1)T_{i+1}}{8(i-1)}$ [AP2.15]

In a similar manner, a three point approximation for the second order radial derivative can be obtained by volume averaging from point i-1 to point i+1. The resulting formula is as follows:

$$\frac{1}{\xi}\frac{\partial}{\partial\xi}\left(\xi\frac{\partial T}{\partial\xi}\right) = \frac{(2i-3)T_{i-1}-4(i-1)T_i+(2i-1)T_{i+1}}{2(i-1)\Delta\xi^2} \qquad \text{[AP2.16]}$$

A discrete form of Equation 7 can be written using equation 16 for the second order radial derivative of temperature and standard central finite differences for the other terms. Radial averaging using Equation 13 will be used to eliminate the odd/even disconnect that can occur when central finite differences are employed for the first order axial derivative. Replacing the terms in Equations 7, 8 and 9 with central finite differences and averaging the convective flow term over the radial dimension results in the following expressions:

$$\frac{Tg_{j,i}^{n+1}-Tg_{j,i}^{n}}{\Delta t} =$$

$$-\frac{v_z}{\psi L 2\Delta x}\frac{(2i-3)\left(Tg_{j+1,i-1}^{n}-Tg_{j-1,i-1}^{n}\right)+4(i-1)\left(Tg_{j+1,i}^{n+1}-Tg_{j-1,i}^{n+1}\right)+(2i-1)\left(Tg_{j+1,i+1}^{n}-Tg_{j-1,i+1}^{n}\right)}{8(i-1)}+$$

$$\frac{\alpha_g}{\psi R^2\Delta\xi^2}\left(\frac{(2i-3)T_g{}^n_{j,i-1}-4(i-1)T_g{}^{n+1}_{j,i}+(2i-1)T_g{}^n_{j,i+1}}{2(i-1)}\right)+\frac{\alpha_g}{\psi L^2\Delta x^2}\left(T_g{}^{n+1}_{j-1,i}-2T_g{}^{n+1}_{j,i}+T_g{}^{n+1}_{j+1,i}T_g\right)-\frac{x_c(1-\psi)\lambda_c}{\psi}\left(T_{g_{j,i}}{}^{n+1}-T_{c_{j,i}}{}^{n+1}\right)-\frac{x_f(1-\psi)\lambda_f}{\psi}\left(T_{g_{j,i}}{}^{n+1}-T_{f_{j,i}}{}^{n+1}\right)$$

[AP2.17]

$$\frac{T_{c_{j,i}}{}^{n+1}-T_{c_{j,i}}{}^n}{\Delta t}=\frac{\alpha_c}{(1-\psi)R^2\Delta\xi^2}\left(\frac{(2i-3)T_{c_{j,i-1}}{}^n-4(i-1)T_{c_{j,i}}{}^{n+1}+(2i-1)T_{c_{j,i+1}}{}^n}{2(i-1)}\right)+\frac{\alpha_c}{(1-\psi)L^2\Delta x^2}\left(T_{c_{j-1,i}}{}^{n+1}-2T_{c_{j,i}}{}^{n+1}+T_{c_{j+1,i}}{}^{n+1}T_g\right)-\lambda_c\left(T_{c_{j,i}}{}^{n+1}-T_{g_{j,i}}{}^{n+1}\right)$$

[AP2.18]

$$\frac{T_{f_{j,i}}{}^{n+1}-T_{f_{j,i}}{}^n}{\Delta t}=\frac{\alpha_f}{(1-\psi)R^2\Delta\xi^2}\left(\frac{(2i-3)T_{f_{j,i-1}}{}^n-4(i-1)T_{f_{j,i}}{}^{n+1}+(2i-1)T_{f_{j,i+1}}{}^n}{2(i-1)}\right)+\frac{\alpha_f}{(1-\psi)L^2\Delta x^2}\left(T_{f_{j-1,i}}{}^{n+1}-2T_{f_{j,i}}{}^{n+1}+T_{f_{j+1,i}}{}^{n+1}\right)-\lambda_f\left(T_{f_{j,i}}{}^{n+1}-T_{g_{j,i}}{}^{n+1}\right)$$

[AP2.19]

The right side of these equations with all values at the same time are the residuals at point (j,i). The residuals are computed at each time step to monitor the approach to steady-state.

A line implicit solution in the axial direction will be used to integrate the discrete equations to the steady-state solution. This results in a block tri-diagonal system of linear equations:

$$\left(-\frac{v_z}{4\psi L\Delta x}-\frac{\alpha_g}{\psi L^2\Delta x^2}\right)T_g{}^{n+1}_{j-1,i}+\left[\frac{1}{\Delta t}+\frac{2\alpha_g}{\psi}\left(\frac{1}{R^2\Delta\xi^2}+\frac{1}{L^2\Delta x^2}\right)+\frac{(1-\psi)(x_c\lambda_c+x_f\lambda_f)}{\psi}\right]T_g{}^{n+1}_{j,i}-\frac{(1-\psi)x_c\lambda_c}{\psi}\lambda_c T_c{}^{n+1}_{j,i}-\frac{(1-\psi)x_f\lambda_f}{\psi}\lambda_f T_f{}^{n+1}_{j,i}+\left(\frac{v_z}{4\psi L\Delta x}-\frac{\alpha_z}{\psi L^2\Delta x^2}\right)T_g{}^{n+1}_{j+1,i}=$$

$$\frac{T_g{}^n_{j,i}}{\Delta t}-\frac{v_z}{2\psi L\Delta x}\frac{\left[(2i-3)\left(T_g{}^n_{j+1,i-1}-T_g{}^n_{j-1,i-1}\right)+(2i-1)\left(T_g{}^n_{j+1,i+1}-T_g{}^n_{j-1,i+1}\right)\right]}{8(i-1)}+\frac{\alpha_g}{\psi R^2\Delta\xi^2}\left(\frac{(2i-3)T_g{}^n_{j,i-1}+(2i-1)T_g{}^n_{j,i+1}}{2(i-1)}\right)$$

[AP2.20]

$$\left(-\frac{\alpha_c}{(1-\psi)\mathrm{L}^2\Delta\mathrm{x}^2}\right)T_{c}{}_{j-1,i}^{n+1} - \lambda_c T_{g}{}_{j,i}^{n+1} + \left[\frac{1}{\Delta\mathrm{t}} + \frac{2\alpha_c}{(1-\psi)}\left(\frac{1}{\mathrm{R}^2\Delta\xi^2} + \frac{1}{\mathrm{L}^2\Delta\mathrm{x}^2}\right) + \lambda_c\right]T_{c}{}_{j,i}^{n+1} + \left(-\frac{\alpha_c}{(1-\psi)\mathrm{L}^2\Delta\mathrm{x}^2}\right)T_{c}{}_{j+1,i}^{n+1} =$$

$$\frac{T_{c}{}_{j,i}^{n}}{\Delta\mathrm{t}} + \frac{\alpha_c}{(1-\psi)\mathrm{R}^2\Delta\xi^2}\left(\frac{(2i-3)T_{c}{}_{j,i-1}^{n} + (2i-1)T_{c}{}_{j,i+1}^{n}}{2(i-1)}\right)$$

[AP2.21]

$$\left(-\frac{\alpha_f}{(1-\psi)\mathrm{L}^2\Delta\mathrm{x}^2}\right)T_{f}{}_{j-1,i}^{n+1} - \lambda_f T_{g}{}_{j,i}^{n+1} + \left[\frac{1}{\Delta\mathrm{t}} + \frac{2\alpha_f}{(1-\psi)}\left(\frac{1}{\mathrm{R}^2\Delta\xi^2} + \frac{1}{\mathrm{L}^2\Delta\mathrm{x}^2}\right) + \lambda_f\right]T_{f}{}_{j,i}^{n+1}$$

$$+ \left(-\frac{\alpha_c}{(1-\psi)\mathrm{L}^2\Delta\mathrm{x}^2}\right)T_{f}{}_{j+1,i}^{n+1}$$

$$= \frac{T_{f}{}_{j,i}^{n}}{\Delta\mathrm{t}} + \frac{\alpha_f}{(1-\psi)\mathrm{R}^2\Delta\xi^2}\left(\frac{(2i-3)T_{f}{}_{j,i-1}^{n} + (2i-1)T_{f}{}_{j,i+1}^{n}}{2(i-1)}\right)$$

[AP2.22]

The boundary condition at the inlet for these energy balances is a fixed temperature. The zero axial derivative at the exit of the tube is accounted for using a one-sided three point derivative.

$T_{1,i}^{n+1} = T_{inlet}$ and $T_{k}{}_{M-1,i}^{n} - 4T_{k}{}_{M,i}^{n+1} + 3T_{k}{}_{M+1,i}^{n+1} \Big/ 2\Delta z = 0$, k=gas, catalyst and fiber.

This set of 3x(M+1) equations was solved for different radial coordinates sweeping from the tube wall to one point away from the centerline. The solutions were updated as soon as new values were computed. At the centerline the radial derivative is zero, so the values at the second radial point were used for the centerline values.

A three point one-sided derivative that maintains second order accuracy is as follows:

$$\frac{\partial T}{\partial \xi} = \frac{T_{i-2} - 4T_{i-1} + 3T_i}{2\Delta\xi} \qquad \text{[AP2.23]}$$

Inserting Equation 23 into Equation 10 for either the gas, catalyst or fiber phase gives a formula for updating the temperature of that phase at the wall:

$$\left(T_w - T_{k}{}_{j,i}^{n+1}\right) = \frac{k_g}{h_{gw}R}\frac{T_{k}{}_{j,i-2}^{n} - 4T_{k}{}_{j,i-1}^{n} + 3T_{k}{}_{j,i}^{n+1}}{2\Delta\xi}$$

Rearranging this equation results in the following expression:

$$T_{k\,j,i}^{\,n+1} = \frac{T_{w\,j} + \frac{k_g}{h_{gw} R 2 \Delta \xi} \left(4 T_{k\,j,i-1}^{\,n} - T_{k\,j,i-2}^{\,n} \right)}{1 + 3 \frac{k_g}{h_{gw} R 2 \Delta \xi}} \qquad \text{[AP2.24]}$$

The k subscript represents the gas, catalyst or fiber phase.

Appendix III

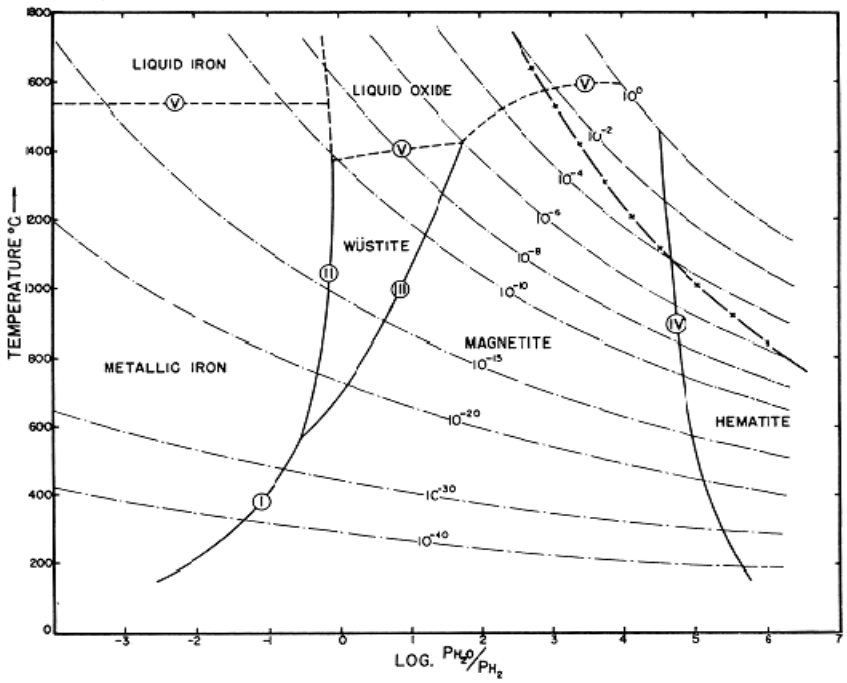

AP Figure 1 Phase Diagram for Iron Magnetite[i]

The following figure is used to illustrate the trends and possible phase change with respect to temperature for Iron. At a LTFT, the risk of phase change is minimal. The risk increases when running a HTFT.

[i] Muan A. "Phase Equilibria at high temperatures in Oxide Systems involving Changes in Oxidation States." *American Journal of Science* 256 (1958): p171-207

Appendix IV

Steam Reactor and Furnace

The Steam Reforming Reactor was modeled as a fired heat exchanger. Where the numbers of tubes and cross sectional area were calculated using the following equations listed below. The following results are for Case B as an example

Ap Table 1. Summary of Size

SIZING:	Packed Bed	MFEC
WHSV [lbs NGAS/hr/lb Cat]	1.25	1.25
Cat Density [lbs/ft^3]	54	54
Flow Rate NGAS [lb/hr]	7200	6821
Amount Catalyst [lbs]	5760	5457
Volume Catalyst [ft^3]	107	101
Bed Voidage	0.45	0.45
Steam Reactor Volume [ft^3]	194	184
Flowrate [Ft^3/hr]	5379000	49724
Flowrate [Ft^3/s]	1494	1494
Volume, [Cubic ft]	75	69
Diameter, [Ft]	8	8
Height, Ft	4	4
Number of Tubes:	9864	9864
Tube Diameter [ft]	0.167	0.167
Surface Area of Stm Reactor [ft ^2]	65	65
Shell Wall Thickness, [ft]	0.5	0.5
Tube thickness, [ft]	0.0262	0.0262
Total Weight [Tonne]	269	256

$$\text{Amount of Catalyst} = \frac{FlowrateNgas}{WHSV} \qquad \text{(AP4.1)}$$

$$\text{Steam Reactor Volume} = \frac{volumeofCatalyst}{1 - BedVoidage} \quad \text{(AP4.2)}$$

$$\text{Area of Reactor} = \frac{SteamreactorVolume}{Lengthofreactor} \quad \text{(AP4.3)}$$

[ii] $$N_{tubes} = \frac{Areaofreactor}{TubeArea * 0.3} \quad \text{(AP4.4)}$$

The length of the tubes was calculated from the reformer volume. By specifying the tube diameter, the cross sectional area was calculated. The Steam Reformer consists of a fired furnace which is ignored.

FTS Reactor

Ap Table 2. Summary of Size

	Packed Bed	MFEC
Number of Tubes:	2050	1100
Tube Diameter [ft]	0.167	0.167
Tube Length [ft]	42	30
Tube Volume [ft^3]	0.86	0.44
Total Tube Volume (w/o catalyst voidage) [ft^3]	1758	393
Catalyst Voidage	0.38	0.75
Reactor Volume [ft^3]	949	110
Reactor Volume, [m^3]	27	3
Cat Density [lbs/ft^3]	943	1500
Amount Catalyst [lbs]	55904	9198
Wall Thickness, [ft]	0.5	0.5
Density of Steel, [lb/ft3]	553	553
Total Volume,[ft3]	1496	597
Total Wight, [Tonne]	375	128

The following formulas listed below are the calculations that were made in order to figure out the cost of the FTS reactor and its size.

$$Tv = \Pi r^2 L \quad \text{(AP4.5)}$$

[ii] Seider, W.D. Seader, J.D. and Lewin, D.R.. *Process Design Principles*. John Wiley and Sons Inc. NY. 2nd Ed. 2004.

Tube Volume

$$Tv_{w/outcatalyst} = Tv * N_{tubes} \tag{AP4.6}$$

Total tube Volume w/out Catalyst

$$R_v = \frac{Tv_{w/outcatalyst}}{\alpha} \qquad R_A = N_{tubes}\Pi * T_{diameter} * T_{length} \tag{AP4.7}$$

Distillation Towers

In order, evaluate the distillation column size, certain assumptions were made. These assumptions include no foaming; the sieve trays area ratio is greater than 0.1. The final assumption was that there is 24 in. spacing between the trays. A 4 minute liquid hold up was assumed in the reflux accumulator drums.

Ap Table 3. Summary of Size

Dimensions of Distillation Tower		Reflux Accumulator Drum	
Fraction, f	0.8	Flow rate, Ib/Min	16118
Foaming Factor, F_F	1	Liquid Hold Up	4
Hole Area factor, F_{HA}	1	Volumetric Flow rate cft	64472
Surface tension, σ_{H2O} (dyne/cm)	72.7	Vessel Volume cft	107453.
Surface tension, σ_{HC} (dyne/cm)	22.7	Length (Ft)	85.508
σ (dyne/cm)	17.26	Diameter (ft)	40
Surface Tension factor, F_{ST}	0.97	Ratio	2.13
Density, ρ_G (g/cm^3)	0.0051		
Density, ρ_L (g/cm^3)	0.683		
Gas, mass velocity, G (g/s)	100044		
Liquid, mass velocity, L (g/s)	84629		
Flow ratio, F_{LG}	0.073		
Flooding Correlation for sieve, C_{SB} (ft/s)	0.37		
Capacity, parameter, C (ft/s)	0.359		
Vapor flooding velocity, U_f (ft/s)	4.126		
D_T (ft)	7		
H (ft)	36		
E, fractional Weld efficiency	0.850		

$$t_P = \frac{P_d D}{2SE - 1.2P_d} \tag{AP4.8}$$

This is the wall thickness [inches]

$$P_d = \exp\left[0.60608 + 0.91615*\left(0.91615*Ln(P_0)\right) + 0.0015655*(\ln(P_O))^2\right] \quad \text{(AP4.9)}$$

Po is the operating pressure. In order to calculate the diameter of the Column, the following equation was used;

$$D_T = \left(\frac{4G}{FU_f \Pi(1-\frac{A_d}{A_T})\rho_G}\right)^{\frac{1}{2}} \quad \text{(AP4.10)}$$

where $U_f = C\left(\frac{\rho_l - \rho_G}{\rho_G}\right)^{\frac{1}{2}}$ (AP4.11)

The parameter is for towers with perforated sieve plates.

We assumed $(\frac{A_d}{A_T}) = 0.1$ because the flow ratio, parameter F_{LG} was less than 0.1

Where the weight is related to the thickness of the shell, and Height and diameter of the column

$$W = \Pi(D + t_S)(L + 0.8D)(t_S\rho) \quad \text{(AP4.12)}$$

Ap. Table 4. Results of Distillation Column Size

	PB	MFEC
COLUMN COST	**7 ft diameter**	**5 ft diameter**
Wall thickness, ts [ft]	0.0833	0.0833
Column Diameter, Di [ft]	7	5
Column Height, L [ft]	36	36
p (CS) [lb/ft^3]	490	490
Column weight, W [lb]	37785	11733

Flash

It is assumed that the material of construction will be carbon steel.

Ap. Table 5. Results of Distillation Column Comparison

SIZING:		
Umax, Ft/Sec	3.63	3.51
K, Ft/sec	0.35	0.35
Pl, liquid Density, Ib/Ft^3	35.83	46.75
Pv, Vapor Density, Ib/FT^3	0.33	0.46
Vapor Rate Ft^3/hr	134400	1183000
Vapor Flowrate Ft^3/s	37.33	328
Diameter, Ft	3.61	10.916
Height, Ft, Hl	5.46	0.210
Height Hv 4	4	4
Total Height or Length [Ft]	9.45	4.21
t, Liquid Hold up, [mins]	4	4
Liquid Flow rate, [Ft^3/s]	3.87	0.510
Thickness, [in]	1.440	1.87
Pd, internal Design [Psig]	813.5	358
Di, inside diameter, [Inches]	43.42	130
S, Max allowable Stress of Shell Material, [psi]	15000	15000
E, fractional Weld efficiency	0.85	0.85
Po, Operating Pressure, [psig]	720	300
Temperature inside the flash, [F]	100	150

Max Vapor Velocity

$$U\max = \left(K * \frac{P_l - P_v}{P_V} \right)^{\frac{1}{2}} \quad \text{K = 0.35 w/Demister} \qquad \text{(AP4.13)}$$

$$D\min = \left(\frac{4Q_v}{\Pi U \max} \right)^{\frac{1}{2}} \qquad \text{(AP4.14)}$$

Overall , Height = $H_l + H_v$. Assumed , Liquid Holdup, t_l is about 4 mins

$$H_l = \left(K * \frac{4 * t_l * Q_l}{\Pi * D^2} \right) \qquad \text{(AP4.15)}$$

Ap. Table 6. Summary weight of Flash Columns

The Flash	Separation Flash	H20 Flash
Total volume is [Ft^3}	97	394
Thickness [Ft]	0.12	0.156
Head Volume [ft^3]	10	93
Shell [Ft^3]	12	22
Total Vol [Ft^3]	33	209
den of SS [Ib/cft]	505	505
W [Ib]	16903	105921

Heat Exchangers

The following are sample calculations use. The Total spreadsheet cannot be shown

Ap. Table 7. Summary weight of Flash Columns

	B22	B23
Q[Btu/hr]	5,701,431	10,855,268
T_process_1[F]	90	100
T_process_2[F]	950	950
T_medium_1[F]	1384	1327
T_medium_2[F]	1327	1290
DT1	434	377
DT2	1237	1190
DT2-DT1	803	813
ln(DT2/DT1)	1	1
T_mean	767	707
R	0.1	0.04
S/P	15	23
Ft	1	1
U[Btu/hr-sqft-F]	150	150
A[ft2]	50	79
Shell Radius[ft]	4	5
total no of tubes	496	804
Shell ID thickness[ft]	0.03125	0.03125
tube tickness[ft]	0.00583	0.00583
p (CS) [lb/ft^3]	490	490
Tube Weight[Ibs]	24281	39358
Shell Weight[Ibs]	98908	157532
Weight[Ibs]	123189	196890
Weight[tonne]	56	89
Volume[ft3]	251	402
Volume[m3]	7	11

Hydro-cracking

Ap. Table 8. Summary Hydro-cracking Unit

HYDROCRACKING	
Hydrocracking yield(%)	80
WAX input to the process (kg/h)	750
residue unreacted (kg/h) (recycle)	150.00
total wax input (kg/h)	900.00
Hydrogen that reacts (kg/h)	4.5
Hydrogen excess (kg/h)	1.35
total H2 input reactor (kg/h) 65% of total wax input, weight	5.85
TOTAL INPUT (kg/h)	905.85
	with a yield of 5% (weight) for gas, 15% gasoline and 80% diesel
diesel produced (kg/h)	603.60
nafta produced (kg/h)	113.18
gas produced (kg/h) only saturated gases	37.73
TOTAL OUTPUT (kg/h)	755.85

Ap. Table 9. Summary Hydro-cracking Unit Variables Used in Aspen

		distribution		
diesel (saturated hydrocarbon)	PM (kg/kmol)	weight fraction	kg/h (reactor output)	**Yield (*)**
C12	170	0.1627	98.23	0.1084
C13	184	0.1587	95.76	0.1057
C14	198	0.1508	91.02	0.1005
C15	212	0.1426	86.09	0.0950
C16	226	0.1398	84.39	0.0932
C17	240	0.1298	78.32	0.0865
C18	254	0.1156	69.78	0.0770
tot		1.000	603.60	
gas	kg/h produced	**Yield**		
CH4	9.43	0.0104		
C2H6	9.43	0.0104		
C3H8	9.43	0.0104		
C4H10	9.43	0.0104		
tot	37.73			

	distribution			
gasoline	weight fraction	kg/h produced	**Yield**	
C5	0.014	1.61	0.0018	5
C6	0.028	3.21	0.0035	6
C7	0.065	7.40	0.0082	7
C8	0.146	16.48	0.0182	8
C9	0.237	26.79	0.0296	9
C10	0.253	28.64	0.0316	10
C11	0.257	29.04	0.0321	11
tot	1.000	113.18		tot

	distribution	
atoms of C	weight fraction	**Yield**
19	0.130312751	0.0216
20	0.103849238	0.0172
21	0.086206897	0.0143
22	0.071371291	0.0118
23	0.059743384	0.0099
24	0.052927025	0.0088
25	0.04691259	0.0078
26	0.042502005	0.0070
27	0.037690457	0.0062
28	0.034482759	0.0057
29	0.030473136	0.0050
30	0.028468324	0.0047
31	0.026463512	0.0044
32	0.023255814	0.0039
33	0.021251002	0.0035
34	0.020048115	0.0033
35	0.018043304	0.0030
36	0.016439455	0.0027
37	0.015236568	0.0025
38	0.014033681	0.0023
39	0.013231756	0.0022
40	0.011627907	0.0019
41	0.010825982	0.0018
42	0.009222133	0.0015
43	0.008821171	0.0015
44	0.008420209	0.0014
45	0.008019246	0.0013
46	0.007217322	0.0012
47	0.006014435	0.0010
48	0.005613472	0.0009
49	0.004811548	0.0008
50	0.004410585	0.0007
51	0.004009623	0.0007
52	0.003608661	0.0006
53	0.002806736	0.0005

54	0.002405774	0.0004
55	0.002004812	0.0003
56	0.002004812	0.0003
57	0.002004812	0.0003
58	0.001202887	0.0002
59	0.000801925	0.0001
60	0.000801925	0.0001
61	0.000400962	0.0001

Appendix V

Fe/Cu/K/La- Al_2O_3

POLYMATH Report
Nonlinear Regression (mrqmin)

15-Mar-2010

Model: C02 = A*0.3189+B*(1-0.0039*((C01+273.15)-533))

Variable	Initial guess	Value	95% confidence
A	0.8	0.9842637	0.3476149
B	0.3	0.4598872	0.1051788

NOTE: Calculations exceeded the maximum number of iterations.

Nonlinear regression settings
Max # iterations = 64
Tolerance = 0.0001

Precision

R^2	0.9046731
R^2adj	0.8951405
Rmsd	0.0040368
Variance	0.0002347
Chi-Sq	0.234663
Alamda	1.0E+52

General

Sample size	12
Model vars	2
Indep vars	1
Iterations	65

Source data points and calculated data points

	C01	C02	C02 calc	Delta C02
1	210	0.855	0.8631779	-0.0081779
2	210	0.85	0.8631779	-0.0131779
3	220	0.84	0.8452423	-0.0052423
4	230	0.83	0.8273067	0.0026933
5	240	0.84	0.8093711	0.0306289
6	250	0.79	0.7914354	-0.0014354
7	250	0.82	0.7914354	0.0285646
8	260	0.76	0.7734998	-0.0134998
9	270	0.75	0.7555642	-0.0055642
10	270	0.755	0.7555642	-0.0005642
11	275	0.74	0.7465964	-0.0065964
12	280	0.73	0.7376286	-0.0076286

Fe/ Al_2O_3

POLYMATH Report
Nonlinear Regression (mrqmin)

15-Mar-2010

Model: C02 = A*0.3189+B*(1-0.0039*((C01+273.15)-533))

Variable	Initial guess	Value	95% confidence
A	0.8	-3.409247	2.462831
B	0.3	1.59965	0.7217882

NOTE: Calculations exceeded the maximum number of iterations.

Nonlinear regression settings
Max # iterations = 64
Tolerance = 0.0001

Precision

R^2	0.8305575
R^2adj	0.802317
Rmsd	0.0116821
Variance	0.0014557
Chi-Sq	0.8734233
Alamda	1.0E+46

General

Sample size	8
Model vars	2
Indep vars	1
Iterations	65

Source data points and calculated data points

	C01	C02	C02 calc	Delta C02
1	220	0.73	0.7610511	-0.0310511
2	230	0.7	0.6986648	0.0013352
3	230	0.71	0.6986648	0.0113352
4	235	0.635	0.6674716	-0.0324716
5	235	0.685	0.6674716	0.0175284
6	240	0.675	0.6362784	0.0387216
7	250	0.62	0.573892	0.046108
8	260	0.46	0.5115057	-0.0515057

$Fe/SiO_2/Al_2O_3$

POLYMATH Report
Nonlinear Regression (mrqmin)

15-Mar-2010

Model: C02 = A*0.3189+B*(1-0.0039*((C01+273.15)-533))

Variable	Initial guess	Value	95% confidence
A	0.8	-1.295405	2.327632
B	0.3	0.9090909	0.6949198

NOTE: Calculations exceeded the maximum number of iterations.

Nonlinear regression settings
Max # iterations = 64
Tolerance = 0.0001

Precision

R^2	0.9406308
R^2adj	0.9109462
Rmsd	0.0036927
Variance	0.0001091
Chi-Sq	0.0218182
Alamda	1.0E+48

General

Sample size	4
Model vars	2
Indep vars	1
Iterations	65

Source data points and calculated data points

	C01	C02	C02 calc	Delta C02
1	230	0.6	0.6018182	-0.0018182
2	240	0.57	0.5663636	0.0036364
3	250	0.52	0.5309091	-0.0109091
4	250	0.54	0.5309091	0.0090909

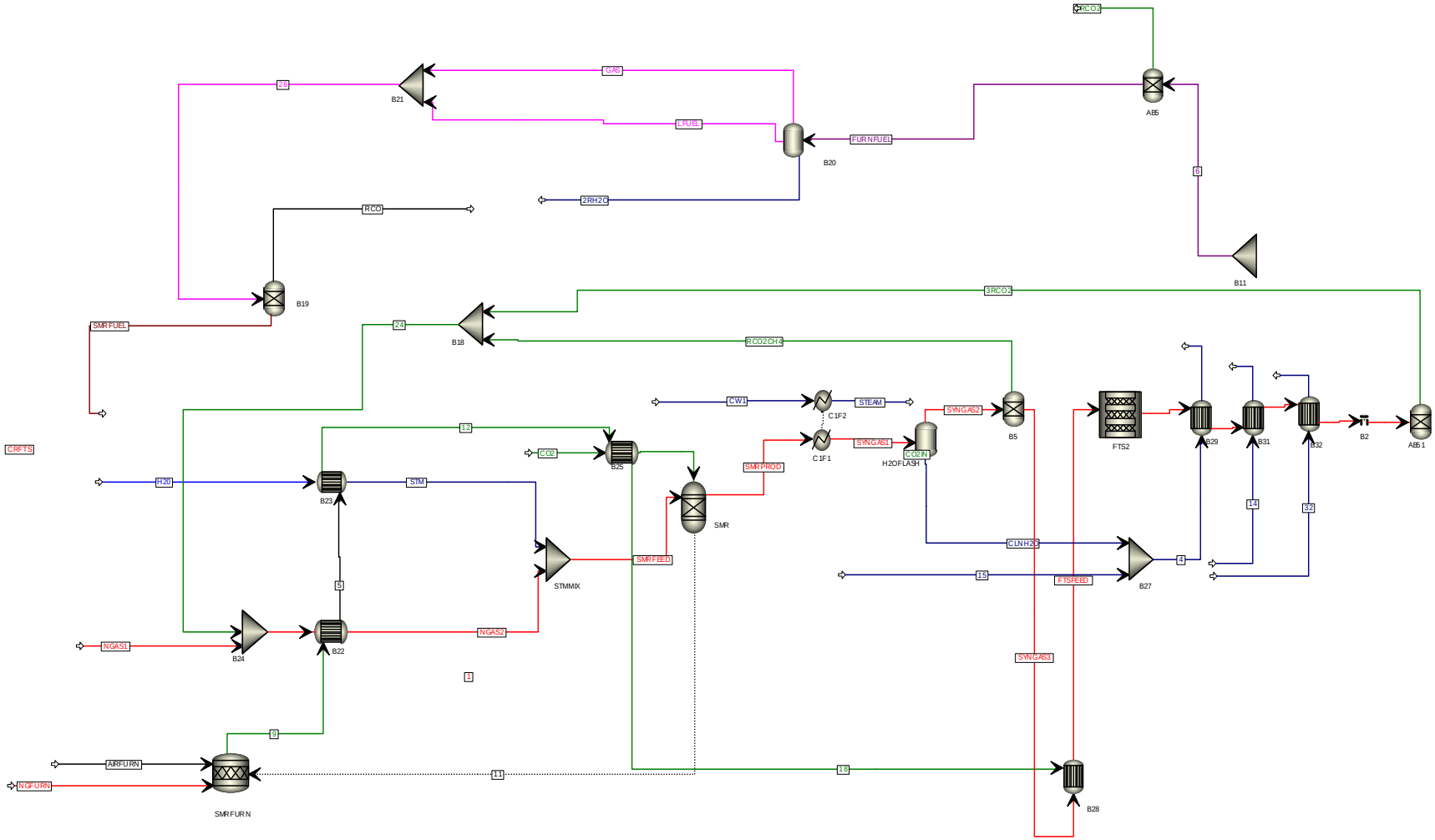

Aspen Flowsheet Upstream

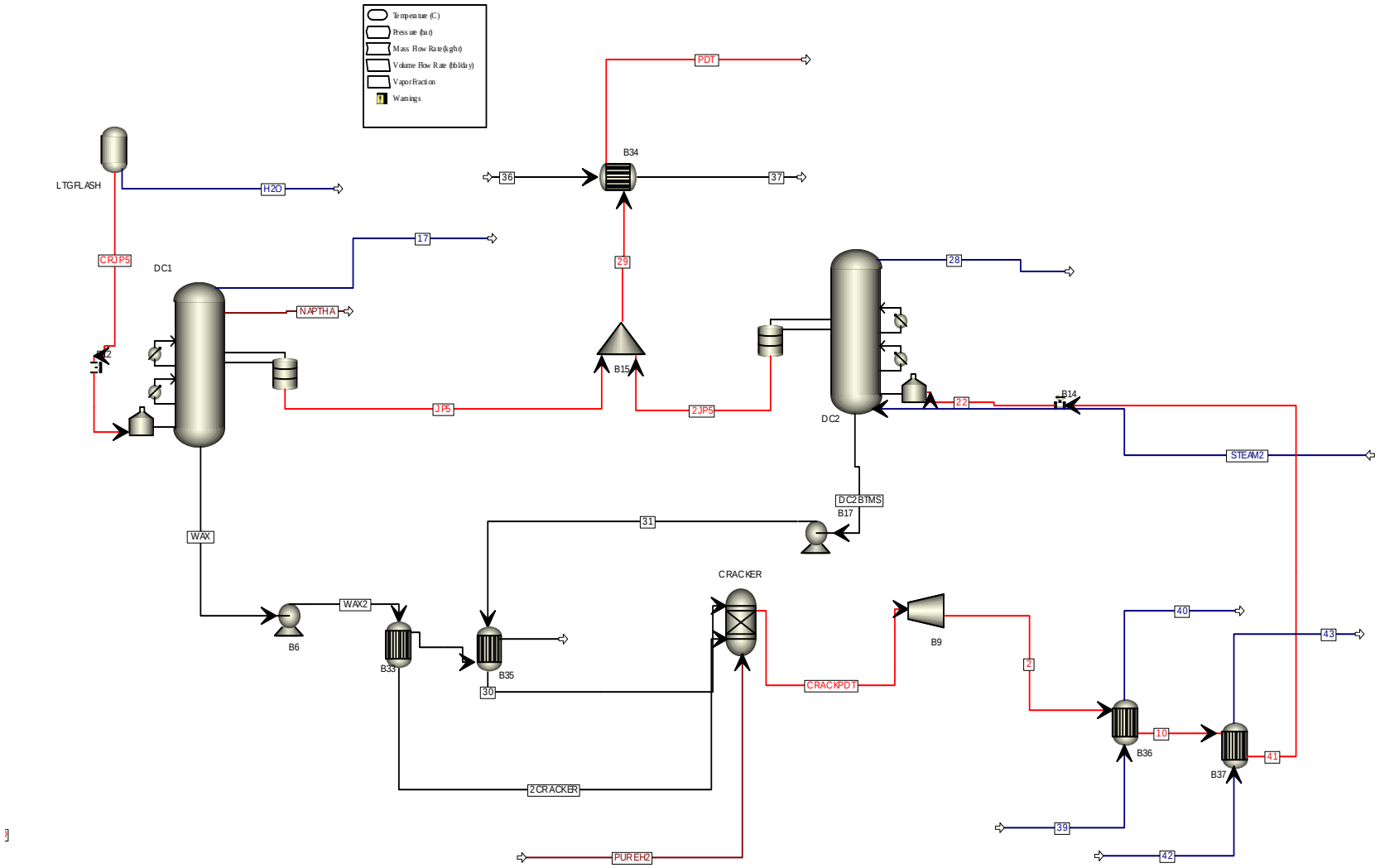

Aspen Flowsheet Downstream